Moments of the Magnetic and Hamiltonian Variety – New Perspectives on Historic Approaches to the Electronic Correlation Energy and its Properties

by

Bradley Kyle Ganoe

A dissertation submitted in partial satisfaction of the

requirements for the degree of

Doctor of Philosophy

in

Chemistry

in the

Graduate Division

of the

University of California, Berkeley

Committee in charge:

Professor Martin Head-Gordon, Chair
Professor Eric Neuscamman
Professor Steve Louie

Summer 2023

Moments of the Magnetic and Hamiltonian Variety – New Perspectives on Historic Approaches to the Electronic Correlation Energy and its Properties

Abstract

Moments of the Magnetic and Hamiltonian Variety – New Perspectives on Historic Approaches to the Electronic Correlation Energy and its Properties

by

Bradley Kyle Ganoe

Doctor of Philosophy in Chemistry

University of California, Berkeley

Professor Martin Head-Gordon, Chair

Much progress in the theoretical sciences is founded on the application of insight from modern developments and techniques to approaches previously-considered unattractive. This dissertation is concerned with the many-body problem inherent to descriptions of the electronic wavefunction for molecular systems. We begin by developing the intractable exact solution, describe realizable approximations from the many-body to a single-body picture, and cover a range of approaches in recovering the accurate description of the energy from the approximate solution: the quantity of most interest in the chemical sciences. Special considerations for the problem when the bodies are under the effect of a static external applied field are taken into consideration for the same approximations.

We first focus on the description of this problem via high-order cumulants of the Hamiltonian. The use of cumulants is traditionally plagued by the infeasibility of evaluating even low-order powers of the Hamiltonian, especially in comparison to techniques developed in the perturbative description of the energies. Considering the success of selective summation of infinite perturbative terms with added low-order contributions, which today constitute the 'gold standard' of our field, we introduce similar techniques to the span of the moments themselves for use in their respective methodologies. Harkening back to the simplest approximation of electron fluctuations through the doubly-excited manifold, we develop the Double Connected Moments (DCM(N)) approximation and evaluate its use in the Connected Moments Expansion (CMX), a realizable approach to the Horn-Weinstein Theorem.

Moving beyond the energy, we then seek to obtain properties of significant pertinence to the physical sciences: the magnetic magnetizabilities and chemical shieldings used to probe problems of all scales. General solutions for the energy of a molecular system in the presence of an externally applied and internally induced magnetic field are presented for arbitrary electronic wavefunctions by explicit consideration of the magnetically dependent Hamiltonian and naturally complexified wavefunction. While the analytic approach has advantages

in computational tractability, the availability of their use for modern methods becomes an increasingly opaque procedure that may be ultimately fruitless in their descriptions. The general method allows the piloting across a swath of methodologies; towards this, we implement the general method and test the magnetic properties of the regularized orbital-optimized family of solutions in perturbation theory.

To whom it may concern.

In Memory of Mom.

Contents

Acknowledgments

I am grateful to the many folks whose compassion and humanity have made this arduous journey possible. There were far more exits than the intended one; I surely would have strayed if not for their critical support. The shoulders of giants are far too large to scale alone.

Valeria Kleiman,
for wonderful lectures that lit up my eyes;
Rod Bartlett,
for enrapturing my mind with many-body theory;
Ajith Perera & Dominika Zgid,
for their astounding undergraduate mentorship;
Teresa Head-Gordon & Eran Rabani,
for expanding my pedagogical breadth;

Martin Head-Gordon,
for truly exceeding in his role as graduate advisor, his insight and encouragement in our discussions, and the patience with which he approaches both research and individuals.

Bill, Sharon, Nigel, & Barb,
for their eternal love and care;
Skye and Andrew,
for their kindness and friendship;
Beatrice, Ian, Silvia, Jessalyn, Will, & many other companions,
for the stories far more interesting than this one;
My colleagues at the Pitzer Center,
for making a most hospitable and exciting workplace;
The California Pacific Medical Center, especially Assad Hassoun & Adil Wakil,
for their role in my survival via organ transplantation;

Alex, Harvey, Hazel, & Marlon,
who make this existence beyond beautiful and brighten each day.

Chapter 1

Introduction

It was the irregularities of the lunar theory that had kept Newton awake at night – a model of the 3-body orbit was hoped to pare down the error of the moon's orbit to within $2'$ - $3'$, yet instead accounted for about $10'$ off observation in practice. In the preface to *Principia*, the structure of the world and its accurate description was hoped to be elucidated completely by forces, still under search at the time, repelling and attracting these bodies in kind. The cycle of model refinement in the many-body problem towards increasingly accurate predictions of phenomena persists to this day (and its sleepless nights), perhaps most interestingly to this author for its appearance in the quantum theory of particles. As a fundamental postulate, quantum mechanics dictates that the value of any property O may be elucidated[1–3] by the expectation of the many-body operator $\hat{O}$

$$\hat{O} = \hat{O}_{(0)} + \sum_{p} \hat{O}_p + \sum_{p \neq q} \frac{1}{2!} \hat{O}_{pq} + \sum_{p \neq q \neq r} \frac{1}{3!} \hat{O}_{pqr} + \cdots \tag{1.1}$$

constituting the zero-, one-, two-, three-, $\cdots$ body interactions among particles p,q,r,$\cdots$ acting on the exact mathematical description of this state, known as the wavefunction $|\Psi\rangle$, from which the exact physical properties of the system may be determined

$$\langle \hat{O} \rangle = \frac{\langle \Psi | \hat{O} | \Psi \rangle}{\langle \Psi | \Psi \rangle} \tag{1.2}$$

To the best of our collective knowledge to date, this holds true subject to:

1. The limitations of the Haag-Kastler axioms[4] to only certain systems[5], or the dropping of the Spectrum Condition allowing the creation of the Feynman perturbation series[6–9] constructing the perturbative Quantum Field Theory (pQFT),

2. The inaccessibility of the Einstein-Hilbert action[10, 11] defining gravitational dynamics on a spacetime background as a rigorous quantized field[12],

3. Gödel's Incompleteness Theorems[13] resulting in the impossibility of the Hilbert program[14, 15] and a complete and consistent description of the universal wavefunction,

with no hitherto verifiable evidence to counter this claim[16]. Its continued success in the evaluation of physical properties and fundamental relations of systems across the physical sciences is continually evidence, and has accounted for the most accurate theoretical prediction from any scientific field, the evaluation of the fine-structure constant[17] and magnetic moments of leptons[18], relative to experimental evidence our species has yet derived.

1.1 The Many-Body Electronic System

Thankfully, perhaps of most interest to quantum chemists are situations in which these limitations are not applicable, and we may freely use the pQFT approach allowing quantum mechanics with relativistic corrections to wholly define our field. In particular, we seek to use the Hamiltonian describing both the motion and electromagnetic forces among electrons and nuclei defined as

$$\hat{H}(r_i, R_N) = -\sum_N \frac{\nabla_N^2}{2M_N} + \sum_{N<M} \frac{Z_N Z_M}{|R_{NM}|} - \sum_i \frac{\nabla_i^2}{2} - \sum_{iN} \frac{Z_N}{|r_i - R_N|} + \sum_{i<j} \frac{1}{r_{ij}} \tag{1.3}$$

where r_i and R_N refer to the coordinates of the electron i and nucleus N, R_{NM} and r_{ij} the distance between nuclei N and M and electrons i and j respectively, and M_N and Z_N are the mass and charge of nuclei N and the standard atomic units have been used. These may be grouped as above in the general operator based on the electron count of each individual contribution

$$\hat{H}(r_i, R_N) \equiv \hat{H} = \hat{H}_0 + \sum_i \hat{H}_i + \sum_{i<j} \hat{H}_{ij} \tag{1.4}$$

The quantum mechanical description of the electron in a field of clamped nuclei in the Born-Oppenheimer approximation is sufficient for a vast array of chemical systems[2, 19]; in this work we shall keep our focus on the ground state solutions, avoiding the breakdowns of the Born-Oppenheimer product[20, 21], and the separable electronic wavefunction becomes an excellent starting point for the *ab initio* models created in quantum chemistry:

$$\Psi(r_i, R_N) = \Psi_e(r_i, R_N)\Phi_N(R_N) \tag{1.5}$$

in which the total molecular wavefunction is now written as a direct product of the nuclear and electronic wavefunctions, the latter of which may be handled by a parameterization in the field of the nuclear positions $\{R_N\}$. In the rest of this work, we take the electronic wavefunction to be the many-body system of interest. Describing the total energy of the system in terms of this Hamiltonian in the Schrödinger equation[22]

$$\hat{H}(r_i, R_N)\Psi_e(r_i, R_N, t) \equiv \hat{H}|\Psi(t)\rangle = i\frac{\partial}{\partial t}|\Psi(t)\rangle \tag{1.6}$$

offers a route to predicting the dynamics of any system in state $|\Psi(t)\rangle$ given the interactions of these particles: an exciting step towards the very dream outlined in *Principia*. As the

solution to this equation may be described via a trivial phase factor dependent on the initial conditions,

$$|\Psi(t)\rangle = e^{-i\hat{H}(r_i,R_N)t}\,|\Psi(0)\rangle \tag{1.7}$$

we are often interested in the description of the stationary eigenstates in the time-independent formulation of the Schrödinger equation that allow us to describe the static properties of molecular systems

$$\hat{H}|\Psi\rangle = E|\Psi\rangle \tag{1.8}$$

Quickly, it was realized that for all but the simplest set of particles that the conjunction of the many-body problem and the quantum mechanical description of bodies was wholly intractable, and one must approach both the wavefunction and its energy in an approximate way[22–24]. The route to solution has taken many forms, but perhaps among the more common approaches is the use of the Expansion Theorem[25], in which we may expand any normalizable function of spatial and spin coordinate state $\psi(\mathbf{x}) = \psi(\mathbf{r})\sigma(\omega_i)$ in an introduced basis of orthonormal one-particle functions:

$$\psi(\mathbf{x}) = \sum_k \Phi_k(\mathbf{x}) \int \psi(\mathbf{x}_1)\Phi_k^*(\mathbf{x}_1)dx_1 \tag{1.9}$$

for which we are particularly interested in the set of functions $\Phi_k(\mathbf{x}_i)$ of electron coordinates $\mathbf{x}_i$, with $i = 1, 2, \cdots, n$ and no specific constraint yet on symmetries. In practice, the exact infinite-dimensional expansion is not accessible to deterministic approaches, so a finite-basis is used to define a set of configurations whose algebraic approximations approach the exact limit as more configurations are considered. The successive use of theorem for this truncated basis may be used to expand $|\Psi\rangle$:

$$\Psi(\mathbf{x}_1, \mathbf{x}_2, ..., \mathbf{x}_n) = \sum_{\mathbf{k}} \Phi_{k_1}(\mathbf{x}_1)\Phi_{k_1}(\mathbf{x}_1)\cdots\Phi_{k_n}(\mathbf{x}_n)C(\mathbf{k}) \tag{1.10}$$

with the coefficients defined

$$C(\mathbf{k}) = C(k_1, k_2, \cdots, k_n) \tag{1.11}$$

$$= \int \Psi(\mathbf{x}_1, \mathbf{x}_2, \cdots, \mathbf{x}_n)\Phi_{k_1}^*(\mathbf{x}_1)\Phi_{k_2}^*(\mathbf{x}_2)\cdots\Phi_{k_n}^*(\mathbf{x}_n)dx_1dx_2\cdots dx_n \tag{1.12}$$

and offering a convenient framework to define the configuration in the Hilbert space as a selection among the ordered n k-indices meeting the normalization condition

$$\sum_{\mathbf{k}} |C(\mathbf{k})|^2 = \int |\Psi|^2 dx_1 dx_2 \cdots dx_n \tag{1.13}$$

and leaves the coefficients anti-symmetric under the permutations of parity p in coordinates x_i due to the fermionic statistics requirement inherent of spin-$\frac{1}{2}$ particles

$$PC(\mathbf{k}) = (-1)^p C(\mathbf{k}) \tag{1.14}$$

and, in a convenient permutation among dummy indices,

$$\Psi(\mathbf{x}_1, \mathbf{x}_2, ..., \mathbf{x}_n) = \sum_{\mathbf{k}} C(\mathbf{k}) \sum_{P} (-1)^p P_k \Phi_{k_1}(\mathbf{x}_1)\Phi_{k_2}(\mathbf{x}_2)\cdots\Phi_{k_n}(\mathbf{x}_n) \tag{1.15}$$

$$\Psi(\mathbf{x}_1, \mathbf{x}_2, ..., \mathbf{x}_n) = \sum_{k_1<k_2<\cdots<k_n} C(\mathbf{k}) \det\{\Phi_{k_1}(\mathbf{x}_1)\Phi_{k_2}(\mathbf{x}_2)\cdots\Phi_{k_n}(\mathbf{x}_n)\} \tag{1.16}$$

showing that the exact wavefunction of an electronic system, in a now simplified notation, is a summation over k configurations

$$|\Phi_k\rangle = (N!)^{-\frac{1}{2}} \det\{\Phi_{k_1}(\mathbf{x}_1)\Phi_{k_2}(\mathbf{x}_2)\cdots\Phi_{k_n}(\mathbf{x}_n)\} \tag{1.17}$$

with coefficients

$$C_k = (N!)^{\frac{1}{2}} C(\mathbf{k}) \tag{1.18}$$

for a total electronic wavefunction of state as

$$|\Psi\rangle = \sum_k C_k |\Phi_k\rangle \tag{1.19}$$

whose numbers of configurations grow *factorially* with respect to the number of particles. It is from this problem that the whole of quantum chemistry has been spawned: a convenient framework with which to describe exactly the state of interest (to within the limitations denoted above) of all chemical systems[26], yet not an achievable framework with which to do so for all but the smallest of systems; from here, approximations must be made.

1.1.1 The Density Matrix: Creating Fewer-Body Methods

Perhaps the most general route to achievable approximations[27] is described through the system operator Γ that it takes the form

$$\Gamma(\mathbf{x}_1, \mathbf{x}_2, \cdots, \mathbf{x}_n | \mathbf{x}'_1, \mathbf{x}'_2, \cdots, \mathbf{x}'_n) = |\Psi(\mathbf{x}_1, \mathbf{x}_2, \cdots, \mathbf{x}_n)\rangle\langle\Psi(\mathbf{x}'_1, \mathbf{x}'_2, \cdots, \mathbf{x}'_n)| \tag{1.20}$$

that has the properties of a true mathematical projector:

1. Self-adjoint ($\Gamma^\dagger = \Gamma$)
2. Positive semi-definite ($\Gamma \geq 0$)
3. Trace of unity ($\mathrm{Tr}\Gamma = 1$)

such that the kernel, known as the N-particle density matrix, replaces the fermionic wavefunction under the conditions of

1. idempotency $\Gamma = \Gamma^2$

2. anti-symmetry ($\Gamma(\mathbf{x}_1, \mathbf{x}_2, ...) = -\Gamma(\mathbf{x}_2, \mathbf{x}_1, ...) = \Gamma(\mathbf{x}_1, \mathbf{x}_2, ...)$

The stipulation this presents may be used in a number of ways to make solutions more tractable, but of most interest to us is successively tracing the N-body density matrix to form any p-body reduced density matrix on the k vectors

$$\begin{gathered}\Gamma(\mathbf{x}_1, \mathbf{x}_2, \cdots, \mathbf{x}_p | \mathbf{x}'_1, \mathbf{x}'_2, \cdots, \mathbf{x}'_p) = \\ \binom{N}{p} \int \Gamma(\mathbf{x}_1, \mathbf{x}_2, \cdots, \mathbf{x}_p, \mathbf{x}_{p+1}, \cdots, \mathbf{x}_n | \mathbf{x}'_1, \mathbf{x}'_2, \cdots, \mathbf{x}'_p, \mathbf{x}_{p+1}, \cdots, \mathbf{x}_n) dx_{p+1} \cdots dx_n\end{gathered} \tag{1.21}$$

down to the two special cases of the two-particle reduced density matrix (2RDM) and the one-particle reduced density matrix (1RDM)

$$\begin{gathered}\Gamma(\mathbf{x}_1, \mathbf{x}_2 | \mathbf{x}'_1, \mathbf{x}'_2) = \\ \binom{N}{2} \int \Gamma(\mathbf{x}_1, \mathbf{x}_2, \mathbf{x}_3, \cdots, \mathbf{x}_n | \mathbf{x}'_1, \mathbf{x}'_2, \mathbf{x}_3, \cdots, \mathbf{x}_n) dx_3 \cdots dx_n\end{gathered} \tag{1.22}$$

$$\begin{gathered}\Gamma(\mathbf{x}_1 | \mathbf{x}'_1) = \\ \binom{N}{2} \int \Gamma(\mathbf{x}_1, \mathbf{x}_2, \cdots, \mathbf{x}_n | \mathbf{x}'_1, \mathbf{x}_2, \cdots, \mathbf{x}_n) dx_2 dx_3 \cdots dx_n\end{gathered} \tag{1.23}$$

These two forms are particularly useful, as our Hamiltonian of interest is an at-most two-particle operator and its exact expectation under the normalization condition $\langle \Psi | \Psi \rangle = 1$ may now be writen

$$\begin{gathered}\langle \Psi | \hat{H} | \Psi \rangle = \mathrm{Tr}(\hat{H}\Gamma) \\ = E_{\mathrm{nuc}} + \int \hat{H}_1 \Gamma(\mathbf{x}_1 | \mathbf{x}'_1) dx_1 + \int \hat{H}_{12} \Gamma(\mathbf{x}_1, \mathbf{x}_2 | \mathbf{x}'_1, \mathbf{x}'_2) dx_1 dx_2\end{gathered} \tag{1.24}$$

allowing for a more tractable approach to the exact energy. The use of the 2RDM to express the exact energy directly in a tractable form given its slew of N-Representability conditions to ensure a one-to-one mapping with the exact wavefunction is an open area of research in the field[28, 29]; instead, we here take the traditional single-particle theory constituting the averaged potential felt first introduced by Slater[30] with which to recover the remainder portion, often referred to as the correlation energy.

1.1.2 A single-particle theory

The use of the 1RDM as the density of choice was shown by Fock to form a one-electron independent particle theory limited to the now single configuration of purely occupied orbitals[31]

$$|\Psi\rangle = \sum_k C_k |\Phi_k\rangle \approx |\Phi_0\rangle \tag{1.25}$$

whose expectation value with respect to the Hamiltonian yields its energy E_0 in what is referred to as the General Hartree-Fock (GHF)[27] Method with as-of-yet determined restraints on the symmetry

$$E_0 = \frac{\langle \Phi_0 | H | \Phi_0 \rangle}{\langle \Phi_0 | H | \Phi_0 \rangle} \geq E_{exact} \tag{1.26}$$

and its set of molecular orbitals $|\phi_i\rangle$ used in the expansion of the determinant are typically taken as a linear combination of atomic orbitals[32]

$$|\phi_i\rangle \equiv \phi_i(\mathbf{r}) = \sum_\mu C_{\mu i} \eta_\mu(\mathbf{r}) \equiv \sum_\mu C_{\mu i} \, |\eta_\mu\rangle \tag{1.27}$$

composed of the (usually atom-centered) atomic orbitals basis functions $|\eta_\mu\rangle$ and the coefficient $C_{\mu i}$ expanding the moleculer orbital i on the basis function μ from which we approximate the infinite expansion[33, 34]. In the basis of the one-particle functions, this takes the form employing the Slater-Condon (or Löwdin in non-orthogonal) rules[35]

$$E_0 = \sum_i h_{ii} + \frac{1}{2} \sum_{ij} \langle ij || ij \rangle \tag{1.28}$$

where we have simplified from the N-particle matrix elements to the 1- and 2-particle matrix elements and summed over both the integrals

$$h_{ii} = \langle \phi_i | \hat{h} | \phi_i \rangle = \sum_N \langle \phi_i | - \frac{\nabla}{2} - \frac{Z_N}{|r - R_N|} | \phi_i \rangle \tag{1.29}$$

corresponding to the of one-body kinetic and nuclear attraction of electron i from a partition of the electronic Hamiltonian, equivalent to the Hartree orbital energies in the diagonalized case, and the set of integrals

$$\langle ij || ij \rangle = \langle \phi_i \phi_j | \frac{1}{r_{12}} | \phi_i \phi_j \rangle - \langle \phi_i \phi_j | \frac{1}{r_{12}} | \phi_j \phi_i \rangle \tag{1.30}$$

representing the two-body electron repulsion terms between electrons i and j which together account for the averaged electron-electron repulsion energy of the system. Finally, the symmetry-adapted aspects of the wavefunction $|\psi\rangle$ may be derived for any operators $\hat{\Omega}$ that are a constant of motion[36]

$$[\hat{H}, \hat{\Omega}] = \hat{0} \tag{1.31}$$

such that the wavefunction is a simultaneous eigenfunction to both operators

$$\hat{H}\hat{\Omega}|\psi\rangle = \hat{\Omega}\hat{H}|\psi\rangle = \epsilon\hat{\Omega}|\psi\rangle \tag{1.32}$$

and, as a direct consequence of this commutation, the Schrödinger equation of the exact state itself trivially shares a set of eigenfunctions with the operator

$$\hat{\Omega}|\Psi\rangle = \omega|\Psi\rangle \tag{1.33}$$

However, the variationally optimized reference function $\delta\langle\Phi|\hat{H}|\Phi\rangle = 0$ need not satisfy the constraint $\hat{\Omega}|\Phi\rangle = \omega|\Phi\rangle$. In order to address spin, we may decompose the 1RDM explicitly into the Molecular Orbital (MO) coefficients of the occupied orbitals $\mathbf{C}_{occ}$ partitioned into their respective spinfunctions

$$\Gamma(\mathbf{x}_1|\mathbf{x}_1') \equiv \mathbf{P} = \mathbf{C}_{occ}\mathbf{C}_{occ}^{\dagger} = \begin{bmatrix} \mathbf{P}^{\alpha\alpha} & \mathbf{P}^{\alpha\beta} \\ \mathbf{P}^{\beta\alpha} & \mathbf{P}^{\beta\beta} \end{bmatrix} \tag{1.34}$$

In order to match the complex and spin symmetry of the exact wavefunction, the Hartree-Fock one-particle density matrix is required to:

1. Constrain the MO's to the real space $\mathbf{P} = \mathbf{P}(\mathbb{R})$
2. Impose a block diagonal form on the general matrix

$$\mathbf{P} = \begin{bmatrix} \mathbf{P}^{\alpha\alpha} & 0 \\ 0 & \mathbf{P}^{\beta\beta} \end{bmatrix} \tag{1.35}$$

3. Enforce a restriction on the spin densities $\mathbf{P}^{\alpha\alpha} = \mathbf{P}^{\beta\beta}$

Enforcement of all three of these symmetries upon $|\Phi_0\rangle$ leads to the real-space Restricted Hartee-Fock (RHF) set of solutions. Unfortunately, these constraints placed on the variational manifold in the case of RHF may lead to an artificially high energy when the qualitative features of the single determinant $|\Phi_0\rangle$ are unable to replicate the total $|\Psi\rangle$ and symmetry-broken solutions with less constraints may lower the energy[37]. Possible relaxations come in several possible forms

1. Complex Hartree-Fock: Allowing $\mathbf{P} = \mathbf{C}_{occ}(\mathbb{C})\mathbf{C}_{occ}^{\dagger}(\mathbb{C})$
2. Unrestricted Hartree-Fock: Dropping only $\mathbf{P}_{\alpha\alpha} = P_{\beta\beta}$
3. General Hartree-Fock: Dropping block-diagonalization

$$\mathbf{P} = \begin{bmatrix} \mathbf{P}^{\alpha\alpha} & \mathbf{P}^{\alpha\beta} \\ \mathbf{P}^{\beta\alpha} & \mathbf{P}^{\beta\beta} \end{bmatrix} \tag{1.36}$$

for a total of 6 possible Hartree-Fock constraints (Restricted, Unrestricted, General, and their respective complex versions) that may lower the energy, but no longer have the symmetry properties inherent to the true wavefunction. This may be especially of note when the UHF and GHF solutions introduce spin-contamination from the inclusion of states with mixed multiplicities, and intruder states that typically would not energetically contribute may significantly effect the results[38]. This problem has been named the symmetry dilemma.

1.2 Re-Approaching Many-Body Descriptions

In nearly a century and five generations of scientists, we still seek to address this problem through a diversity of methods seeking to satisfy the conditions under which this (or differently chosen) reference function may bring us towards the exact energy, as well as the desiderata useful in making these wavefunctions an applicable tool for the general scientist. The aspirations to achieve such goals have taken on several key features over the decades, but perhaps most readily accepted are the criteria for an approximate but well-defined Model Chemistry via Pople[39]:

1. Target: It ought to make a clear distinction between different modes of molecular behavior, towards a goal of global accuracy within 1 kcal/mol.

2. Formulation: It ought to be continuous, unique, and consistent along the energy manifold, while being as general for as wide a variety of chemical systems as possible.

3. Implementation: It must be realizable within reasonable time and cost of computation.

4. Verification: It ought to be systematically replicate physical observables from the experimental data.

5. Prediction: It ought to properly predict behavior of unknown or disputed systems of chemical interest.

Two approaches will be explored in this thesis. First, we push towards a new Model Chemistry in which the correlation energy not accounted for in the single-particle picture may be accurately and affordably produced. The investigation of new methodologies with unique sets of properties offers a convenient toolbox in which we may assess the validity of the approaches in light of these broad goals. As no extant technique fully satisfies set of desiderata for all interesting chemical problems, probing new techniques to yield niches in difficult-to-address problems or surpassing established methods in the regime of accuracy vs. computational demand are both sufficient qualities to warrant research. Towards this, we seek modified approaches in the description of the electron correlation based not on the accurate modelling of the reference, from which perturbation theory may be used, but instead describing an approach based on the prior work of Löwdin, Horn, and Weinstein[36, 40] in which moments and their cumulants play a key role.

Second, we focus on the access of properties for use by the general chemist, and in particular the ubiquitous set of NMR parameters on which many experimentalists rely upon. While all properties of interest may be derived from the mathematical approach described above, making them calculable does not always follow the trends of improvement in energy. In fact, for several contributions from the magnetic Hamiltonian, our traditional knowledge on accuracy diverges in the evaluation of their respective property. As it stands, the development of methodologies accurately addressing energetics may not always reflect this same success in their evaluation of properties. Combined with the fact that the pace of production of these

methods and, in some cases, the impossibility of accessing such properties via traditional routes, we seek to formulate a generalized framework derived from early work by Cohen, Roothaan, and Pople[41, 42] in which the explicit evaluation of the molecule in the presence of a field may be readily achieved.

1.2.1 The Correlation Problem

We will find it useful to develop the correlation problem in a framework of an arbitrary reference $|0\rangle$, from which we may approach the exact wavefunction under the condition that they have a non-zero overlap and their difference may be defined $|\chi\rangle = |\Psi\rangle - |0\rangle$ to represent the missing determinants. This will allow us to develop several traditional approaches in the field[43], as well as elaborate on some historic methodologies that we will expand upon. The use of the partitioning technique allows us to set up the supermatrix[44]

$$\begin{bmatrix} P\hat{H}P & P\hat{H}Q \\ Q\hat{H}P & Q\hat{H}Q \end{bmatrix} \begin{bmatrix} |0\rangle \\ |\chi\rangle \end{bmatrix} = E \begin{bmatrix} |0\rangle \\ |\chi\rangle \end{bmatrix} \tag{1.37}$$

with the introduced terms of the reference subspace, which acts upon the exact wavefunction to produce the reference

$$P = |\Phi_0\rangle\langle\Phi_0| = |0\rangle\langle 0| \tag{1.38}$$

and the orthogonal subspace, a projection that produces the set of excited configurations of the Hilbert space

$$Q = I - P = \sum_{ia} |_i^a\rangle\langle_i^a| + \frac{1}{4}\sum_{ijab} |_{ij}^{ab}\rangle\langle_{ij}^{ab}| + \cdots \tag{1.39}$$

These operators are particularly useful in the construction of correlated techniques and used in a route to the exact wavefunction directly from the initial reference via substituting the solution to the second equation of the supermatrix

$$Q|\Psi\rangle = (E - Q\hat{H})^{-1} Q\hat{H}P|\Psi\rangle \tag{1.40}$$

implicitly for the form of the exact wavefunction by adding

$$0 = E\hat{H}(E - Q\hat{H})^{-1}|0\rangle - E\hat{H}(E - Q\hat{H})^{-1}|0\rangle \tag{1.41}$$

to the first equation of the supermatrix

$$E\,|\Psi\rangle = \hat{H}\,|0\rangle + \hat{H}(E - Q\hat{H})^{-1} Q\hat{H}|\,|0\rangle \tag{1.42}$$

$$E\,|\Psi\rangle = \hat{H}\,|0\rangle + \hat{H}(E - Q\hat{H})^{-1}(Q\hat{H} - E)|0\rangle + E\hat{H}(E - Q\hat{H})^{-1}|0\rangle \tag{1.43}$$

$$|\Psi\rangle = \hat{H}(E - Q\hat{H})^{-1}|0\rangle \tag{1.44}$$

and by projecting with the reference function and taking the standard intermediate normalization choice yields

$$\langle 0|\Psi\rangle = 1 = \langle 0|\hat{H}(E - Q\hat{H})^{-1}|0\rangle \tag{1.45}$$

Known as the implicit energy formula, which does not directly solve for the true wavefunction, but instead for its energy eigenvalues directly from any arbitrary reference constrained to a non-zero overlap with the exact wavefunction[45]. Inspection in the case of an overlap of unity, which constrains the orthogonal space to $Q = \hat{0}$, trivially yields the identity, but the process of how one proceeds to the energy from any approximation is needed. Seeking a way to address this, we begin from an alternative condition that allows this same equation, and many others throughout the field[46, 47], to be yielded as a direct consequence of the resolvent solution to the inhomogenous Schrödinger equation:

$$(\hat{H} - z \cdot I)|\Psi\rangle = a|\Phi\rangle \tag{1.46}$$

where we have introduced multipliers of z and a that apply, respectively, upon the exact and reference wavefunction in this form of the equation. Quite evidently, the solution in which $a = 0$ necessarily yields the traditional time-indendepent Schrödinger equation with the valuation of z being the eigenenergy of the system. Following the same procedure in the partitioning technique as above, we can express the exact wavefunction

$$|\Psi\rangle = -aR(z)|\Phi\rangle \tag{1.47}$$

where we have now introduced the notation for the resolvent operator, a common tool in use for the solution of inhomogenous differentials more generally, as well a concrete evaluative approach to a, commonly referred to as the Weinstein function

$$R(z) = (z \cdot I - \hat{H})^{-1} \quad a = -\langle\Phi|R(z)|\Phi\rangle \tag{1.48}$$

1.2.2 Methodologies for the Correlation Energy

The framework presented shall be our starting point for correlation methods[44]. Perhaps most obvious, the energy-dependent propagators and the Dyson orbital approach[48, 49] naturally fall out of the definition of the resolvent when $z = E$

$$G(\mathbf{x}', \mathbf{x}', E) = \langle x|\hat{G}(E)|x'\rangle \tag{1.49}$$

$$(E - \hat{H})\hat{G}(E) = 1 \implies \hat{G}(E) = (E - \hat{H})^{-1} \tag{1.50}$$

in which now both the one-particle and many-particle Green's Function family of methodologies may be derived under the typical set of tools to deal with the propagator's inability to be properly inverted. Here we make note of the ability to include within z an arbitrarily small positive or negative imaginary energy, which gives the incoming and outgoing Green's

Functions a solution pushed into either the upper or lower half of the complex planes using the time-evolution operator of

$$i\frac{\partial U(t,t')}{\partial t} = \hat{H}(t)U(t,t') \tag{1.51}$$

to resolve the solutions via a Fourier transform

$$\hat{G}_+(z) = -i\int_0^\infty e^{izt}U(t) = (z-\hat{H})^{-1} \quad (\mathrm{Im}z > 0) \tag{1.52}$$

and

$$\hat{G}_-(z) = i\int_{-\infty}^0 e^{izt}U(t) = (z-\hat{H})^{-1} \quad (\mathrm{Im}z < 0) \tag{1.53}$$

so that if the limit as ϵ tends towards zero exists for either form, then their respective solution

$$\hat{G}_\pm = \lim_{\epsilon\to 0}\hat{G}_\pm(E \pm i\epsilon) \tag{1.54}$$

may be substituted in the solution of the Dyson equation. The other plainly apparent route is that the poles of the Weinstein function yields the (negative) eigenenergies of the system, which one may calculate explicitly and find the divergences of the equation; however, due to the quite pathological nature in the divergence of solutions it is often not feasible to find the set of poles and no such calculation has been performed in the electronic self-energy (at least known to this author). However, one may equivalently use the identity for the inverse of the difference of operators

$$(\hat{A}-\hat{B})^{-1} = \hat{A}^{-1} + \hat{A}^{-1}B(\hat{A}-\hat{B})^{-1} \tag{1.55}$$

in the expansion of the resolvent expansion $R(z) = z^{-1} + z^{-1}\hat{H}R(z)$ and make use of the projection of Q onto the inhomegenous Scrödinger equation

$$Q(\hat{H} - z\cdot I)|\Psi\rangle = Qa|\Phi\rangle = 0 \equiv |\Psi\rangle = \big[1 - \frac{Q\hat{H}}{z}\big]^{-1}|\Phi\rangle \tag{1.56}$$

obtaining a general form of partitioning technique representation of the wave operator in terms of the Hamiltonian. This form is particularly convenient in the derivation of the entire set of perturbation theories[50], in which by choice of linear operators we may separate the Hamiltonian into the zeroth-order portion $\hat{H}_0$ and a small component representing the perturbation $\hat{V}$. Doing the separation before the partitioning in the supermatrix

$$\begin{bmatrix} P\hat{V}P & P\hat{V}Q \\ Q\hat{V}P & Q\hat{V}Q \end{bmatrix}\begin{bmatrix} |0\rangle \\ |\chi\rangle \end{bmatrix} = (E-\hat{H}_0)\begin{bmatrix} |0\rangle \\ |\chi\rangle \end{bmatrix} \tag{1.57}$$

and, whereby following the same technique, we get a modified form of the resolvent solution to the exact wavefunction

$$|\Psi\rangle = \big[1 - \frac{Q\hat{V}}{z - Q\hat{H}_0}\big]^{-1}|\Phi\rangle \tag{1.58}$$

and deriving the wave operator form of Many-Body Perturbation Theory[51, 52]. Much thought has been put into what the best choice of small component and z may be[53], but a ubiquitous choice is known as the Møller-Plesset partitioning of the Hamiltonian, in which the zeroth-order is set as the eigenoperator of the Hartree one-body contributions to the energy[54]

$$\hat{H}_0^{[0]} |\Phi_0\rangle = \epsilon_0 |\Phi_0\rangle \tag{1.59}$$

From here, various choices in the scalar z yield the famous flavors of perturbation theory, which becomes apparent after applying the idempotency of projector Q to yield the traditional resolvents in MBPT

$$\frac{Q\hat{V}}{z - Q\hat{H}_0^{[0]}} = R_0(z)\hat{V} \tag{1.60}$$

Allowing it to stay the exact energy, $z = E$, as we have been doing, one yields the Epstein-Nesbet (EN) variant[55], while the most popular choice is the Raleigh-Schrödinder (RS) perturbation theory[56], where the choice of the Hartree orbital energies, $z = E_0^0$ and the application of the identity may be applied now to the Schödinger equation

$$E = \langle\Phi_0|H|\Psi\rangle = \langle\Phi_0|H[1 - R_0(E_0^0)V]^{-1}|\Phi_0\rangle = \sum_{n=0}^{\infty} \langle\Phi_0|H(R_0V)^n|\Phi_0\rangle \tag{1.61}$$

giving the usual final expression of the Møller-Plesset energy as a sum one may truncate at order n for the E_n order energy referred to as MPn. One final act of convenience instead has us wrap MP1, the averaged two-body contributions of the Hartree-Fock Energy, also into the zeroth-order expression, allowing us to seek instead the correlation energy, ΔE, directly. The use of normal-ordered operators, which directly subtracts off the Fermi vacuum expectation of the operator, enforces that the expectation is zero relative the the reference

$$\hat{O}_{\mathrm{N}} = \hat{O} - \langle O\rangle_0 \implies \langle 0|\hat{O}_{\mathrm{N}}|0\rangle = 0 \tag{1.62}$$

and appropriate modification to normal-ordered operators in the above gives us now the correlation energy with respect to the Hartree-Fock reference:

$$\Delta E = \langle 0|V_{\mathrm{N}}(1 - R_0V_{\mathrm{N}})^{-1}|0\rangle = \sum_{n=0}^{\infty} \langle\Phi_0|V_{\mathrm{N}}(R_0V_{\mathrm{N}})^n|\Phi_0\rangle_{C,L} \tag{1.63}$$

using the subscript C and L to refer to the expectation values of each order as purely the connected and linked contributions of the energy, a term coming from the derivation via Wick's theorem where each contribution must be fully contracted in the series. This ensures that each individual portion in the summation scales with the particle count, $E_n \propto N$ and, where by the Brillouin theorem[57, 58], the one-particle portions of the normal-ordered Hamiltonian collapses to zero when the $\langle 0|V|0\rangle$ portion is subsumed into E_0 so the first surviving term is the second-order energy MP2. As the various electron fluctuations through

the Hilbert space using the normal-order form may never reach the fermi-vacuum (as the expectation would be null), any connected and linked portions derived from such approaches are at all orders a property that necessarily establishes the size-extensivity of a methodology, and the energy of infinitely separated subsystems A and B

$$E(A+B) = E(A) + E(B) \tag{1.64}$$

will be equivalent whether done in the supersystem or separately. Any connected wavefunction will produce an energy that is both connected and linked[59].

1.2.3 Coupled-Cluster: Renormalization of the Series

Historically, the infinite expansion is not realizable for most many-body Hamiltonians, but because well-approximated low-order expansions often recover a large portion of the energy they have become a preferred route to approximate the exact energy. From this series and the definition of the normal-ordered operators, finding selective contributions to infinite order becomes a practice in worthwhile resummation techniques. It is simple to define the Coupled Cluster[60] amplitudes from the infinite-order MBPT wavefunction.

$$|\Psi\rangle_{\mathrm{MBPT}} - |0\rangle = \sum_{n=1}^{\infty} (\hat{R}_0 \hat{V}_N)^n \, |0\rangle_C = \sum_{m=1}^{N} \hat{T}_m \, |0\rangle \tag{1.65}$$

where each T_m is a resummation of the various terms in the MBPT expasion that create a pair of m hole-particle external pairs lines, commonly referred to as the m-th excitation level, to the maximal possible excitation of N particles out of the reference

$$\hat{T_m} = \frac{1}{(m!)^2} \sum_{\substack{i_1,i_2,\cdots,i_m \\ a_1,a_2,\cdots,a_m}} t_{i_1,i_2,\cdots,i_m}^{a_1,a_2,\cdots,a_m} \{\hat{a}_1^\dagger \hat{i}_1 \hat{a}_2^\dagger \hat{i}_2 \cdots, \hat{a}_m^\dagger \hat{i}_m\} \tag{1.66}$$

by use of the fully-contracted annihilation operators $\hat{i}_m$, removing a particle from the right-hand determinant orbital index i_m, and the creation operators $\hat{a}_m^\dagger$, placing a particle in the right-hand determinant orbital index a_m (as well as the inverse when applied towards the left-hand determinant). Reintroducing the reference and the use of an exponential ansatz to generate both the resummed connected-cluster ($T_m \, |0\rangle$) and disconnected-cluster ($T_m \cdots T_n \, |0\rangle$) contributions to the wavefunction applied to this reference function as a wave operator gives

$$|\Psi\rangle = e^{\hat{T}} \, |0\rangle \qquad \hat{T} = \sum_{m=1}^{N} \hat{T}_m \tag{1.67}$$

$$e^{-\hat{T}} \hat{H}_{\mathrm{N}} e^{\hat{T}} \, |0\rangle = \hat{H}_{\mathrm{N}} [1 + \hat{T} + \hat{T}^2 + \hat{T}^3 + \hat{T}^4] \, |0\rangle_C \tag{1.68}$$

in which the Baker-Campbell-Hausdorff expansion of the similarity-transform and the at-most two-particle nature of the Hamiltonian requires a truncation to four contractions limited

to connected contributions[61, 62] The Coupled-Cluster hierarchy of CCS, CCD, CCSD, and so forth until use of all T_m clusters fully solve the equations via projection of the reference for the energy, and the excited determinants for the T-amplitudes; this procedure is fully equivalent to the entire set of configurations possible at the limit of T_N.

This idea behind selective summations of infinite order terms will feature heavily in chapter two, and in passing it is of note that many different methodologies have their design in this[60, 63–65]. For example, the random-phase approximation is a subset of the T_2 amplitudes used in CCD strictly truncated to pairwise particle-hole lines known as the 'ring diagrams' when taking a diagrammatic approach to the equations[66]. Of most note, the CCSD(T) 'gold standard' achieving the Model Chemistry criteria for a large portion of real systems (save the hefty $O(n^7)$ scaling) is the connected- and disconnected-clusters of infinite order in single and double excitations, while taking an even-tempered sum of triple excitations through 5th-order, and evidently opening the door to infinitely wide arrays of possible methods[67]; much work over the decades of Coupled-Cluster and MBPT have spent detailed analysis on which portions of the Hilbert space contribute significantly to the systems encountered in Chemistry to warrant inclusion and more sophisticated approaches with which to do so.

1.2.4 The Moment Methodologies

Heading back to the inhomogeneous solution, we may instead be willfully indecisive, making no choice of small parameter and proceeding along similar lines as the perturbative case. Doing so, one may yield an equation now with the form[68]

$$E = \langle \Phi_0 | \hat{H} | \Psi \rangle = \langle \Phi_0 | H [1 - \frac{Q\hat{H}}{z}]^{-1} | \Phi_0 \rangle = \sum_{n=0}^{\infty} \langle \Phi_0 | H (z^{-1} Q\hat{H})^n | \Phi_0 \rangle \tag{1.69}$$

which produces one route to solving the implicit energy formula and displaying the origin of the name 'denominator-free perturbation theory' with only a scalar rather than a necessary-to-calculate inverted operator as divisor[69]. The numerators of these objects, which from a mathematical analysis may be classified equivalently as the m-th level cumulants, central moments, or (most useful for our purpose) the connected moments of operators, are useful objects in both analysis and statistics. The fundamental raw moment, the expectation $\langle H \rangle$, is equivalent to its connected moment, but for higher-order terms they will often deviate from one another. From the n-th raw moment of the Hamiltonian, $\langle H^n \rangle$, we may generate the whole set of the connected moments from the moment-generating function

$$\langle H^j \rangle_c = \langle H^j \rangle - \sum_{k=0}^{j-1} \binom{j}{k} \langle H^{k+1} \rangle \langle H^{j-k} \rangle \tag{1.70}$$

which allow their construction. To demonstate with the simple second cumulant, the application of the moment generating function

$$\langle H^2 \rangle_c = \langle H^2 \rangle - \langle H \rangle \langle H \rangle = \langle \Phi_0 | \hat{H} (P + Q) \hat{H} - \hat{H} P \hat{H} | \Phi_0 \rangle \tag{1.71}$$

gives the variance of the Hamiltonian, and the connection to the implicit energy formulation of the Scrödinger equation arises through the generation of all connected moments in the expansion. Rather than using the partial operator approaches inherent to perturbation theory, we may approach the same theoretical methods from a slightly different angle. The eigenenergy solutions may be expressed via the zeros of the bracketing function

$$a = \langle\Phi|H - z \cdot I|\Psi\rangle = \langle\Phi|H|\Psi\rangle - z \tag{1.72}$$

where by enforcing the solution to the manifold of eigenvalue solutions and choice of scalar $Z = E$, it yields the exact eigenenergies of the implicit energy formula and, in analogy to MBPT, may be expanded through n-th order

$$E^n - E^{n-1}\langle H\rangle_c - E^{n-2}\langle H^2\rangle_c - \cdots - E\langle H^{n-1}\rangle_c - \langle H^n\rangle_c = 0 \tag{1.73}$$

yielding, equivalently, Hartee-Fock as the zeroth order energy

$$E = \langle H\rangle_c \equiv E = \langle H\rangle \tag{1.74}$$

and, as before invoking the normal-ordered set of Hamiltonian operators to yield directly the correlation energy and omitting the zero-valued vacuum expectation term

$$\Delta E^n - \Delta E^{n-2}\langle H_{\rm N}^2\rangle_c - \cdots - \Delta E\langle H_{\rm N}^{n-1}\rangle_c - \langle H_{\rm N}^n\rangle_c = 0 \tag{1.75}$$

The connected moments are also invoked in the Horn-Weinstein approach to energies, which makes use of the spectral resolution of a time-dependent reference function[40]

$$|\Phi(t)\rangle = \frac{e^{-tH/2}\,|\Phi\rangle}{\langle\Phi|e^{-tH}|\Phi\rangle^{1/2}} \tag{1.76}$$

where t is a positive constant and uses any approximate ground state wavefunction such that it may always be improved at the $t \to \infty$ limit and will always approach the true ground state of the system. The energy of such a state[70, 71],

$$E(t) = \langle\psi(t)|H|\psi(t)\rangle = \frac{\langle\phi|He^{-tH}|\phi\rangle}{\langle\phi|e^{-tH}|\phi\rangle} \tag{1.77}$$

as will be elaborated on in Chapter 2, constructs from this denominator the raw moments

$$\langle\Phi|e^{-tH}|\Phi\rangle = \sum_{j=0}^{\infty}\frac{(-t)^j}{j!}\,\langle H^j\rangle \tag{1.78}$$

and its logarithmic derivative yields an extensive quantity based on the connected moments of the Hamiltonian, commonly referred to as the Connected Moment Expansion (CMX) methodology and several variants[72–74]. While much less popular than its cousins, these various moments-based methodologies may allow the exact wavefunction to always be achieved for any reference $|\phi\rangle$ (given $\langle\phi|\Psi\rangle \neq 0$) by the application of infinite Hamiltonian operators: By Löwdin's geometric term and by Horn-Weinstein's exponential term. These serve as the basis of expanding the wave operator towards the exact energy where connected moments inherited by the functional form $(\Delta E - Q\hat{H}_N)^{-1}|0\rangle$ are doing all the work in approximating the Hilbert space, but now simply as an implicit definition.

1.3 Magnetic Properties

While energies of various states play a key component throughout all of chemistry, the analysis of spectra is also a valuable tool to the general scientist; among them, the response of a system to the application of the electromagnetic field allows a strongly resolved spectra that has roles in identifying constituent material throughout the chemical and low-energy physical sciences[75, 76]. The set of forces from these fields are still incorporated purely in the electromagnetic force, so while our general approach as above is still valid, the construction of the Hamiltonian now under the effects of an external applied field and the natural internal field of the system's response requires some adaptation[77–79].

The consideration of the Lorentz force imposed on a particle in the presence of an external field in the classical picture

$$\vec{F}(\vec{r},t) = q(\vec{E}(\vec{r},t) + \vec{v}\vec{B}(\vec{r},t)) \tag{1.79}$$

where $\vec{E}(\vec{r},t)$ is the electric field, $\vec{B}(\vec{r},t)$ the magnetic field, and $\vec{v}$ its velocity allows us to establish the effect of Maxwell's laws on our system of interest. Two convenient quantities to work with in the framework of static fields are the scalar potential and vector potential associated with the electric and magnetic field, respectively

$$\phi(\vec{r}) = -\vec{r}\cdot\vec{E} \tag{1.80}$$

$$\vec{A}(\vec{r}) = \frac{1}{2}\vec{B}\times\vec{r} \tag{1.81}$$

which by their definitions are not uniquely defined with respect to their related fields; thus, introducing a simultaneous gauge transformation, which we know must necessarily not effect the physical reality of the field for which any of the set of solutions describe; we may infer that there must be a form invariance with respect to such an arbitrary transformation. While this may be done explicitly via the Dirac equation and the special relativistic considerations applicable[22], the most common route is to take the approximation of the small component. The relativistic term in one of the two components of the Dirac equation may be back-substituted into the other and, knowing that $m_e c^2 >> E + e\hat{\phi}(\vec{r})$, keep only the first term and approximate[80]:

$$\frac{c^2}{E + e\hat{\phi}(\vec{r}) + m_e c^2} = \frac{1}{2m_e}\left(1 - \frac{E + e\hat{\phi}(\vec{r})}{2m_e c^2}\right) \tag{1.82}$$

obtaining a much simpler route in the non-relativistic limit that persists in most of chemistry from the full Hamiltonian of a system under a magnetic field.

1.3.1 Molecules under a Magnetic Field

The magnetic properties of molecules allow us to probe them at the atomic scale, allowing for a broad range of applications: from development of new materials, to the very diagnostics used in medicine. To describe this process, we introduce the canonical momentum

that alters the mechanical momentum of the field-free particles under the minimal coupling approximation:

$$\hat{\pi}_i = (-i\nabla - e\mathbf{A} + \sum_k e\mathbf{A}_k)^2 \tag{1.83}$$

where we have the typical momentum, the vector potential introduced by the field directly, and now including the vector potential as introduced by Ramsey in the limit that the typical Lamb diamagnetic theory[81] needed correction related to the induced magnetic moments of the nuclear centers k

$$\mathbf{A}_k(\mathbf{r}) = \alpha^2 \sum_k \frac{\mathbf{M}_k \times (\mathbf{r} - \mathbf{r}_k)}{|\mathbf{r} - \mathbf{r}_k|^3} \tag{1.84}$$

The Hamiltonian with explicit dependence on the external magnetic field and nuclear magnetic moment may then be expanded by considering the terms introduced by this canonical momentum in the Hamiltonian, considerably expanding the terms at hand

$$\begin{aligned}
\hat{H} = &\frac{1}{8}\big(\mathbf{B}^2\mathbf{r}_i^2 - (\mathbf{B}\cdot\mathbf{r}_i^2)\big) + \frac{1}{2}\sum_i^n \boldsymbol{B}\cdot\boldsymbol{L}_i + \alpha^2 \sum_i^n \sum_K^N \frac{\boldsymbol{m}_K \cdot \boldsymbol{L}_{iK}}{r_{iK}^3} \\
&+ \frac{\alpha^2}{2}\sum_i^n \sum_K^N \frac{(\boldsymbol{B}\cdot\boldsymbol{m}_K)(\boldsymbol{r}_{iN}\cdot\boldsymbol{r}_{iK}) - (\boldsymbol{B}\cdot\boldsymbol{r}_{iK})(\boldsymbol{r}_{iN}\cdot\boldsymbol{m}_K)}{r_{iK}^3} \\
&+ \frac{\alpha^4}{2}\sum_i^n \sum_{KL}^N \frac{(\boldsymbol{m_K}\cdot\boldsymbol{m}_L)(\boldsymbol{r}_{iK}\cdot\boldsymbol{r}_{iL}) - (\boldsymbol{m_K}\cdot\boldsymbol{r}_{iL})(\boldsymbol{r}_{iK}\cdot\boldsymbol{m}_L)}{r_{iK}^3 r_{iL}^3} \\
&- \frac{1}{2}\sum_i^n \nabla_i^2 - \sum_i^n \sum_K^N \frac{Z_K}{|\mathbf{r}_{iK}|} + \sum_{i<j} \frac{1}{|\mathbf{r}_i - \mathbf{r}_j|}
\end{aligned} \tag{1.85}$$

Indices i, j refer to electrons, K, L refers to nuclei, the angular momentum operator of electron j around nucleus K is $\boldsymbol{L}_{jK} = -i\mathbf{r}_K \times \nabla_j$, and α is the fine structure constant. These terms may be put into a physical picture by decomposing the product in the canonical momentum[82]:

1. The first term, the diamagnetic magnetizability (DM), is a direct result of the squared external field;

2. The second, the paramagnetic shielding (PS), is a direct coupling of the external field to the electronic motion;

3. the third is the paramagnetic spin-orbit (PSO) and couples the induced field from the magnetic moments of the nuclei with the electronic motion;

4. the fourth is the diamagnetic shielding (DS) coupling the external field to the induced field of the magnetic moments;

5. and finally the fifth new term is the diamagnetic spin-orbit (DSO) coupling the induced fields of the magnetic moments between different nuclear centers K and I.

The remaining terms are, as in the beginning of the chapter, the explicit terms due to the motion and Coulombic forces in the electronic Hamiltonian. While this is rather more complicated in form than the traditional approach, the terms introduced at the non-relativistic level do not require any two-electron interactions, just an expanded set of nuclear-electron terms related to the (both external and internal) field and field gradients of the first kind introduced by the new canonical momentum[83]. These terms are often coupled relative to their order in perturbation theory; the one-electron terms linear in the perturbation are referred to as $H^{[1]}$, while terms quadratic are likewise termed $H^{[2]}$.

1.3.2 Yielding Magnetic Properties

The changes in energy with respect to the field yield a plethora of information that give experimentalists useful information. Limited to second-order properties, the quantities of interest that may be described as various derivatives with respect to this Hamiltonian's energy are:[82, 84]

1. The magnetizabilities (also known as magnetic susceptibilities) are the magnetic equivalent of the susceptibility of a molecule to an electric field. A smaller magnetizability is associated with a smaller resistance to the effects of a field. Trivially, a system with no magnetizability is neither repelled by nor attracted to an external field. Only the DM and PS term contributes to the derivative:

$$E^{(2)}(\mathbf{B}) = \left.\frac{\partial^2 E(\mathbf{B})}{\partial B_\alpha \partial B_\beta}\right|_{B_\alpha=0, B_\beta=0} \tag{1.86}$$

2. The nuclear shieldings (also known as the chemical shift) are the changes associated with the presence the electrons have on the effective field felt at each nuclear center K. A smaller nuclear shielding is indicative of a lesser deviation away from the Lamb shift. A deshielding may occur, in which the effective force felt is actually more than predicted by the nuclear Zeeman term. The PS, DS, and PSO terms all contribute:

$$E^{(1)}(\mathbf{B}, \mathbf{M}_k) = \left.\frac{\partial^2 E(\mathbf{B}, \mathbf{M}_k)}{\partial B_\alpha \partial M_{k\beta}}\right|_{B_\alpha=0, M_{k\beta}=0} \tag{1.87}$$

where indices α and β are cartesian components with respect to spatial orientation. In passing, we note that additional terms related to the interaction of nuclear spin with the above concepts introduces the Fermi-Contact, Paramagnetic Spin-Orbit, and Spin-Dipole contributions which, alongside DSO[85], contribute to the scalar couplings (also known as the spin-spin coupling) property that is outside the scope of this work.

A second aspect of the introduction of a field is that the wavefunction naturally complexifies in its presence. While in an infinite basis this presents no issue, any finite-basis methodology introduces a gauge-dependence due to the arbitrariness of the transformation. Due to this, one must account for the gauge directly in the construction of the atomic orbitals[86]. Thankfully, the first-order wavefunction with respect to the field introduces a gauge origin to the atomic orbitals $\chi(\mathbf{r})$ to the basis ω_μ, centered on nucleus N, and given as

$$\omega_\mu(\mathbf{r};\mathbf{A}_N) = \exp\left(-i\mathbf{A}_N\cdot\mathbf{r}\right)\cdot\chi(\mathbf{r}), \tag{1.88}$$

and the vector potential becomes an arbitrary linear function of the gauge origin introduced, often referred to as either the London or gauge-including atomic orbitals (GIAO). This is a sufficient condition on which to ensure properties are independent of the choice in gauge; though the atomic orbitals themselves are not (this has resulted in a shift away from historic terminology such as gauge-invariant and gauge-independent atomic orbitals)[87, 88]. With the two major roadblocks accounted for in describing the many-body electronic problem in the presence of the field, we may now seek routes to obtain these properties. Solutions for this have taken three distinct forms over the years, each with their own strengths and weaknesses

1. The sum-over-states approach[81], in which the exact magnetic wavefunction is explicitly written order-by-order and truncated, whereby the many-body state implicitly included is approximated

$$|\Psi(\mathbf{B}\rangle \approx |\Psi_0(0)\rangle + i\mathbf{B}\sum_k^a \frac{\langle\Psi_0(0)|H^{[1]}(\mathbf{B})|\Psi_k^a(0)\rangle}{E_0(0)-E_k^a(0)}\,|\Psi_k^a(0)\rangle \tag{1.89}$$

   in which we have invoked the exact single-excitation states $|\Psi_k^a\rangle$ and their eigenenergies E_k^a and have used here the first-order perturbation with respect to the magnetic field[80, 89]. In a more useful form, we may then derive the first- and second- order properties as their perturbative expansion

$$E^{(1)}(\mathbf{B}) = \langle 0|\hat{H}^{[1]}|0\rangle \tag{1.90}$$

$$E^{(2)}(\mathbf{B}) = \langle 0|\hat{H}^{[2]}|0\rangle - 2\sum_{i,a}\frac{\langle 0|\hat{H}^{[1]}|\Phi_i^a\rangle\,\langle\Phi_i^a|\hat{H}^{[1]}|0\rangle}{E_i^a - E_0} \tag{1.91}$$

   and may be now computed with knowledge of the reference function and excitation energies.

2. by invocation of the generalized Hellman-Feynman theorem[90, 91], any property that may be written as the derivative with respect to the energy of a particular methodology's wavefunction may be expanded

$$\frac{\partial E(\mathbf{B})}{\partial \mathbf{B}_\alpha} = \langle\frac{\partial\Psi(\mathbf{B})}{\partial\mathbf{B}_\alpha}|\hat{H}(\mathbf{B})|\Psi(\mathbf{B})\rangle + \langle\Psi(\mathbf{B})|\frac{\partial\hat{H}(\mathbf{B})}{\partial\mathbf{B}_\alpha}|\Psi(\mathbf{B})\rangle + \langle\Psi(\mathbf{B})|\hat{H}(\mathbf{B})|\frac{\partial\Psi(\mathbf{B})}{\partial\mathbf{B}_\alpha}\rangle \tag{1.92}$$

and successively iterated such that when the contributions from the field are small, we may make use of formal power series and the first-order and second order properties are written analytically as

$$E^{(1)}(\mathbf{B}) = \langle \Psi^0 | \hat{H}^{[1]} | \Psi^0 \rangle \tag{1.93}$$

$$E^{(2)}(\mathbf{B}) = \langle \Psi^0 | \hat{H}^{[2]} | \Psi^0 \rangle + \langle \Psi^0 | \hat{H}^{[1]} | \Psi^1(\mathbf{B}) \rangle \tag{1.94}$$

yielding a similar first-order term as in the sums-over-states expression and now may use the explicit perturbative Hamiltonian and its matrix elements for any wavefunction of interest, now through second order[92–94].

3. One may take a fully numerical approach, in which the finite-field and the full molecular magnetic Hamiltonian is explicitly applied to the field-dependent wavefunction, and then one may take finite differences as usual. While the most conceptually simple, it requires the full set of matrix elements to be computed in the complex space that the wavefunction now rests in.[95, 96]

Traditionally, the first approach has seen limited usage, as knowledge of the set of *exact* singly-excited states is often a high hurdle. The second route is by far the most common, as the nature of the matrix elements needed in the evaluation are fairly straightforward to create analytic solutions for various real-space methodologies in existence via methods such as such as the Coupled-Perturbed SCF equations, the method of Lagrange Multipliers, or the use of the Λ equations in the many-body picture. The difficulty introduced by them is limited to developmental challenges; the introduction of these analytic solutions is often tedious, and doing so efficiently (such as being able to perform on a small subset among many nuclear centers) can be an ever increasing challenge as more sophisticated methodologies arise. Among some of the newest ones, especially with no well-defined wavefunction, analytic access might be forthright impossible. As methodologies in modern development often pose excellent energetics as their first goal in a quest of speed vs. accuracy, whether this translates to successful properties is not always assured and one may find that the years-long endeavor is fruitless.

In this limit, it would be useful to evaluate many different methodologies in the framework of the third option, where limitations to extant (and often long to code) second-order properties may be hard to come by for any recent method. Testing these methods with the finite-field approach can filter out which would be worthwhile pursuing for properties. The challenge presented then is to code explicitly all the terms contributing to the magnetic Hamiltonian, while also accounting for the, now necessarily complex, wavefunctions from which we calculate. In almost an inversion, the derivatives themselves are trivial to obtain from numerical finite difference, while the creation of matrix elements serves the main challenge. However, upon doing so, any methodology implemented in complex arithmetic as outlined in the case of the complex Hartree-Fock equations and their correlated equivalents are easily accessible to evaluation. This shall be the focus of the third and fourth chapter of this text for the magnetizabilities and nuclear shieldings, respectively.

1.4 Works Outside the Scope

We often find ourselves in the unfortunate situation that the *ab initio* theories cannot readily access problems of all scales. As the magnetic properties of systems are used on the atomic, biologic, geologic, and astronomic scales, developing techniques to use this tool beyond small chemical systems is worthwhile. We here mention works contributed to by the author for the description of NMR in crystallography and biological molecule by description through use of machine-learning algorithms based on their quantum mechanical description. The full body of these works may be found in their respective citations[97, 98]

1.4.1 A Multi-Resolution 3D-DenseNet for Chemical Shift Prediction in NMR Crystallography

We have developed a deep learning algorithm for chemical shift prediction for atoms in molecular crystals that utilizes an atom-centered Gaussian density model for the 3D data representation of a molecule. We define multiple channels that describe different spatial resolutions for each atom type that utilizes cropping, pooling, and concatenation to create a multi-resolution 3D-DenseNet architecture (MR-3D-DenseNet). Because the training and testing time scale linearly with the number of samples, the MR-3D-DenseNet can exploit data augmentation that takes into account the property of rotational invariance of the chemical shifts, thereby also increasing the size of the training dataset by an order of magnitude without additional cost.

1.4.2 Efficient Calculation of NMR Shielding Constants Using Composite Method Approximations and Locally Dense Basis Sets

This paper presents a systematic study of applying composite method approximations with locally dense basis sets (LDBS) to efficiently calculate NMR shielding constants in small and medium-sized molecules. The pcSseg-n series of basis sets are shown to have similar accuracy to the pcS-n series when n $\geq$ 1 and can slightly reduce compute costs. We identify two different LDBS partition schemes that perform very effectively for density functional calculations. We select a large subset of the recent NS372 database containing 290 H, C, N, and O shielding values evaluated by reference methods on 106 molecules to carefully assess methods of the high, medium, and low compute costs to make practical recommendations. Our assessment covers conventional electronic structure methods (DFT and wavefunction) with global basis calculations, as well as their use in one of the satisfactory LDBS approaches, and a range of composite approaches, also with and without LDBS. Altogether 99 methods are evaluated. On this basis, we recommend different methods to reach three different levels of accuracy and time requirements across the four nuclei considered.

1.5 Outline

1.5.1 Chapter 2

Ab initio methods based on the second-order and higher connected moments, or cumulants, of a reference function have seen limited use in the determination of correlation energies of chemical systems throughout the years. Moment-based methods have remained unattractive relative to more ubiquitous methods, such as perturbation theory and coupled cluster theory, due in part to the intractable cost of assembling moments of high-order and poor performance of low-order expansions. Many of the traditional quantum chemical methodologies can be recast as a selective summation of perturbative contributions to their energy; using this familiar structure as a guide in selecting terms, we develop a scheme to approximate connected moments limited to double excitations. The tractable Double Connected Moments (DCM(N)) approximation is developed and tested against a multitude of common single-reference methods to determine its efficacy in the determination of the correlation energy of model systems and small molecules. The DCM(N) sequence of energies exhibits smooth convergence towards limiting values in the range of $N = 11 - 14$, with compute costs that scale as a non-iterative $O(M^6)$ with molecule size, M. Numerical tests on correlation energy recovery for 54 small molecules comprising the G1 test set in the cc-pVDZ basis show that DCM(N) strongly outperforms MP2 and even CCD with a Hartree-Fock reference. When using an approximate Brueckner reference from orbital-optimized (oo) MP2, the resulting oo:DCM(N) energies converge to values more accurate than CCSD for 49 of 54 molecules. This work is in preparation.

1.5.2 Chapter 3

Magnetic properties of molecules such as magnetizabilities represent second order derivatives of the energy with respect to external perturbations. To avoid the need for analytic second derivatives and thereby permit evaluation of the performance of methods where they are not available, a new implementation of quantum chemistry calculations in finite applied magnetic fields is reported. This implementation is employed for a collection of small molecules with the aug-cc-pVTZ basis set to assess orbital optimized (OO) MP2 and a recently proposed regularized variant of OOMP2, called κ-OOMP2. κ-OOMP2 performs significantly better than conventional second order Møller-Plesset (MP2) theory, by reducing MP2's exaggeration of electron correlation effects. As a chemical application, we revisit an old aromaticity criterion called magnetizability exaltation. In lieu of empirical tables or increment systems to generate references, we instead use straight chain molecules with the same formal bond structure as the target cyclic planar conjugated molecules. This procedure is found to be useful for qualitative analysis, yielding exaltations that are typically negative for aromatic species and positive for antiaromatic molecules. One interesting species, N_2S_2, shows a positive exaltation despite having aromatic characteristics[99].

1.5.3 Chapter 4

We developed and implemented a method-independent, fully numerical finite difference approach to calculating NMR shieldings, using gauge-including atomic orbitals. The resulting capability can be used to explore non-standard methods given only the energy as a function of finite applied magnetic fields and nuclear spins. For example, standard second order Møller-Plesset theory (MP2) has well-known efficacy for ^{1}H and ^{13}C shieldings, and known limitations for other nuclei such as ^{15}N and ^{17}O. It is therefore interesting to seek methods that offer good accuracy for ^{15}N and ^{17}O shieldings without greatly increased compute costs, as well as exploring whether such methods can further improve ^{1}H and ^{13}C shieldings. Using a small molecule test set of 28 species, we assessed two alternatives: κ regularized MP2 (κ-MP2) which provides energy-dependent damping of large amplitudes and MP2.X, which includes a variable fraction, X, of third order correlation (MP3). The aug-cc-pVTZ basis was used, and CCSD(T) results were taken as reference values. Our κ-MP2 results reveal significant improvements over MP2 for ^{13}C and ^{15}N, with the optimal κ value being element-specific. κ-MP2 with $\kappa = 2$ offers 30% RMS error reduction over MP2. For ^{15}N, κ-MP2 with $\kappa = 1.1$ provides 90% error reduction vs MP2, and 60% error reduction vs CCSD. On the other hand, MP2.X with scaling factor 0.6 outperformed CCSD for all heavy nuclei. These results can be understood as providing renormalization of doubles amplitudes to partially account for neglected triple and higher substitutions, and offer promising opportunities for future applications[100].

Chapter 2

Hamiltonian Moments

2.1 Introduction

The majority of quantum chemical methods begin from the Schrödinger equation and make approximations in an effort to efficiently find an acceptably accurate expectation value of the Hamiltonian $E = \langle\phi|H|\phi\rangle$. As the approximate wavefunction $|\phi\rangle$ approaches the exact ground state wavefunction $|\psi_0\rangle$, our approximate expectation value approaches the true energy. Fine tuning this approach takes many forms, but generally begins from a reference wavefunction such as the Hartree-Fock determinant or the antisymmetrized product of strongly orthogonal geminals, and then determining the correlation energy of the system to approach the exact energy or values that are within 'chemical accuracy' for various systems. Popular among these are methods based around some variant of perturbation theory, in which the correlation energy of the system:

$$\Delta E_{\text{exact}} = \langle 0|V_{\text{N}}|\psi_0\rangle = \sum_{m=0}^{\infty} \langle 0|V_{\text{N}}[R_0 V_{\text{N}}]^m|0\rangle \tag{2.1}$$

is expanded in a series approximation, with V_{N} being the normal-ordered perturbation operator and R_0 being a resolvent operator based on the expansion. Different partitionings and reference functions give rise to well-known perturbation series expansions[101], such as Brillouin-Wigner[102], Rayleigh-Schrödinger[103], or Møller-Plesset[104] if performed with a Hartree-Fock reference. In the latter case, the resolvent is then simply $R_0 = (F - \langle 0|F|0\rangle)^{-1}$, where F is the mean field Fock operator.

The Coupled Cluster expansion[105–108] may likewise be obtained through the use of an exponential wavefunction ansatz and its projection onto a reference and some set of substituted or excited determinants. One may also explore the Hilbert space variationally such as in the CI, CASSCF[109] and DMRG[110] schemes. What all these methods have in common is that the expectation value of the Hamiltonian is the primary quantity of interest. It is interesting to note that additional expectation values implicitly arise in many of these,

such as the variance, or second moment, of the energy:

$$\mu_2 = \langle H^2 \rangle - \langle H \rangle^2 \tag{2.2}$$

In the variational methods, the variance approaches zero as the expectation value of $\langle H \rangle$ approaches the exact energy (i.e. as $|\phi\rangle$ approaches the exact eigenstate, $|\psi\rangle_0$). The variance also becomes an important quantity in the coupled cluster equations,[111] which can be made apparent by inserting the identity in the variance expression

$$\mu_2 = \langle H(P+Q)H \rangle - \langle HPH \rangle = \langle HQH \rangle = \langle H^2 \rangle_{\rm c} \tag{2.3}$$

We use P to mean the projective subspace of the reference function and Q its orthogonal subspace such that $P+Q=I$ and $\mu_2 = \langle H^2 \rangle_{\rm c}$ to mean the second cumulant or equivalently the second connected moment of the Hamiltonian. The amplitude equations are solved using $Q\bar{H}P = 0$, where $\bar{H}$ is the similarity-transformed Hamiltonian, which results in a value of $\mu_2 = 0$ within the space, Q, within which the cluster equations are solved.

Moments play a central role in an alternate approach, the so-called t-expansion of Horn and Weinstein[112]. This approach begins from the observation that a given approximate ground state wavefunction, $|\phi\rangle$ can always be improved by defining:

$$|\psi(t)\rangle = \frac{e^{-tH/2}\,|\phi\rangle}{\langle\phi|e^{-tH}|\phi\rangle^{1/2}} \tag{2.4}$$

where t is a positive constant. This result can be readily proven by expanding $|\psi(t)\rangle$ in terms of the exact eigenstates, or one can recognize that Eq. 2.4 corresponds to propagating $|\phi\rangle$ in imaginary time for duration $t/2$. Indeed $|\psi(t)\rangle$ becomes the exact wavefunction in the limit as $t \to \infty$. The imaginary time evolution is routinely treated in various flavors of Quantum Monte Carlo (QMC)[113–115] which map this procedure onto stochastic processes to recover better approximations to a trial reference[116, 117]. Deterministically, the energy associated with $|\psi(t)\rangle$ is:

$$E(t) = \langle\psi(t)|H|\psi(t)\rangle = \frac{\langle\phi|He^{-tH}|\phi\rangle}{\langle\phi|e^{-tH}|\phi\rangle} = -\frac{Z'(t)}{Z(t)} \tag{2.5}$$

Here $Z(t)$ is a Maclaurin series containing expectation values of powers of the Hamiltonian operator, $\langle H^j \rangle = \langle\phi|H^j|\phi\rangle$:

$$Z(t) = \langle\phi|e^{-tH}|\phi\rangle = \sum_{j=0}^{\infty} \frac{(-t)^j}{j!} \langle H^j \rangle \tag{2.6}$$

$Z'(t)$ is defined as:

$$Z'(t) = \frac{dZ(t)}{dt} = -\sum_{j=0}^{\infty} \frac{(-t)^j}{j!} \langle H^{j+1} \rangle \tag{2.7}$$

Thus the expression for $E(t)$ above is the logarithmic derivative of $Z(t)$. The result for the energy can be generalized to other operators, O, to yield an expression for $O(t)$ which is likewise exact in the limit as $t \to \infty$.[112]

The promise of the t-expansion is that for an arbitrary reference $|\phi\rangle$ satisfying $\langle\phi|\Psi\rangle \neq 0$, the exact energy cannot only be approached by the conventional variational approach of treating $\langle H\rangle$ as accurately as possible by improving the trial function, $|\phi\rangle$. Instead, exactness can also be attained by deriving an energy expression in terms of coefficients, μ_j that involve powers of the Hamiltonian, evaluated with a fixed approximate wavefunction:

$$E(t) = \sum_{j=0}^{\infty} \frac{(-t)^j}{j!} \mu_{j+1} \tag{2.8}$$

Simple powers of the Hamiltonian, $\langle H^j\rangle$, scale as powers of the system volume, V^j, whilst of course the energy is linear in the volume (extensive). Thus the coefficients, μ_j that enter the expansion above, defined by the negative quotient of the two power series, $Z'(t)$ and $Z(t)$, must also scale linearly in the volume. These μ_j coefficients are the *connected moments*, $\mu_j = \langle H^j\rangle_c$, which may be defined in the diagrammatic sense of connectedness, or equivalently by evaluating the power series quotient to obtain the c_j term by term. Thus $\mu_1 = \langle H\rangle$, $\mu_2 = \langle H^2\rangle - \langle H\rangle^2$, $\mu_3 = \langle H^3\rangle - \langle H\rangle\langle H^2\rangle - \langle H^2\rangle_c \langle H\rangle$, etc, and in general:

$$\mu_j \equiv \langle H^j\rangle_c = \langle H^j\rangle - \sum_{k=0}^{j-1} \binom{j}{k} \mu_{k+1} \langle H^{j-k}\rangle \tag{2.9}$$

Turning the t-expansion into a practical computational method is a non-trivial challenge. Creating regular expressions for this series has resulted in various extrapolations[118, 119]. At low order, amongst the most promising of these is the Connected Moment Expansion (CMX)[120, 121]. A useful form of the CMX can obtained by presuming that an N^{th} order approximation to $E(t)$, Eq. 2.8, can be expressed as a sum of $(N-1)$ decaying exponentials, $A_i e^{-b_i t}$, and obtaining the coefficients by matching low order terms in the power series expansions.[121] In the resulting CMX models, an N^{th} order approximation, CMX(N) to the ground state energy may be succinctly written[121] in terms of the lowest $2N-1$ connected moments, and the inverse of an $(N-1)\times(N-1)$ matrix constructed from those moments:

$$E^{(N)} = \mu_1 - \begin{bmatrix}\mu_2 & \mu_3 & \cdots & \mu_N\end{bmatrix} \begin{bmatrix} \mu_3 & \mu_4 & \cdots & \mu_{N+1} \\ \mu_4 & \mu_5 & \cdots & \mu_{N+2} \\ \vdots & \vdots & \ddots & \vdots \\ \mu_{N+1} & \mu_{N+2} & \cdots & \mu_{2N-1} \end{bmatrix}^{-1} \begin{bmatrix}\mu_2 \\ \mu_3 \\ \vdots \\ \mu_N\end{bmatrix} \tag{2.10}$$

In particular, CMX(1) is simply the energy of the reference (i.e. μ_1), and the two lowest order corrections to the reference energy, CMX(2) and CMX(3), have energies defined as

$$E_{\text{CMX(2)}} = \mu_1 - \frac{\mu_2^2}{\mu_3} \tag{2.11}$$

and

$$E_{\mathrm{CMX}(3)} = \mu_1 - \frac{\mu_2^2}{\mu_3} - \frac{\mu_3(\mu_4\mu_2 - \mu_3^2)}{\mu_5\mu_3 - \mu_4^2} \tag{2.12}$$

respectively. CMX(4) requires moments up to μ_7 and the inverse of a 3×3 moment matrix. Several variants[122, 123] have also been developed to help rid the original expansion of singularities, and combine the terms in different combinations.

The t-expansion is not the only place these connected moments have been the central quantity in determining the energy. Löwdin's implicit energy formula[68]

$$1 = \langle\Phi|H(E - PH)^{-1}|\Phi\rangle \tag{2.13}$$

may be expanded[124] using the identity

$$(\hat{A} - \hat{B})^{-1} = \hat{A}^{-1} + \hat{A}^{-1}\hat{B}(\hat{A} + \hat{B})^{-1} \tag{2.14}$$

to obtain an approximate expression for the roots of the energy:

$$E^{(N)} = \mu_1 E^{(N-1)} + \mu_2 E^{(N-2)} + \cdots + \mu_{(N-1)} E^{(1)} + \mu_N \tag{2.15}$$

This set of equations requires the N lowest connected moments to evaluate the N^{th}-order approximation to the energy in the denominator-free perturbation theory.[124]. At second order the result is $E^{(2)} = \mu_1 + (\mu_2)^2/\mu_1$. If one optimizes the constant energy denominator associated with the first order wavefunction, the CMX(2) result is recovered at second order, with the third order correction going to zero.

The CMX-based moments approaches and alternatives have been investigated across both model [119, 125–135] and real [123, 125, 130, 136–140] systems in lattice gauge theory, quantum chromodynamics, and quantum chemistry, which has been well reviewed by Amore[141]. The convergence and analytic behaviors of these methods have been the focus of several studies in the literature and their strengths and limitations have been well evaluated[130, 136, 142–145]. Focusing on the problem of the correlation energy of molecular systems, moment-based methods have remained a niche topic of research relative to standard coupled cluster or many-body approaches based on the Schrödinger equation, with only a small catalogue of papers using moments-based methods for electronic structure[121, 124, 132, 146–148]. Of particular note is the Method of Moments Coupled Cluster (MMCC) approach[149, 150], which acknowledges that the exact energy may be retrieved from any Coupled Cluster reference with energy E_{CC} via the formalism of β-nested equations by projecting onto the asymmetric energy expression

$$\delta E = E - E_{CC} = \frac{\langle\Psi_0|(H - E_{CC})e^T|0\rangle}{\langle\Psi_0|e^T|0\rangle} \tag{2.16}$$

This forms an approximate hierarchy of non-iterative corrections yielded through better approximations to $|\Psi_0\rangle$ by including terms related to the excitation space neglected in the Coupled Cluster amplitudes, but are extant in the general moment contributions to the

exact energy[151]. For example, use of a CCSD wavefunction in MMCC requires only up to hextuply-excited configurations; while the triple excitations and higher do not factor into the amplitude equations and/or second moment, they do survive in the exact representation of Equation 2.16.

One reason for this is the cost to assemble these connected moments and the order to which one needs them to approach quantitative accuracy. Early correlation energy studies[121, 152] compared the lowest order CMX expansions to the similar Møller-Plesset series. In weakly correlated systems, the CMX(2) underperforms MP2 both in terms of energy whilst requiring greater computational costs. Assembling μ_3 requires $O(N^6)$ tensor contractions, which is the most costly step in the evaluation of CMX(2) with a Hartree-Fock reference. In fact, CMX(2) is fully equivalent to the Unsöld approximation to MP2[124], which helps explain this underperformance in the weakly-correlated region. Despite this quantitative failure, some successes have been reported in the strongly-correlated regions of bond breaking, where many traditional single-reference quantum chemical methods break down or become prohibitive in cost and the Unsöld approximation does not diverge, unlike the traditional MP2 approximation. Going to the next order, CMX(3) requires the assembly of μ_5, requiring $O(N^8)$ operations which is already cost-prohibitive for molecules of medium-size (the same scaling as full CCSDT, for example). We also note that there has been recent interest in the connected moments as an approach for performing molecular electronic structure calculations on quantum computers.[153, 154]

Efforts to truncate the many-body expansion of the Full CI (FCI) problem in a computationally tractable way has led to many different ansatze to approximate the ground-state energy of the system. The most successful quantum chemical approaches typically cover subset of the FCI expansion. An order-by-order truncation in the fluctuation parameter results in the regular MP(n) expressions, but more sophisticated summations are possible. RPA, for example, is equivalent to an infinite sum over the ring diagrams in the perturbation expansion[155]. Infinite-order resummations of the perturbative terms also result in various coupled cluster methodologies. The MBPT series summed over all possible doubly excited states, DMBPT(∞)[156], is formally equivalent to CEPA(0)[157] and linearized CCD[158]. This perturbative analysis[159] holds true for various CC expansions[160, 161] as well, with a notable example being CCSD(T)[162, 163] as all connected singles and doubles to infinite-order, as well as triples through fourth-order with a perturbative fifth-order correction of the triple's contribution to the single's amplitudes[164]. Several approximations reliant on removing terms in the series have arisen and has been well reviewed recently[165].

Despite the success of these selective summations in perturbation theory, no comparable scheme has been reported in approximating connected moments for use in the CMX-based methodologies reliant on their use. Keeping in mind what has been successful in the perturbative case, we report a methodology to approximate the connected moments using a selective summation constrained to the doubly-excited manifold and apply these approximate connected moments in place of their vastly more expensive exact counterparts. We design a recursive algorithm to construct approximated connected moments, and use these terms to assess the validity in their use for approximating correlation energies across a range

of small molecules and report stable results up through twentieth order in the CMX expansion.

2.2 The Doubles Connected Moment Approximation

To begin evaluating finite-order CMX approximations we must specify a reference from which to construct the connected moments. In this work, we shall take both the Hartree-Fock determinant, $|\phi\rangle = |\Phi_{HF}\rangle$, and the SCF reference generated via orbital optimized (OO) MP2 orbital optimization,[166–168] $|\phi\rangle = |\Phi_{OOMP2}\rangle$ as our zeroth-order wavefunctions. The latter is a simple approximation to the exact Brueckner determinant which is best single reference.[169, 170] Use of only the occupied molecular orbitals in the reference serves us both as a simple model from which to understand the behavior of approximate moment methods in relation to traditional single-reference methodologies as well as providing a unified scheme from which we may generate approximate connected moments. Unlike in the case of CCSD, in which we expect the typical orbital insensitivity owed to the Thouless theorem[118], DCM(N) does not have the orbital relaxation effects associated with singles, so meaningful energy changes may be expected when we change reference. DCM(N) also benefits from the fact that the (exact) Brueckner determinant maximizes overlap between the reference and exact wavefunctions. The convergence of the CMX series relies on that overlap and a closer starting determinant should therefore more rapidly approach the true expectation value.[135]

We can then define $\hat{H}_{\mathrm{N}} = \hat{H} - E_0$ (note that all connected moments above μ_1 are invariant to adding a constant to $\hat{H}$) using the expectation value of the determinant, E_0, as the reference result in the CMX(1) energy. It may be beneficial to discuss the nature of the low-order canonical-orbital case qualitatively before developing the general semi-canonical all-order expressions. Going further in the series, one can construct[152]

$$\mu_2 = \langle H_{\mathrm{N}}^2 \rangle_c = \langle 0 | H_{\mathrm{N}} Q H_{\mathrm{N}} | 0 \rangle = \frac{1}{4} \sum_{ijab} \langle ij||ab\rangle \langle ab||ij\rangle \tag{2.17}$$

as the second-order connected moment for the canonical orbitals, with $\langle ij||ab\rangle$ being the anti-symmetrized two-electron matrix elements in standard notation.[35]. In particular, double substitutions from occupied orbitals $i, j, k, \cdots$ to virtual orbitals $a, b, c, \cdots$ are the only part of Q that makes non-zero contributions to μ_2 in Hartree-Fock. The next moment, μ_3 also involves only contributions from double substitutions in the cannonical case leading to:[152]

$$\begin{aligned} \mu_3 = \langle H^3 \rangle_c = &\sum_{ijabcd} \frac{1}{8} \langle ij||ab\rangle \langle ab||cd\rangle \langle cd||ij\rangle + \sum_{ijklab} \frac{1}{8} \langle ij||ab\rangle \langle ij||kl\rangle \langle kl||ab\rangle \\ &- \sum_{ijkabc} \langle ij||ab\rangle \langle kb||ic\rangle \langle kj||ac\rangle - \sum_{ijab} \frac{1}{4} |\langle ij||ab\rangle|^2 \Delta_{ij}^{ab} \end{aligned} \tag{2.18}$$

where $\Delta_{ij}^{ab} = \epsilon_i + \epsilon_j - \epsilon_a - \epsilon_b$ are the orbital eigenenergy differences; these one-particle terms are now in the numerator of just the final term, in contrast to their position in the denominator

for all terms in perturbation theory. This presents an exclusively doubles theory in the construction of the CMX(2) energy. The higher-order moments may be evaluated via the same scheme, and of course increasingly large subspaces of Q begin to make contributions in the exact case. Specifically, while $H_N |\Phi_0\rangle$ contains up to double substitutions, $H_N H_N |\Phi_0\rangle$ contains single, double, triple and quadruple substitutions (S,D,T,Q). Therefore, like the MP4 energy, μ_4 also contains S,D,T,Q contributions and requires $\mathcal{O}(N^7)$ compute effort. In addition, μ_4 contains one 'MP2-like' term with two Fock operators and three 'MP3-like' terms with a single Fock operator after combining the complex-conjugate cases.

Similar to MP5, μ_5 requires $\mathcal{O}(N^8)$ computational effort to evaluate 9 classes of terms (SS, SD, ST, DD, DT, DQ, TT, TQ, QQ), plus the set of Δ-containing terms, to enable construction of the CMX(3) energy via Eq. 2.12. Higher terms require yet greater computational effort, analogous to the corresponding Møller-Plesset energy terms[159, 171], but without orbital energy difference denominators. With the system-scaling increasing by one power per order of CMX, and the number of distinct terms or diagrams exploding, it is clear that while direct implementation of CMX(3) is challenging, CMX(4) which requires μ_7, is essentially prohibitive.

Clearly there is a strong resemblance between the connected moments, $\mu_j = \langle H^j \rangle_c = \langle 0|H_\mathrm{N}[QH_\mathrm{N}]^j|0\rangle$ and the corresponding j^th order Møller-Plesset energy, $E^j = \langle 0|V_\mathrm{N}[R_0 V_\mathrm{N}]^j|0\rangle$, as each involves the same power of the fluctuation potential. There are also key differences. The most obvious distinction is the lack of the resolvent R_0 operator in μ_j, which instead features a projection operator, Q, onto the orthogonal space. This eliminates Møller-Plesset energy eigenvalue denominators from the moments expressions. Another difference is that in the moments approach, there was no determination of a small parameter, unlike the perturbative case. This may help avoid perturbation theory breakdowns. When the HF reference is used, this results in moments expression where some terms include Δ-dependence in the numerator, as seen in Eq. 2.18. We note the advantage of additive separability of the Δ-containing moment numerator terms compared to the perturbation theory energy denominators. Instead of $(j-1)$ Δ^{-1} in all terms of the j^th order energy, there are terms containing up to Δ^{j-2} in the j^th connected moment.

Diagonal Fock components are typically the dominant numeric value in the evaluation of $\langle \Phi_{ij}^{ab}|H_\mathrm{N}|\Phi_{kl}^{cd}\rangle$. This fact is also why MP2 recovers most of the correlation energy in weakly correlated (large orbital gap) systems. In such systems, because the gap is large, so too is $\left|\Delta_{ij}^{ab}\right|_\infty$, and therefore the doubles amplitudes are small relative to one: $|R_0 V_\mathrm{N}|0\rangle|_\infty << 1$. Letting the largest doubles amplitude have magnitude $t_\mathrm{max} << 1$, we then expect the magnitude of the MP3 energy to be smaller than MP2 by roughly this same factor because it involves one more power of $R_0 V_\mathrm{N}$. For MP4, the connected triples and quadruples give rise to larger eigenenergy differences such as Δ_{ijk}^{abc} and Δ_{ijkl}^{abcd} which is compounded with the presence of one more power of $R_0 V_\mathrm{N}$ in the MP4 energy. Connected doubles tend to dominate in single-reference cases which is one of the strengths of the CC methods, as its most basic form functions as a resummation of these terms through infinite order. Heuristically, the energetic contributions of the singles and triples cancels against the quadruples, contributing another advantage that has led to the success of even low-order perturbation theory and

methods constrained to only doubles.

We shall now introduce the approximations to the construction of the various higher-order moments by exploiting these very same arguments, likewise considering the single-determinant case. In this instance, the dominant terms in μ_3 ought to be the MP2-like term mentioned above. In μ_4, the MP2-like term scaling as $|\Delta_{ij}^{ab}|^2$ is roughly an order of magnitude larger than the MP3-like terms scaling as Δ_{ij}^{ab}, and so forth. Though we lack the benefit of inverse energy difference decay, we see that at each N-th order cumulant, the largest expected term is always contained in the connected doubles, keeping the comparison to PT relevant. Going outside the single reference case, these terms may cease to be the largest. However, unlike in Møller-Plesset where near degeneracies cause a singularity in the equations, the terms do not diverge in the connected moments and merely tend towards zero. This leaves the dominant small-gap terms as those containing no Fock operators. This suggests that evaluating the connected moments within just the subspace of doubles would be a worthwhile venture just as it has been in the case of CC and PT theory.

In the case of semicanonical orbitals, the exact μ_2 includes an additional term corresponding to a sum over the Fock contributions from non-Brillouin singles, $|f_i^a|^2$, yet ameliorated in magnitude by their approximate Brueckner-like nature. Non-Hartree-Fock reference determinants would have these singles contributions neglected in such an approximation, which otherwise would only begin formally at μ_4. Similar use of these orbitals in work on perturbation theory had found that approximations neglecting these singles contributions at third-order are sufficient in the construction of low-order energies. As the CMX matrix equation is of a more complex form than the sum, we desire to keep an even-tempered approach to the description of the Hilbert space at each level of the moments. Thus, we retain only doubles even at low-order in this description of both the canonical and semi-canonical case of our equations.

The doubles approximation to the connected moments will be defined by replacing the resolution $(P+Q)$ by $(P+D)$ where D is the doubles subspace of the orthogonal Hilbert space: $D = \frac{1}{4}\sum_{ijab} |\Phi_{ij}^{ab}\rangle \langle\Phi_{ij}^{ab}|$. In analogy to DMBPT($\infty$) and LCCD, we can begin by defining the intermediate integral tensors and now incorporating off-diagonal elements of the doubles:

$$(ij||ab)_1 = \langle ij||ab\rangle \tag{2.19}$$

and

$$\begin{aligned}(ij||ab)_2 =& \frac{1}{4}\sum_{kl} \langle ij||kl\rangle \langle kl||ab\rangle + \frac{1}{4}\sum_{cd} \langle ij||cd\rangle \langle cd||ab\rangle \\ &- \sum_{kc} \langle ik||cb\rangle \langle jc||ka\rangle - \sum_{k} P(ij) \langle ik||ab\rangle f_{kj} + \sum_{c} P(ab) \langle ij||ac\rangle f_{bc}\end{aligned} \tag{2.20}$$

Here $P(pq)$ is the standard anti-symmeterizer function for electrons p and q, $(ij||ab)_1$ is identical to a raw anti-symmeterized two-electron integral and the terms in $(ij||ab)_2$ comprise the hole ladder, particle ladder, ring term, and the 'MP2-like' delta terms of μ_3 respectively,

which takes the form of $-\langle ij||ab\rangle\,\Delta_{ij}^{ab}$ in the Hartree-Fock case. From here, we may generate the 20 skeletal diagrams contributing to the μ_4 doubles: 16 reminiscent of the doubles contribution to MP4, as well as three MP3 like terms with a single Fock contribution and one MP2 like term with two Fock contributions by a simple recursion:

$$\begin{aligned}(ij||ab)_{n+1} = &\frac{1}{2}\sum_{cd}\langle cd||ab\rangle\,(ij||cd)_n + \frac{1}{2}\sum_{kl}\langle kl||ij\rangle\,(kl||ab)_n \\ &- \sum_{k} P(ij)(ik||ab)_n f_{kj} + \sum_{c} P(ab)(ij||ac)_n f_{bc} \\ &+ \sum_{kc}\big[\,\langle kb||jc\rangle\,(ik||ca)_n - \langle jc||ka\rangle\,(ik||cb)_n \\ &- \langle kb||ic\rangle\,(jk||ca)_n + \langle ka||ic\rangle\,(jk||cb)_n\big]\end{aligned} \tag{2.21}$$

All terms of higher order may be generated directly from the previous intermediate. Simple contraction of these intermediates results in the doubles approximation to the connected moments (DCM):

$$\mu_{2n-1}^{D} = \sum_{ijab}(ij||ab)_n(ij||ab)_{n-1} \tag{2.22}$$

and

$$\mu_{2n}^{D} = \sum_{ijab}|(ij||ab)_n|^2 \tag{2.23}$$

Like LCCD or DMBPT(∞) or even CCD and CCSD, the limiting step in the formulation of the intermediates is the $\mathcal{O}(o^2v^4)$ particle ladder contraction, similar to the MP3 energy or the CCD/CCSD amplitudes equation. However, unlike CCD/CCSD, this does not require solving a non-linear set of equations and, outside of the recursion, no iterations for the determination of amplitudes or energies are needed in the formation of the intermediates. One may then use the values of the approximate moments μ_{2n-1}^{D} in place of the exact μ_{2n-1} to yield the DCM(N) approximations to the full CMX(N) model.

2.3 Implementation

The code necessary to form $(ij||ab)_{n+1}$, and therefore the necessary doubles connected moments, $\mu_{2n-1}^{D}, \mu_{2n}^{D}$ was implemented in a development version of the Q-Chem quantum chemistry program,[172, 173] which has also been used to carry out the all-electron calculations for each methodology in the following examples. Two other important aspects of the implementation should be mentioned.

First, unlike in the PT case, higher-order moments do not generally shrink in value except in the (rather pointless) case of an exact reference function, for which the second order and

higher connected moments all evaluate to zero. However, μ_k has dimensionality E^k and is dominated by terms with $(\Delta_{ij}^{ab})^{k-1}$. The largest value whose largest value of (Δ_{ij}^{ab}) is:

$$\Delta_{\max} = \max_{ijab} \Delta_{ij}^{ab} \tag{2.24}$$

We then redefine the energy scale such that $E' = E/\Delta_{\max}$ to keep the moments from exploding in value. In turn the scaled energy can be rescaled after the CMX algorithm is applied to obtain the final DCM(N) energy.

Second, we do not explicitly invert the $(N-1)\times(N-1)$ matrix of moments that enters Eq. 2.10. Rather we solve a set of linear equations:

$$\begin{bmatrix} \mu_3 & \mu_4 & \cdots & \mu_{N+1} \\ \mu_4 & \mu_5 & \cdots & \mu_{N+2} \\ \vdots & \vdots & \ddots & \vdots \\ \mu_{N+1} & \mu_{N+2} & \cdots & \mu_{2N-1} \end{bmatrix} \begin{bmatrix} \zeta_2 \\ \zeta_3 \\ \vdots \\ \zeta_N \end{bmatrix} = \begin{bmatrix} \mu_2 \\ \mu_3 \\ \vdots \\ \mu_N \end{bmatrix} \tag{2.25}$$

and then evaluate:

$$E^{(N)} = \mu_1 - \begin{bmatrix} \mu_2 & \mu_3 & \cdots & \mu_N \end{bmatrix} \begin{bmatrix} \zeta_2 \\ \zeta_3 \\ \vdots \\ \zeta_N \end{bmatrix} \tag{2.26}$$

This improves numerical stability in the case where the coefficient matrix may be near singular.

Having discussed the necessity of scaling, we next present some specific data for the water example. As a reference point, the unscaled approximate moments from μ_4 to μ_{39} span a range of over 57 orders of magnitude! For various scaling factors, we show both the logarithm of the scaled range of the approximate DCM(N) moments and the energy differences (in μH) between calculated DCM(N) energies using different rescalings in Table 2.1.

The range of magnitudes of the scaled connected moments is very satisfactory ($< 10^4$) for all scalings considered. We focus on the behavior of the the highest-order DCM(N) energies for different scaling factors multiplied by $\Delta_{\max}^{-1}$, from 0.85 to 1.25 and compared against the value of 1.1. Even including the unscaled approach, all energies through DCM(5) are the same within machine precision, while this is true of all scaled moment approaches tested here through DCM(11). The fact that the higher order DCM(N) energies show differences of $\mathcal{O}(10^0 - 10^2)$ μH suggests that solving the linear equations, Eqs. 2.25 may involve some ill-conditioning even in scaled energy units.

Based on the data presented in Table 2.1, as well as tests on other members of the G1 data set, we decided to employ a scaling factor of $1.1\Delta_{\max}^{-1}$ in the moment generating procedure, followed by multiplying its reciprocal value back to the DCM(N) energy in order to re-scale back to atomic units.

Method	Scaling Factor							
	0.85	0.90	0.95	1.00	1.05	1.15	1.20	1.25
DCM(14)	119.5	127.9	-6.0	-6.0	-4.4	-0.4	0.8	1.0
DCM(15)	138.6	-12.5	-8.8	-6.8	-3.6	2.7	5.7	10.1
DCM(16)	-25.2	-20.5	-15.6	-10.7	-5.5	5.6	12.0	18.1
DCM(17)	35.0	42.2	49.9	58.1	-3.2	1.7	4.9	9.0
DCM(18)	38.2	49.1	-11.8	-8.3	-4.6	2.7	7.3	10.5
DCM(19)	47.1	63.4	-13.2	-9.3	-5.0	4.5	9.0	13.8
DCM(20)	59.8	-20.6	-15.4	-10.7	-5.3	5.6	11.1	15.5
Log Range	3.66	2.80	1.97	1.19	0.52	1.18	1.78	2.36

Logarithmic Range of 1.1 is 0.57

Table 2.1: Difference in energies (in μH) and Logarithmic Range of Approximate Moments by Scaling Factor on top of $\Delta_{\max}^{-1}$. Energies are relative to 1.1

2.4 Results and Discussion

2.4.1 G1 Test Set

We shall address the accuracy of the DCM method for a wide range of small molecules as a measure of its usefulness for the description of chemical systems. Towards this end, we compare the energies of CMX(2), DCM(N), MP2, CCD, CCSD, and CCSD(T) against ASCI+PT2 with a cc-pVDZ basis across 54 systems contained in the first-row G1 test set[174–177] at the geometries described in the original paper and its references. We note that we use the original geometries of the G1 test set in place of the Feller geometries, with a re-evaluated ASCI+PT2 for the exact energies. All ASCI+PT2 calculations were converged to within 10 μH accuracy and serve as an effectively converged full CI calculation.

As the nature of the DCM series' convergence was not known before this work, we will report its behavior for specific systems in addition to the general statistics of the test set. In particular, low-order CMX has been reported to occasionally converge to excited states in the case of a dominant excited state configuration.[178] Erroneously, CMX was thought to converge to incorrect values in seminal works[121], but it was demonstrated that this was an excited state energy of the system[141]). In the spectral representation of Horn-Weinstein, as one reaches high orders, all excited states ought to be sufficiently damped away such that only the ground state survives. However this condition is not necessarily ensured in our subsection of the Hilbert space limited to doubles, nor is the monotonic nature of the series. It is a useful task to assess the convergence of the DCM(N) series to determine if the Nth term in the series improves over the previous value. We begin by inspecting some representative systems of DCM(N)'s behavior in the G1 test set: H_2O, F_2, C_2H_6, CN, and Li_2.

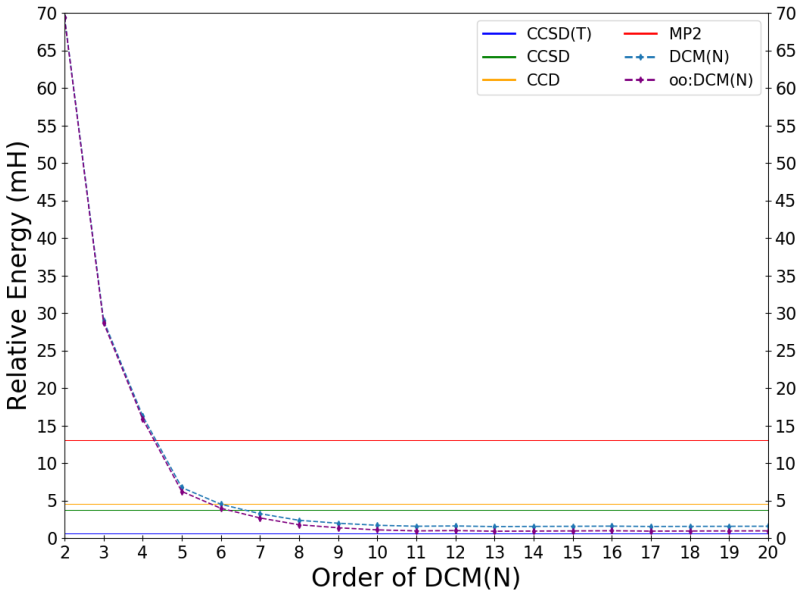

Figure 2.1: The total energy of water in cc-pVDZ for various DCM(N) and oo:DCM(N) orders.

2.4.2 H_2O

Water has served as a test molecule for the behavior of high-order perturbation theory since early algorithms were developed, including sets of selective summations towards the infinite limit which we seek to likewise address[156]. Therefore, it serves as a useful comparison to begin to understand the behavior of the DCM(N) series. In Figure 2.1, we depict order-by-order the DCM(N) and oo:DCM(N) energies relative to the exact energy of H_2O in the cc-pVDZ basis, while a more resolved image focused on just the 4th order and higher terms are depicted in Figure 2.2. The energy errors of some common methods (MP2, CCD, CCSD and CCSD(T)) relative to the exact energy are depicted as horizontal lines.

Referring to Fig. 2.1, CMX(2) and oo:DCM(2) are evidently a very poor description of electron correlation, with over 5 times larger error than the (cheaper) MP2 method. We also see that low-order DCM(N) is insufficient for quantitative accuracy; DCM(N) is inferior to CCD and CCSD until DCM(6) and DCM(7), respectively. However the fact that the DCM(N) sequence crosses over with CCD and CCSD is exciting, and, perhaps, unexpected. Fig. 2.2 provides a zoomed in view of the approach of the sequence of DCM(N) values towards a potential DCM(∞) limit. The sequence settles down to be close to an apparent limit by DCM(11). There is non-monotonic behavior with variations in the value differing by less than 0.1 mH until DCM(14); after this all energetic changes are no larger than 30

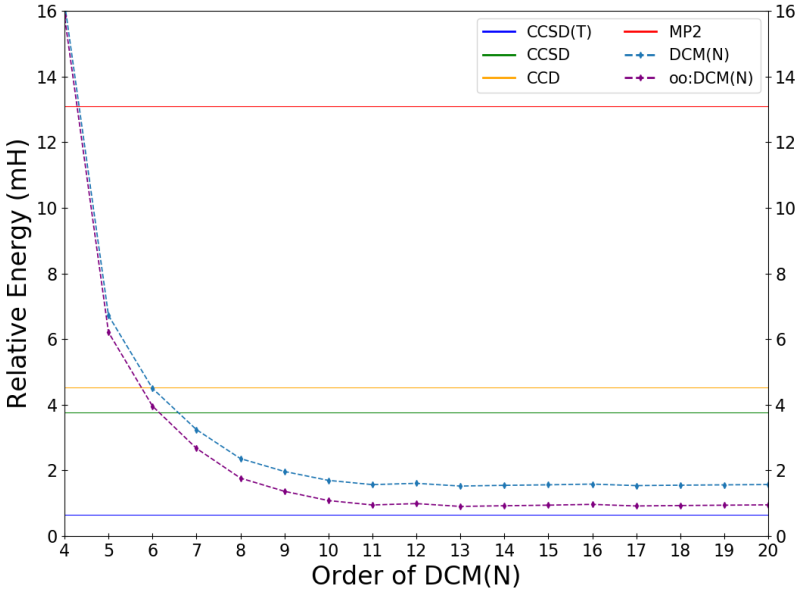

Figure 2.2: The total energy of water in cc-pVDZ for various DCM(4) and oo:DCM(4) and beyond.

μH.

This convergence behavior is reminiscent of the best behavior seen in the case of conventional Møller-Plesset perturbative series, such as for water at R_e in very small basis sets.[179] However, even well-behaved closed shell systems such as the Ne atom exhibit poor convergence and even divergence in slightly larger basis sets such as aug-cc-pVDZ.[180] By contrast, the exact CMX series has a monotonic approach to exactness. However, we have no guarantee that our doubles approximation will replicate the monotonicity of CMX, and therefore oscillations are a possibility. In this regard, the data shown in Figs. 2.1 and 2.2 is very encouraging as the DCM(N) sequence appears quite stable, at least up through DCM(20) in the tested cc-pVDZ basis. One can explain this by the fact that the products of small eigenenergies in the denominator contributing to this behavior in perturbation theory go towards zero in the corresponding moments. Most intriguingly, both the HF- and oo- based DCM(N) methods outperform their fellow O(N^6) CCD and CCSD methods in water. The DCM(N) methods even recover a substantial fraction of the triples contribution, particularly when using the OOMP2 reference determinant.

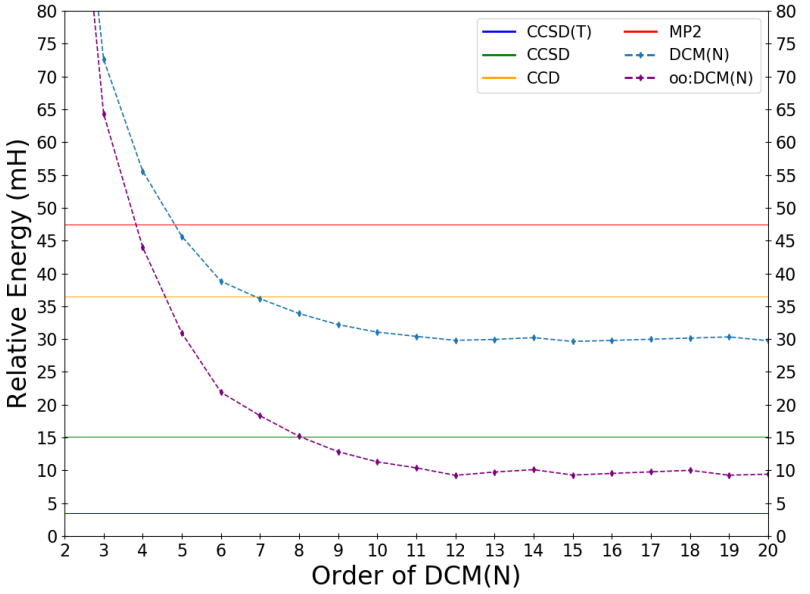

Figure 2.3: The total energy of the CN radical in cc-pVDZ for various methods by order of DCM(N) and oo:DCM(N).

2.4.3 CN & C_2H_6

The cyano radical and ethane present two interesting examples of the behavior of the DCM(N) sequence of energies. They are, respectively, the worst performers in the test set for DCM(N) and CCSD when comparing the magnitude of their errors based on the HF wavefunction. In the case of CN, CCSD outcompetes DCM(N) by 15mH, with Figure 2.3 showing the values of DCM(N) by order.

In fact, CN exhibits the largest error across the entire test set for DCM(N). We see an immediate clue as to the origin of the error from the fact that CCD shows an even larger error, that is about 20% worse than the DCM(N) sequence, and over twice as large as CCSD. If this is truly an issue associated with the lack of singles, approximate Brueckner-like orbitals would help ameliorate the error associated with orbital relaxation. Indeed the much better performance of oo:DCM(N) suggests this is the case, as the error is reduced by roughly a factor of 3 (or 20 mH), with the correlation energy below that of CCSD by DCM(9). As a result, CN is not the worst performer within the dataset for oo:DCM(N). This title instead belongs to SO_2, in which both oo:DCM(13) and oo:DCM(20) have a 31.6 mH error compared to CCSD's 25.1 mH.

The ethane molecule presents an interesting contrast in that CCSD is most out-performed by the DCM(N) sequence. Figure 2.4 shows the behavior of the energy with respect to

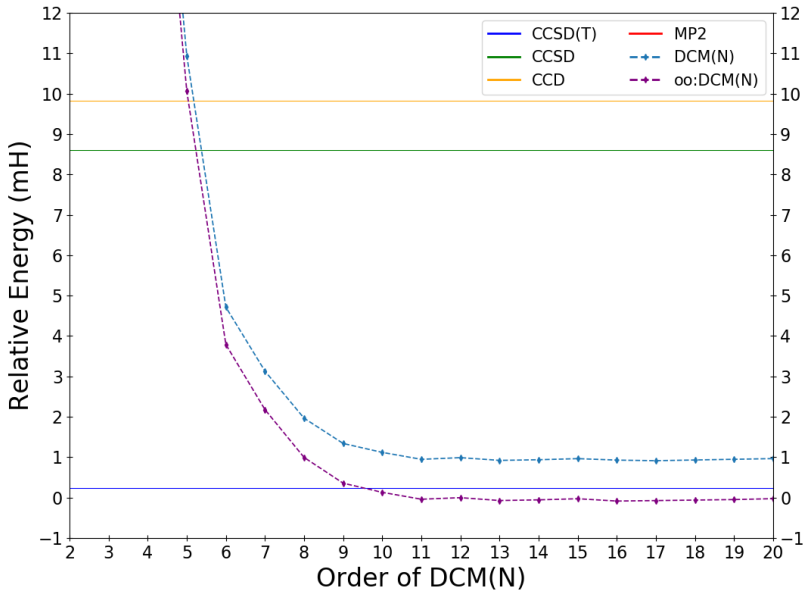

Figure 2.4: The total energy of the ethane molecule in cc-pVDZ for various methods by order of DCM(N) and oo:DCM(N).

DCM(N) order as before, with CCSD and CCD showing errors of roughly 8 and 9 mH relative to the CCSD(T) level of chemical accuracy. This example is not so much a case of poor performance of either CCD or CCSD, as remarkably good performance of the DCM(N) sequence. The limiting error of DCM(N) is only about 1 mH, and the oo:DCM(N) sequence has error that is less than 0.1 mH, and is clearly superior to CCSD(T), which is in error by 0.24 mH. This example suggests that the importance of triple substitutions in the oo:DCM(N) hierarchy may be less than in the usual coupled cluster hierarchy.

2.4.4 F_2 & Li_2

Figure 2.5 shows the correlation energy errors of the DCM(N) and oo:DCM(N) sequences relative to several standard methods for the case of the fluorine dimer using restricted orbitals. F_2 is known to exhibit significant diradicaloid character, and in fact is not even bound at the mean-field Hartree-Fock level. In this case, we see the most significant oscillatory patterns in the DCM(N) energies out of the full set of molecules. Non-smooth decreases in the correlation energy occur until DCM(11), at which point the more minor changes we saw before swell to span a range of 1.5 mH between the troughs and peaks of oo:DCM(12)/oo:DCM(13) and oo:DCM(16)/oo:DCM(17), with slightly smaller values in the Hartree-Fock reference case. Despite this slightly troubling behavior, the DCM(N) values significantly surpass the

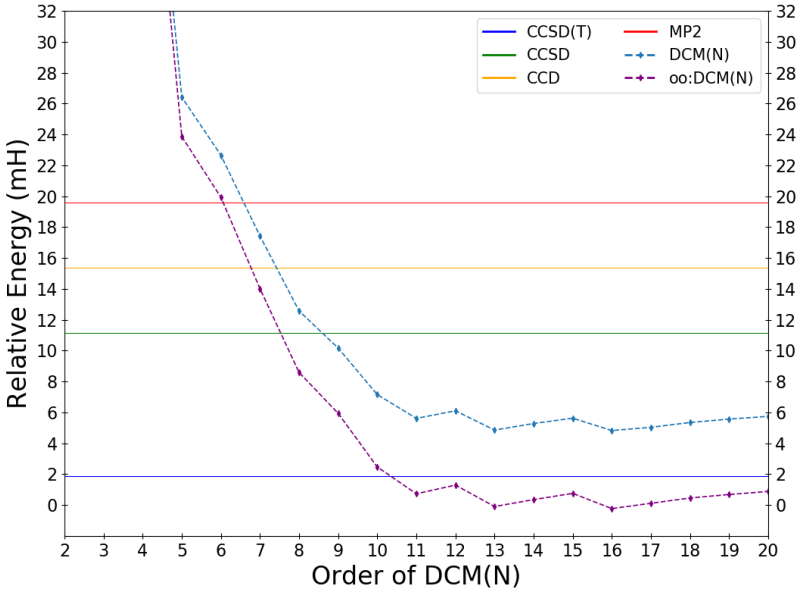

Figure 2.5: The total energy of the F2 molecule in cc-pVDZ for various methods by order of DCM(N) and oo:DCM(N).

CCSD energy even before the oscillations occur. In the oo:DCM(N) case, the energies even improve upon the costlier CCSD(T) method.

The lithium dimer exhibits nonvariational behavior for the DCM(N) energies, as shown in Figure 2.6. While CCD, CCSD, and CCSD(T) are all within chemical accuracy for this effectively 2-electron system, both the DCM(N) and oo:DCM(N) sequences show more than 10 times larger error, with energies going below the exact energy by up to 3.4 mH. The slightly worse behavior in the case of oo:DCM(N) suggests that this is not a deficiency associated with the singles. Whether the resummation structure or the moment structure is the cause of this undesirable behavior is unclear to us at present. Non-variational behavior is observed in LiH also, although the effect is less severe. We note our presentation of the order-by-order analysis for various molecules illustrates that different behavior can arise from one system to the next. We additionally note that it seems to be generally true that the first non-monotonic values occur between DCM(11) and DCM(14), which is also the range where values appear to also approach limiting values in well-behaved cases.

2.4.5 Results across the G1 Test Set

The statistical results across the G1 test set are contained within Table 2.2, where the RMSD of the various methodologies discussed are shown for both the Hartree-Fock and

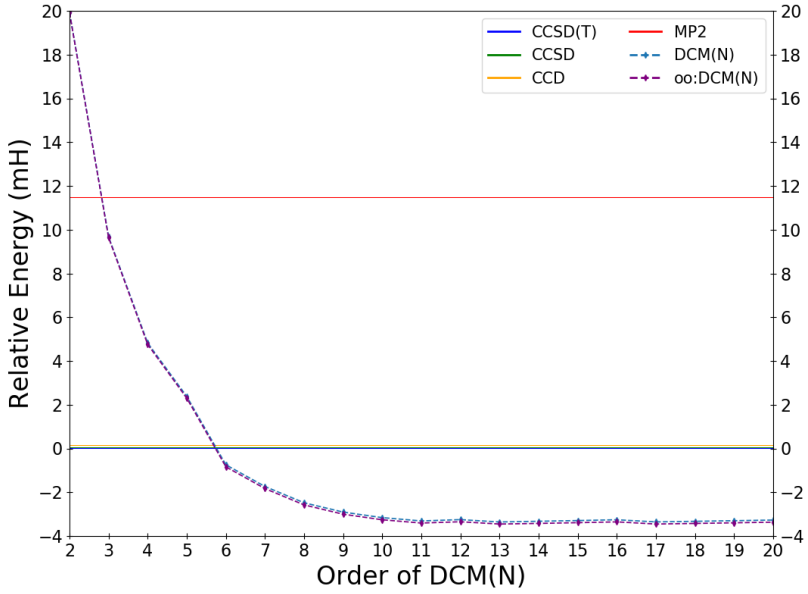

Figure 2.6: The total energy of Li_2 in cc-pVDZ for various methods by order of DCM(N) and oo:DCM(N).

OO reference determinants. The data has been arranged with respect to the entire set as well as two subsets: one containing molecules with only row 1 and 2 atoms, followed by the complement subset containing row 3 atoms. As expected, low-order DCM(N) energies are not useful methods, in line with our understanding of the poor energetic performance of CMX from past investigations. We also note there is no improvement, and in fact even slightly poorer performance of oo:DCM(2) and oo:DCM(3) compared to their Hartree-Fock counterparts.

Consistent with our examination of individual cases, the most exciting results concern the convergence of DCM(N) energies, and especially the oo:DCM(N) energies to very useful values by DCM(11-14) or oo:DCM(11-14). Seeking a direct comparison of the purely doubles methods with similar orbitals, we see a notable improvement over the CCD energies as one iterates through the DCM(N) cycles across both the whole set and the partitions. This improvement is most significant for row 1 and 2 molecules, in which all orders from 12th and onwards improve upon CCD by a margin of over 5 mH. The improvement is less notable among molecules with row 3 atoms, where the same comparison only yields a single mH improvement. Together, this results in an overall improvement of 3.3 mH in the energies of the double methods, despite the lack of the disconnected-cluster contributions allowing for indirect excitations related to $\hat{T}_2^2$ in the CCD amplitudes.

Moving to the comparison of CCSD, it is useful to use the oo:DCM(N) values not just

Method	HF RMSD			Method	OO RMSD		
	All	Row 1+2	Row 3		All	Row 1+2	Row 3
CCSD(T)	1.42	1.32	1.53	-	-	-	-
CCSD	9.98	9.49	10.58	-	-	-	-
CCD	13.60	13.58	13.62	-	-	-	-
MP2	27.80	24.93	31.12	-	-	-	-
CMX(2)	114.29	101.78	128.67	oo:DCM(2)	115.29	101.72	130.76
DCM(3)	76.69	48.14	102.39	oo:DCM(3)	77.04	46.79	103.79
DCM(4)	55.60	30.96	76.45	oo:DCM(4)	55.34	28.93	77.05
DCM(5)	30.22	18.89	40.40	oo:DCM(5)	29.32	16.07	40.45
DCM(6)	23.44	14.56	31.40	oo:DCM(6)	22.20	11.36	31.02
DCM(7)	19.88	12.26	26.67	oo:DCM(7)	18.50	8.76	26.18
DCM(8)	14.90	10.60	19.07	oo:DCM(8)	13.07	6.86	18.18
DCM(9)	12.46	9.59	15.40	oo:DCM(9)	10.43	5.73	14.38
DCM(10)	11.26	8.90	13.73	oo:DCM(10)	9.16	4.96	12.67
DCM(11)	10.45	8.51	12.53	oo:DCM(11)	8.22	4.54	11.33
DCM(12)	10.31	8.44	12.32	oo:DCM(12)	8.10	4.50	11.15
DCM(13)	10.43	8.32	12.64	oo:DCM(13)	8.27	4.35	11.50
DCM(14)	10.27	8.44	12.23	oo:DCM(14)	8.06	4.47	11.09
DCM(15)	10.33	8.38	12.41	oo:DCM(15)	8.11	4.39	11.22
DCM(16)	10.36	8.24	12.58	oo:DCM(16)	8.19	4.27	11.40
DCM(17)	10.41	8.32	12.61	oo:DCM(17)	8.22	4.35	11.41
DCM(18)	10.37	8.40	12.45	oo:DCM(18)	8.14	4.43	11.24
DCM(19)	10.38	8.43	12.44	oo:DCM(19)	8.15	4.39	11.28
DCM(20)	10.34	8.27	12.51	oo:DCM(20)	8.15	4.28	11.34

Table 2.2: RMSD of approximate methods for the correlation energy relative to (nearly) exact selected configuration interaction results (in mH) across the G1 test set, evaluated in the cc-pVDZ basis.

for their quantitative improvement, but also due in part to their approximate Brueckner-like nature that ameliorates orbital relation effects, a property already inherent to CCSD with its orbital insensitivity. For the row 1 and 2 containing molecules, oo:DCM(N) of 12th order and higher improves the energies by a margin of over 5 mH, while across the entire set this value is a more modest value of just under 2mH due to the smaller improvements in the row 3 molecules. Whether the smaller improvements for row 3 containing molecules are a feature of the summation scheme or the moments approach more generally is not clear without additional investigation. It is worth noting that values of oo:DCM(N) after 12th-order are superior relative to CCSD for 49 of the 54 molecules in the G1 test set. Most of the RMSD error stems from a few systems in which the errors are high, such as the previously mentioned SO. In fact, the successful cases are significant enough for oo:DCM(N) to outcompete even CCSD(T) in 15 of the systems tested here.

We also note that the same trend of rising values found in the order-by-order DCM(N) and oo:DCM(N) energy analysis for individual cases holds true in a statistical sense as well. There is some variation in the solutions, but DCM(14) exhibits the smallest RMSD in both the HF and OO cases as energies begin to oscillate. Despite this, anything 12th-order and higher are no more than 0.21 mH above this energy error for both sets of reference determinants.

As mentioned above, DCM(N) scales as the same polynomial power of system size as the CCD and CCSD equations. Specifically, the construction of $(ij||ab)_n$ is needed to assemble μ^D_{2N-1}, and making $(ij||ab)_n$ involves $N-1$ particle ladder contractions, which roughly makes DCM(N) as costly as $N-1$ iterations of the CCD amplitudes. While the pilot code has not undergone heavy optimization, it may still be useful to mention preliminary timings in constructing the amplitudes versus the doubles connected moments. For the largest system, Si_2H_6, CCSD yields 81.3 seconds per cycle, for a total of 650.6 seconds in solving the Coupled Cluster equations. By comparison, DCM(N) required 42.6 seconds per cycle, resulting in DCM(14) being just under the CCSD timing at 596.5 seconds. We can anticipate that when CCSD convergence is slow, the DCM(N) models are a fairly straightforward way to evaluate correlation energies with comparable, or even improved, values due to its single shot nature.

2.4.6 N_2 Dissociation

The potential energy surface corresponding to breaking the triple bond of N_2 has served as a benchmark case in the evaluation of new correlation methodologies such as CI and CC studies through very high orders, and new multi-reference CC approaches, including the many different flavors of Fock-Space MRCC, State-Universal MRCC, and Valence-Universal MRCC[181–183]. N_2 has several valuable properties for benchmarking, beginning with the need to treat both dynamic and static correlation along the dissociation coordinate. While fairly well described by a single determinant at the equilibrium geometry, the triple bond dissociation requires the interaction of 6 active electrons to recouple the two ^{4}N atoms. N_2 is also an excellent case for testing spatial and spin symmetry (breaking) as a function of bond-breaking. While low-order CC techniques fail qualitatively when using a spin-restricted

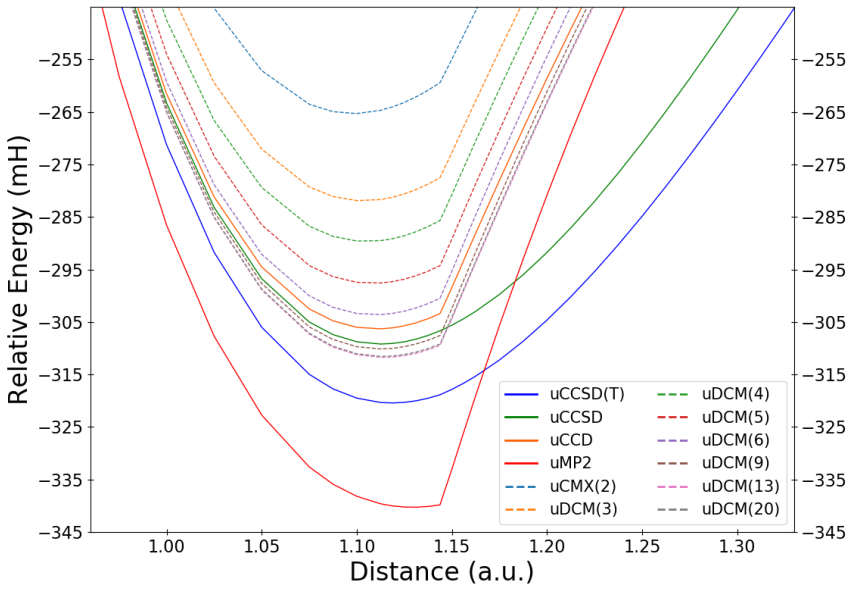

Figure 2.7: Approximations to the total energy of N_2 in the vicinity of the equilibrium geometry with a UHF reference for correlation methods including representatives of the uDCM(N) sequence. Energies are reported relative to two ^{4}N atoms for each method.

reference determinant, the use of a spin-polarized reference allows one to obtain quantitative accuracy at dissociation at the cost of losing the spin purity inherent to the true wavefunction.

Figure 2.7 shows N_2 dissociation in the cc-pVDZ basis using a spin-polarized reference determinant, comparing UMP2, UCCD, UCCSD, and UCCSD(T) against the DCM(N) sequence. To begin, we focus on the convergence of the sequence near the bottom of the well for the Hartree-Fock case before considering the entire curve or the oo:DCM(N) case. For readability, we have omitted some orders, but nevertheless one can see the same trends as before: there is variation of the DCM(N) energies on the sub-mH energy scale after DCM(11). As usual, the traditional purely double methods of uMP2 and uCCD both exhibit a very visible first derivative discontinuity[184] at the Coulson-Fischer point, while uCCSD and uCCSD(T) are both able to circumvent this behavior (at least on the graphical scale) via the inclusion of singles. Lacking orbital relaxation due to singles, the uDCM(N) family of methods share the behavior of uMP2 and uCCD with a pronounced first derivative kink at all orders. However, the actual energetic predictions of the uDCM(N) sequence follows the trends as seen for the G1 test set: uDCM(N) surpasses uCCD by uDCM(6) regardless of whether we are in the unpolarized or spin-polarized regimes.

As other work has recently shown, the inclusion of an orbital-optimized reference delays the onset of the Coulson-Fischer point and one may recover better qualitative description

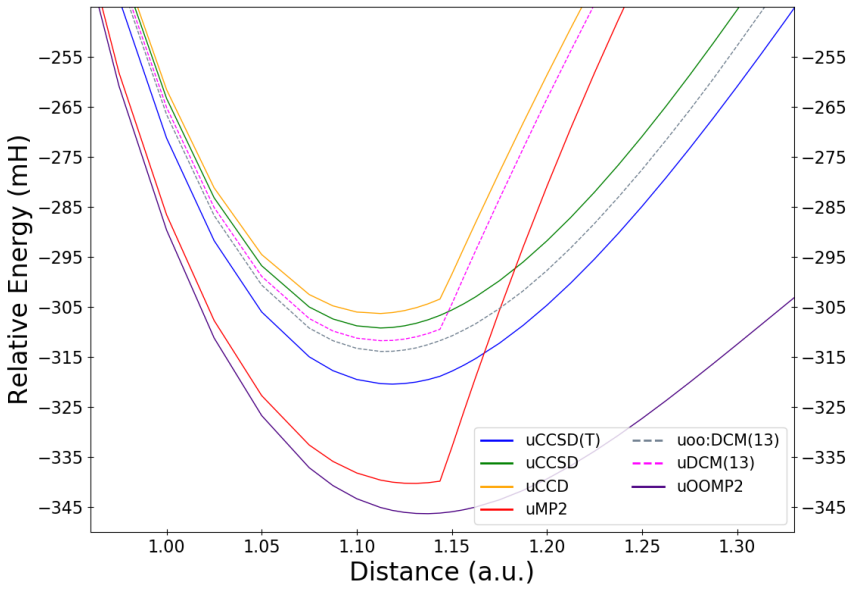

Figure 2.8: Approximations to the total energy of N_2 in the vicinity of the equilibrium geometry with a UHF reference for correlation methods including uDCM(13) and uooDCM(13) as high order representatives of the uDCM(N) sequence. Energies are reported relative to two ^{4}N atoms for each method.

within the well. Combined with the performance in energetics, this makes uoo:DCM(N) an excellent candidate to evaluate in the same way. As the uDCM(13) is the lowest order to reach the convergence limit, we now focus on only this order for both sets of orbitals to make the trend more apparent. Figure 2.8 shows results similar to above near the well, while 2.9 shows the behavior up through the qualitative failure and through the point where the uOOMP2 curve turns over (note that UOOMP2 does not exhibit a Coulson-Fischer point, as has been extensively discussed elsewhere[167, 185]). The uoo:DCM(N) curve does in fact recover the correct qualitative behavior near equilibrium and well after Hartree-Fock's spin-polarization transition.

Interestingly, even as the OOMP2 curve begins to turn over, the uoo:DCM(13) results are able to delay this to be more in line with the uCC methods. By the time the former reaches its maxima, this is no longer the case and both begin to diverge after this point. However, it is notable that the moments approach delays the turning point as well. Of course, while the the uDCM(13) does have its discontinuity, the curve does not diverge. Additionally, uoo:DCM(13) is able to surpass quantitatively all methods here relative to CCSD(T), now resting at 6.4 mH away rather than CCSD's 11.2 mH.

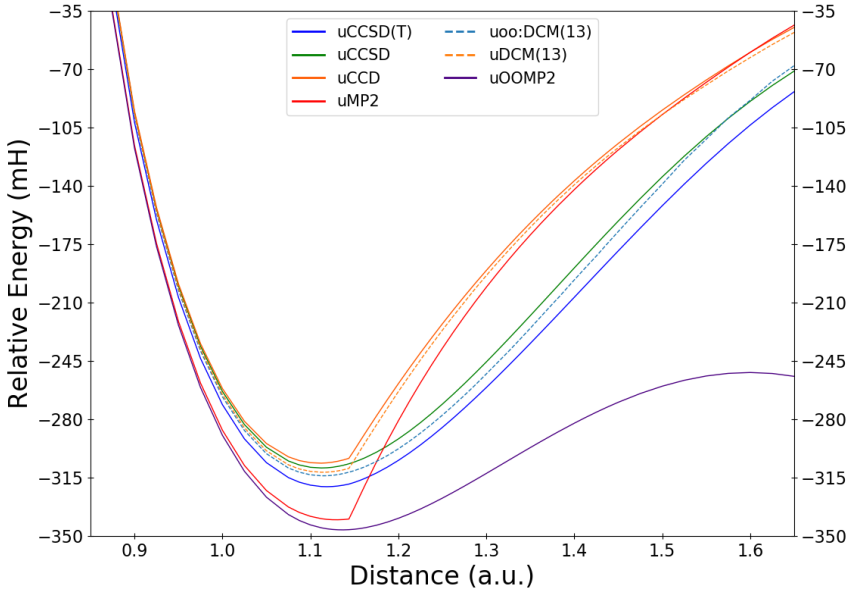

Figure 2.9: Approximations to the total energy of N_2 across the potential curve with a UHF reference for correlation methods including uDCM(13) and uooDCM(13) as high order representatives of the uDCM(N) sequence. Energies are reported relative to two ^{4}N atoms for each method.

2.5 Conclusions

The purpose of this work was to revisit the connected moment expansion (CMX) in order to introduce an approximation analogous to those that have been successful in widely used single-reference correlation methods such as coupled cluster theory. The exact moments (powers of the Hamiltonian) that enter the CMX expressions have compute costs that rise incredibly steeply with the power, which makes these otherwise attractive non-iterative methods unfeasible in practice. To circumvent the computational bottleneck, we decided to evaluate the moments using only the doubles part of the Hilbert space that is strongly orthogonal to a single reference such as the Hartree-Fock determinant, or an approximate Brueckner determinant. We call this approach the Doubles Connected Moments (DCM) expension, and, via the CMX framework, it gives rise to a tractable sequence of DCM energies, DCM(N), for N $= 1 \cdots \infty$. Beyond $N = 1$, each DCM(N) energy can be evaluated with compute cost that scales the same as an iteration of the CCD or CCSD equations. The fact that DCM(N) energies are constructed from connected moments allows the method to retain the important property of size-extensivity of the exact CMX(N) energies.

The DCM(N) methods have been implemented to employ single-references that can be

either Hartree-Fock or approximate Brueckner from orbital-optimized MP2 (oo), and can be either spin-restricted or unrestricted. The resulting methods were then assessed on the correlation energies of the 54 small molecules (and radicals) in the G1 data set, against virtually exact results from selected configuration interaction, as well as standard MP2, CCD, CCSD, and CCSD(T). Interestingly, we observe that DCM(N) for N > 10 performs quantitatively well relative to infinite order doubles methods such as CCD and CCSD. These are perhaps the first tractable calculations using the moments approach that appear potentially viable for chemical applications. Statistically, the oo:DCM(N) energies outperform CCSD for the correlation energy, while the Hartree-Fock-based DCM(N) energies outperform CCD for the correlation energy. Examination of both individual and collective results shows generally smooth convergence patterns to limiting values by DCM(11-14).

The DCM(N) methodology looks useful already although we stress that it is important to explore questions of numerical stability, and basis set extension carefully in future work. If those results are positive, as seems quite likely, then there are practical ways in which the methodology can be systematically improved. First, one may refine the approximation of the moments to include further contributions. In particular, one can easily imagine the construction of SDCM(N) by including the singles contributions to μ_2 and higher. Additionally, there are opportunities to further optimize the implementation. For example, the most costly step in DCM(N) is the contraction of the particle ladder terms, and the use of the tensor hypercontraction (THC) formalism would bring the scaling of DCM(N) down to $\mathcal{O}(M^4)$ with molecule size, as in the case of MP3. [186] There are likewise opportunities to consider more efficient implementations of higher connected contributions such as triples. For example, the μ_4 connected triples may be calculated in $O(M^6)$ time unlike its analogue in the MP4 case where a 6-index denominator results in its most expensive contribution scaling as $O(M^7)$. Though this specific contribution is still relatively intractable at $O(v^6)$ (where v is the number of virtual orbitals), the potential factorizability of the method provides further opportunities for use of THC and Resolution-of-the-Identity (RI).

Especially in situations that exhibit an interplay of strong and weak correlation, the DCM(N) approach may be a blueprint for further refinement of more sophisticated yet still low-cost references, such as strongly orthogonal geminal wavefunctions[187] or the coupled cluster valence bond (CCVB) reference.[188, 189] Indeed the prior success seen using low-order CMX with APSG and CAS reference wavefunctions suggests there is potential for new progress in this direction, based on retaining the affordability and promising accuracy that is a key feature of DCM(N).

2.6 Supplementary Information

The S.I. for this work will soon be be accessible on Arxiv under "The Doubles Connected Moments Expansion: A Tractable Approximate Horn-Weinstein Approach for Quantum Chemistry" before it is to be submitted for publication. Any pre-print data will gladly be provided by BG.

Chapter 3

Molecular Magnetizabilities Computed Via Finite Fields

3.1 Introduction

The magnetizability, $\boldsymbol{\xi}$ of a molecule is the magnetic analog of the electric polarizability. $\boldsymbol{\xi}$ is a second order property that describes the temperature-independent quadratic change of the energy of a molecule, $\delta E(\mathbf{B}) = -\frac{1}{2}\mathbf{B}^\dagger\boldsymbol{\xi}\mathbf{B} + \ldots$, in response to the presence of a magnetic induction, $\mathbf{B}$. Thus $\boldsymbol{\xi}$ is a 3×3 matrix (or symmetric rank-2 tensor). For molecules with non-zero total angular momentum (most commonly, unpaired electron spins), there is an additional temperature-dependent contribution that depends directly on the total spin, and, when present, it is typically the largest contribution. $\boldsymbol{\xi}$ also yields the temperature-independent magnetic moment, $\mathbf{m(B)}$ of a molecule induced by $\mathbf{B}$, as $\mathbf{m(B)} = \boldsymbol{\xi}\mathbf{B}+\ldots$. For more background material on magnetostatics and the magnetizability, we refer the reader to several excellent textbooks.[190–192]

The calculation of magnetic properties is based on the pioneering work by Ramsay in the early 1950s.[193–200] Owing to these efforts, the calculation of Nuclear Magnetic Resonance (NMR) chemical shielding tensors and indirect spin-spin coupling tensors (both second order properties) nowadays belongs to the standard repertoire of the computational chemist and complements the experimental interpretation of NMR spectra.[83, 201] While magnetizabilities are not amongst the most commonly calculated molecular properties, they have some established roles in chemistry. The main role is molecular magnetism in inorganic chemistry, where unpaired spins and orbital angular momentum are routinely characterized.[202] That is not our focus, so we turn next to applications that do not depend on such contributions. In general, the magnetizability tensor is far more difficult to obtain experimentally than chemical shieldings and spin-spin couplings due to the large experimental error bars,[203] so the need for accurate calculations that serve as benchmarks for the experiments is particularly high. At the level of fundamental molecular properties, the magnetizability tensor connects directly to several spectroscopic observables including the molecular Zeeman effect,

the Cotton-Mouton effect, and the interpretation of microwave spectra.[190–192] Separately, in a broader chemical context, it has long been recognized[204] that the magnetizability of aromatic molecules may be enhanced or "exalted" relative to non-aromatic analogs because of the presence of a closed path (or paths) where electrons may move freely in the aromatic case, versus the absence of such a path in the non-aromatic case. Accordingly, calculations of magnetizability exaltations[205, 206] represent perhaps the main chemical application of this molecular property in closed shell, stable molecules. Interestingly, it has also been reported that the level of agreement between mean-field Hartree-Fock magnetizabilities of aromatic molecules and experimentally derived values is significantly poorer for aromatic molecules than for non-aromatic organic molecules.[207]

Magnetizabilities have been calculated fairly early[208, 209] and a plethora of electronic structure methods are available for this task: Magnetizabilities at the levels of Hartree-Fock (HF),[210, 211] density fitted HF,[212] Density Functional Theory (DFT),[213] Current-Density Functional Theory (CDFT),[214] Magnetic-Field Density Functional Theory (BDFT),[215] the Second-Order Polarization Propagator Approximation (SOPPA),[216] various Coupled-Cluster Polarization Propagator Approximations (CCDPPA, CCSDPPA),[216] Linearized Coupled-Cluster Doubles (L-CCD),[217, 218] Coupled-Cluster Singles and Doubles (CCSD),[219] Multiconfigurational Self-Consistent Field (MCSCF),[207, 210] Second- and Third-Order Møller-Plesset Perturbation Theory (MP2 and MP3),[217, 218, 220, 221] as well as Resolution-of-the-Identity MP2 (RI-MP2)[222] have been reported. Relativistic effects have been included in the calculation of magnetizabilities at the MP2 level as well.[223]

The "gold-standard" for the calculation of magnetizabilities is CCSD with a perturbative triples correction (CCSD(T))[224] at the complete basis set limit, which has been used to generate the reference data in one of the few benchmark studies for magnetizabilities.[225, 226] However, due to the steep scaling of CCSD(T) and the resulting rapid increase of computational cost with increasing system size, such calculations are prohibitive for larger molecules. Hence, more cost-efficient methods for the accurate calculation of magnetizabilities are desirable.

MP2 is a technique that scales with the fifth power of the number of basis functions ($O(\mathrm{N}^5)$) and has been used successfully in a multitude of applications. While NMR shielding constants calculated with MP2 are typically of satisfying accuracy,[201] the results for magnetizabilities are generally disappointing and often worse than the HF results.[222] This observation has been attributed to the subtle influence of electron correlation on magnetizabilities and the propensity of MP2 to overestimate this effect.

The challenges of MP2 for accurately describing electron correlation have at least two origins. First, it is well-known that HF orbitals yield charge distributions that are too ionic; this limitation can be addressed by optimizing orbitals in the presence of MP2 correlation.[227–230] Second, the form of MP2 correlation means that the total energy is not bounded from below and can become non-variational (i.e. over-correlated) when energy gaps become small. This can be addressed by intelligent denominator regularization schemes (the simplest being just a level shift[185, 231]), or, possibly other formalisms.[232] Recently, some of us have pre-

sented a new approach to regularized Orbital-Optimized MP2 (κ-OOMP2),[233–235], which scales as the fifth power of the number of basis functions, albeit with a larger prefactor than canonical MP2. κ-OOMP2 attenuates the overestimation of electron correlation by canonical MP2 for small-gaps, while leaving large-gap contributions unaltered. The κ-OOMP2 orbitals have also been used to greatly improve the numerical performance of MP3 relative to HF orbitals.[236] Considering these encouraging results, we think it is useful to explore the performance of κ-OOMP2 for magnetizabilities, particularly given the poor performance of MP2 for this property.

In this paper, the implementation and calculation of magnetizability tensors with κ-OOMP2 is presented using a fully numerical approach. This entails evaluating the energy in the presence of specific applied values of magnetic induction, followed by a finite difference evaluation of the magnetizability. Approaches of this type have been employed previously to characterize the electronic structure of molecules in nonuniform magnetic fields.[237] To address the gauge origin problem inherent in the calculation of magnetic properties,[83] we use Gauge-Including Atomic Orbitals (GIAOs),[238] also known as London orbitals. Our results demonstrate that the errors of the numerical derivative as compared to the analytical approach are acceptable, and also suggest that κ-OOMP2 performs significantly better for magnetizabilities than standard MP2.

The rest of the paper is structured as follows: After an in-depth discussion of the theoretical background of the calculation of magnetizability tensors with κ-OOMP2 and evaluating the accuracy of the numerical procedure (Section 4.2), the performance of the new computational method as compared to CCSD(T) reference data, taken from the test set by Lutnæs and co-workers,[225] is assessed (Section 4.3). After some additional benchmark tests on conjugated cyclic molecules, we then consider a chemical example: magnetizability exaltations, which were historically used to evaluate aromaticity of ring molecules. We present a straightforward approach to evaluating the exaltations without the need for empirical reference data. Conclusions are given in Section 4.4.

3.2 Theoretical Background

An in-depth treatment of the quantum chemical calculation of magnetic properties is beyond the scope of this paper. The interested reader is kindly referred to existing reviews on the subject.[201, 239, 240] Instead, here the general design idea of our code (Section 4.2.1), the matrix elements that are required for the calculation of magnetizabilities (Section 4.2.2), the particularities of κ-OOMP2 in the calculation of the magnetizability tensor (Section 3.2.3), details on the implementation and verification of our code (Section 4.2.5) as well as the performance of the numerical implementation compared to analytical results (Section 4.2.7) are discussed.

3.2.1 General Approach

The magnetizability $\boldsymbol{\xi}$ is a 3x3 tensor and can be calculated as the second derivative of the energy E w.r.t. the magnetic field $\mathbf{B}$,[201] with elements

$$\xi_{ij} = -\frac{\mathrm{d}^2 E\left(\{\mathbf{R}_N\}, \mathbf{B}\right)}{\mathrm{d}B_i \mathrm{d}B_j}\bigg|_{\mathbf{B}=\mathbf{0}} \quad . \tag{3.1}$$

Here, $\{\mathbf{R}_N\}$ is the nuclear configuration. The isotropic magnetizability is $\xi_{\mathrm{iso}} = \frac{1}{3}\mathrm{tr}(\boldsymbol{\xi})$. We use Gauge-Including Atomic Orbitals (GIAOs),[238] also known as London orbitals, in the calculation of magnetizabilities to address the gauge-origin problem.[201] A GIAO ω_μ, centered on nucleus N, is given as

$$\omega_\mu(\mathbf{r}; \mathbf{A}_N) = \exp\left(-i\mathbf{A}_N \cdot \mathbf{r}\right) \cdot \chi(\mathbf{r}), \tag{3.2}$$

where $\mathbf{r}$ is the electron coordinate and $\chi(\mathbf{r})$ is a regular Gaussian-type orbital and the vector potential $\mathbf{A}_N$ is

$$\mathbf{A}_N = \frac{1}{2}\mathbf{B} \times \mathbf{R}_{NO}. \tag{3.3}$$

$\mathbf{R}_{NO}$ is the vector from the nucleus N to an arbitrarily chosen gauge-origin O, the latter of which we choose to be the zero vector for convenience.

We use a fully numerical implementation for the calculation of the magnetizability tensor (eq. 4.2). In particular, focusing on the isotropic part of the magnetizability tensor and omitting the electronic and nuclear coordinates in the energy for clarity, we calculate the second derivative of the energy w.r.t. the magnetic field to second order *via*[241]

$$\xi_{ii} = -2\frac{E(\Delta B_i) - E(\mathbf{B} = \mathbf{0})}{\Delta B_i^2} \tag{3.4}$$

Off-diagonal elements of the tensor can be evaluated to second order via the following expression:

$$\xi_{ij} = -\frac{E(\Delta B_i) + E(-\Delta B_i) + E(\Delta B_j) + E(-\Delta B_j) - 4E(\mathbf{B} = \mathbf{0})}{2\Delta B_i \Delta B_j} \tag{3.5}$$

There are also corresponding expressions that are accurate to fourth order,*via*[241] which is as follows for the diagonal elements:

$$\xi_{ii} = -\frac{-\frac{1}{6}E(2\Delta B_i) + \frac{8}{3}E(\Delta B_i) - \frac{5}{2}E(\mathbf{B} = \mathbf{0})}{\Delta B_i^2}, \tag{3.6}$$

ΔB_i is the step in the Cartesian component i of the magnetic field. The choice of this parameter determines the accuracy of the numerical results. An assessment of ΔB_i and its relation to the numerical error is given in Section 4.2.7. The calculation of the magnetizability *via* eqs. 4.6 and 3.6 necessitates the calculation of several energies at different values of

the magnetic field, which has been achieved before.[242, 243] Due to the use of GIAOs, we use a fully complex-valued code throughout our calculations.

Although analytical derivatives are generally to be preferred over their numerical counterparts due to some clear advantages (e.g. typically shorter calculation times, significantly reduced numerical noise, real-valued code, and no need to calibrate/validate a choice of the finite difference step size), we chose a fully numerical scheme here to calculate the magnetizability for the following reasons: Firstly, once the energy expressions in an external magnetic field (cf. Section 4.2.2) are implemented, it is fairly straightforward to add and rapidly test new computational methods for the calculation of magnetic properties, since the cumbersome implementation of the analytical expressions, which needs to be carried out for each level of theory separately, is avoided. Secondly, the implementation of the explicit energy expressions in the presence of an external magnetic field allows the rapid adaption to other properties involving the magnetic field (e.g. chemical shieldings, circular dichroism), since only a handful of new terms needs to be implemented. This is much more cumbersome in the case of analytical calculations. Thirdly, the calculation of magnetic properties like chemical shieldings or spin-spin couplings for only specific nuclei or pairs of nuclei, respectively, can be trivially achieved with numerical derivatives, although analytical calculations of magnetic properties of subsets of atoms have been reported.[244] Finally, parallelization of the code is a trivial task, since the calculations of the perturbed energies can be conducted independently on different computer nodes, with no need of communication between the processors. This is especially valuable considering today's highly parallel computer infrastructure. In principle, given enough processors, the calculation of the magnetizability is roughly as computationally costly as the calculation of an energy in the presence of a finite magnetic field. Hence, in order to test the viability of the κ-OOMP2 method for the calculation of magnetizabilities, we chose a fully numerical approach.

3.2.2 Required Matrix Elements

The Hamiltonian in an external magnetic field is discussed in detail in ref. 245 and an excellent overview on the calculation of matrix elements involving GIAOs can be found in ref. 246. For the sake of brevity, we will in the following only discuss those matrix elements that we have implemented for the calculation of magnetizabilities.

Focusing on the one-electron terms first, the kinetic energy matrix elements are defined as

$$h_{\mu\nu}^{\text{kin}} = \left\langle \omega_\mu \middle| -\frac{1}{2}\nabla^2 \middle| \omega_\nu \right\rangle . \tag{3.7}$$

Using well-known relations,[245] eq. 3.7 can be reduced to linear combinations of overlap integrals $\langle\omega_\mu|\omega_\nu\rangle$ between GIAOs.

One-electron matrix elements associated with electron-nuclear attraction (NA) are defined as

$$h_{\mu\nu}^{\text{NA}} = -\left\langle \omega_\mu \middle| \sum_\alpha \frac{Z_\alpha}{r_\alpha} \middle| \omega_\nu \right\rangle , \tag{3.8}$$

where r_α is the distance between the electron and the nucleus α. The calculation of such matrix elements requires the use of the Boys function with a complex argument. The interested reader is referred to ref. 246 for details.

For the calculation of the magnetizability tensor, two more one-electron terms need to be taken into account. The first one involves the diamagnetic magnetizability (DM) operator,[245]

$$\hat{h}^{\mathrm{DM}} = \frac{1}{8}\left[\mathbf{B}^2 \cdot \mathbf{r}^2 - (\mathbf{B}\cdot\mathbf{r})^2\right]. \tag{3.9}$$

The second one involves the paramagnetic shielding (PS) operator,

$$\hat{h}^{\mathrm{PS}} = -\frac{i}{2}\mathbf{B}\cdot(\mathbf{r}\times\nabla). \tag{3.10}$$

After some straightforward yet somewhat cumbersome algebra, both operators lead to energy expressions that involve only overlap integrals with increased or decreased angular momentum on GIAO ω_ν (see Appendix).

Turning to the two-electron integrals, many schemes for the calculation of the crucial electron repulsion are available. Some of the most prominent ones are known as Taketa-Huzinaga-O-ohata (THO66),[247] McMurchie-Davidson,[248] Rys-quadrature,[249, 250] Gill-Johnson-Pople (GJP),[251] and Head-Gordon-Pople (HGP88).[252] For an efficient calculation of the electron repulsion integrals it is well-known that the optimal choice of algorithm depends on the orbital angular momentum.[246] Initially, we implemented the inefficient but rather straightforward THO66 algorithm to generate reference numbers (cf. Section 4.2.5), but later switched to the much more efficient HGP88 algorithm for production calculations for both 2-electron-4-center integrals for the regular electron repulsion and 2-electron-3-center integrals for the Resolution-of-the-Identity approximation (for which efficient evaluation has recently been described[253]). All values reported in this paper have been generated with the HGP88 algorithm.

Hence, we have only implemented three basic types of integrals, i.e. overlap, nuclear attraction and electron repulsion. All other integrals (kinetic energy, diamagnetic magnetizability and paramagnetic shielding) could be reduced to linear combinations of overlap integrals.

3.2.3 Magnetizabilities with κ-OOMP2

The regularized orbital-optimized MP2 approach (κ-OOMP2) has been presented recently by some of us.[233–235] In the following only a brief overview of the approach that is necessary to understand the gist of the method is given. The interested reader is kindly referred to the original publication for details.

In canonical MP2, the Hylleraas functional L is minimized with respect to the amplitudes t, which yields the MP2 energy,

$$E_{\mathrm{MP2}} = \min_t L[t,\theta]. \tag{3.11}$$

where the Hylleraas functional is

$$L[t,\theta] = \langle\Psi_1\big|\hat{H}\big|\Psi_0\rangle + \langle\Psi_0\big|\hat{H}\big|\Psi_1\rangle + \langle\Psi_1\big|\hat{H}_0 - E_0\big|\Psi_1\rangle \tag{3.12}$$

In OOMP2, the Hylleraas functional is furthermore optimized with respect to orbital rotation parameters θ,

$$\frac{\partial L[t,\theta]}{\partial\theta} = 0 \tag{3.13}$$

This approach yields a set of orbitals that are no longer the Hartree-Fock orbitals, but approximations to Brueckner orbitals.[227, 254–256] As GIAOs are used in the calculation of magnetic properties, the resulting orbitals are still gauge-including. Hence, the results are independent of the (arbitrary) choice of gauge origin. OOMP2 scales as $O(\mathrm{N}^5)$, albeit with a larger prefactor than canonical MP2, due to the requirement to optimize the orbitals iteratively.

In κ-OOMP2, one modifies the Hylleraas functional by damping the two-electron integrals via $\langle ab||ij\rangle \longleftarrow \langle ab||ij\rangle \left(1 - \exp\left(-\kappa\Delta_{ij}^{ab}\right)\right)$ such that the MP2 amplitudes t are modified as

$$t_{ij}^{ab} = \frac{\langle ab||ij\rangle}{\Delta_{ij}^{ab}}\left(1 - \exp\left(-\kappa\Delta_{ij}^{ab}\right)\right), \tag{3.14}$$

Here $\Delta_{ij}^{ab} = \epsilon_a + \epsilon_b - \epsilon_i - \epsilon_j$ in terms of orbital energies, ϵ, of virtual levels, a, b and occupied levels, i, j. These regularized amplitudes lead to the regularized MP2 (κ-MP2) energy expression

$$E_{\kappa\text{-MP2}} = -\frac{1}{4}\sum_{ijab}\frac{|\,\langle ab||ij\rangle\,|^2}{\Delta_{ij}^{ab}}\left(1 - \exp\left(-\kappa\Delta_{ij}^{ab}\right)\right)^2, \tag{3.15}$$

If $\Delta_{ij}^{ab} \to 0$, $t_{ij}^{ab} \to \kappa\,\langle ab||ij\rangle$ instead of ∞, and the corresponding correlation energy contribution tends to zero. This has the obvious advantage that systems with near-degenerate energy levels can be treated, which is problematic with unregularized MP2.[233] The removal of divergence can, in fact, be achieved by a rather simple linear shift as well.[185, 231] The particular form in Eq. 4.12 was chosen not only to regularize the offending energy denominator but also to maintain the well-behaved correlation energy contribution coming from large denominators. When combined with orbital optimization, such an energy-dependent regularizer was found to be essential to outperform unregularized MP2 and OOMP2 over a handful of benchmark sets while restoring the Coulson-Fischer point.[233, 236] Since κ-OOMP2 has displayed a propensity of attenuating the overestimation of electron correlation that canonical MP2 exhibits, κ-OOMP2 is a promising approach to improve the performance of MP2 in the calculation of magnetizability tensors.

Our κ-OOMP2 code uses the resolution-of-the-identity (RI) approximation throughout.[233] In this approach, the fitting basis is a regular Gaussian-type basis and not a GIAO basis, because otherwise the crucial requirement of gauge-independence cannot be met.[212] The Resolution-of-the-Identity approximation has been used before in combination with

MP2 for the calculation of NMR shielding tensors[212, 257] and magnetizabilities.[222] The errors of the RI approximation have been shown to be negligible throughout. The energy before the first orbital-optimization cycle is the RI-MP2 energy, which allows us to calculate magnetizabilities at the RI-MP2 level of theory as well.

3.2.4 Implementation and Code Verification

We have implemented all one- and two-electron integrals given in Section 4.2.2 and κ-OOMP2 using GIAOs in the integral library `libqints` in a developer's version of Q-Chem 5[173, 258] Our code is able to run complex-restricted[234, 235] and complex-general[186, 259] SCF procedures as implemented in `libgscf` and `libgmbpt`, the latter of which is important for the calculation of indirect spin-spin coupling constants (to be presented in a future publication).

In a first step, the matrix elements were tested in order to verify our code. The overlap matrix elements were tested against reference results obtained *via* Mathematica.[260] The Mathematica code for the overlap integrals [261] was adapted for GIAOs; although the kinetic energy integrals can be decomposed to the already verified overlap integrals, the former were tested separately against Mathematica references[262] that were again adjusted for GIAOs. A similar procedure was carried out for nuclear attraction integrals, for which numerical Mathematica references[263] with GIAOs were generated. The diamagnetic magnetizability and the paramagnetic shielding integrals, which are needed in the calculation of the magnetizability tensor, were also implemented in Mathematica to verify our implementation of the relations given in the Appendix. To test the electron repulsion integrals, we implemented both the THO66[247] and the HGP88[252] algorithms in Q-Chem, both for 2-electron-4-center and 2-electron-3-center integrals. Both codes give matching values for any applied magnetic field.

As another (weak) test of the implementation we verified that the overlap, nuclear attraction, kinetic energy and electron repulsion integrals reduce to the results of regular Gaussian type orbitals at zero magnetic field. In the case of the diamagnetic magnetizability and paramagnetic shielding integrals the results are trivially zero if no magnetic field is applied.

In the second verification step, magnetizabilities at the Hartree-Fock level were tested against the Dalton program package.[264] Magnetizabilities at the RI-MP2 level with very large auxiliary basis sets were tested against MP2 results obtained *via* CFOUR.[265] CFOUR was also employed to generate CCSD and CCSD(T) results against which the various MP2 methods can be assessed.

In the third verification step, magnetizabilities at the κ-OOMP2 level were tested at its two limits: $\kappa = 0$ against those at the Hartree-Fock level and $\kappa = \infty$ against those at the OOMP2 level.

3.2.5 Numerical Accuracy of Finite Differences Magnetizability

To evaluate the numerical accuracy of the finite difference scheme, we tested the finite difference HF and RI-MP2 magnetizabilities of various small molecules against analytical HF

and MP2 magnetizabilities obtained via CFOUR. The general issue in choosing an acceptable step size is avoiding numerical noise from limited precision in the energy (step size not too small) whilst also avoiding contamination from higher derivatives the target second order property (step size not too big). We chose C_2H_4 as an example of molecules with small HOMO-LUMO gaps that might be prone to contamination from higher order terms with larger step sizes; H_4C_2O as the largest molecule in the test set that should accentuate numerical error with smaller step sizes; and lastly LiH as an in-between molecule with moderate gap and small size. The cc-pVDZ, aug-cc-pVDZ, and cc-pVTZ basis sets were tested in this manner. The SCF convergence criteria was 10^{-11} a.u., and the cutoff threshold for two electron integrals was 10^{-14} a.u.

In Table 3.1 we present the % error for HF magnetizabilities for the three aforementioned molecules. With the second order finite difference scheme, the optimal step size 10^{-3} a.u. for C_2H_4 and H_4C_2O leads to errors on the order of 10^{-4}% or less for all three basis sets tested; whereas the optimal step size 10^{-4} a.u. for LiH leads to % errors on the order of 10^{-5}% for the cc-pVDZ and cc-pVTZ basis sets, and we observe a shift in aug-cc-pVDZ: the optimal step size 10^{-5} a.u. leads to % error on the order of 10^{-4}%. Overall these results are encouraging because a step size of either 10^{-3} or 10^{-4} is acceptable for all three molecules in all three basis sets.

Table 3.1: Numerical performance of the 2nd order finite difference scheme for the magnetizability of three molecules with varying step size. Values shown as percentage error for Hartree-Fock in 3 basis sets. Reference values were calculated analytically at the same level of theory.

Molecule	B field step size (log_{10} a.u.)						
	-6	-5	-4	-3	-2	-1	0
				cc-pVDZ			
C_2H_4	-16.17	-0.0215	0.0015	0.0001	0.0102	0.8680	-40.29
H_4C_2O	21.94	-0.0671	-0.0002	-0.0001	-0.0147	-2.4506	-6.89
LiH	0.2805	0.0037	0.00003	-0.0001	-0.0110	-1.0189	-11.6254
				aug-cc-pVDZ			
C_2H_4	-0.0910	-0.1765	0.0027	-0.00002	-0.0011	0.3695	-44.6909
H_4C_2O	-20.8518	-0.1618	-0.0002	-0.0002	-0.0232	-1.7756	-75.7206
LiH	-3.0791	0.0002	0.0048	0.0043	-0.0342	-3.1063	-1.3800
				cc-pVTZ			
C_2H_4	-5.5078	-0.1462	0.0017	0.0001	0.0084	0.7034	9.7808
H_4C_2O	16.0834	0.0573	-0.0005	-0.0002	-0.0158	-1.6033	-3.1721
LiH	-3.0657	0.0127	-0.00004	-0.0003	-0.0363	-3.2028	1.8863

The assessment of the numerical accuracy of our finite difference RI-MP2 implementa-

tion of the magnetizability is more complicated, since the RI approximation constitutes an additional error source (CFOUR is using exact integrals). To disentangle the RI error from the error of the numerical procedure, we tested two different auxiliary basis sets (rimp2-cc-pVDZ and rimp2-aug-cc-pVTZ) for the C_2H_4 and H_4C_2O molecules (Tables 3.2 and 3.3). The smaller rimp2-cc-pVDZ basis reveals error limits associated with the RI approximation. With the larger aug-cc-pVDZ and cc-pVTZ basis sets, applying the rimp2-aug-cc-pVTZ auxiliary basis leads to as least an order of magnitude of error improvement. For all three AO basis sets, using rimp2-aug-cc-pVTZ and either 2^{nd} or 4^{th} order finite difference, at least two orders of magnitude in the B field can be identified that deliver errors better than 10^{-2}%. Encouragingly, the optimal range of fields does not appear to depend strongly on the AO basis set for the choices we will use in this work.

Table 3.2: Numerical performance of the finite difference scheme of 2^{nd} or 4^{th} order (FD order) for the magnetizability of C_2H_4 with varying step size. Values shown as percentage error of RI-MP2 with cc-pVDZ, aug-cc-pVDZ, and cc-pVTZ; and respectively with two different auxiliary basis sets. Reference values were calculated analytically at the MP2 level of theory with the respective basis sets.

Auxiliary basis set	FD order	B field step size (log_{10} a.u.)						
		-6	-5	-4	-3	-2	-1	0
		cc-pVDZ						
rimp2-cc-pVDZ	2	-12.60	-0.0923	-0.0516	-0.0520	-0.0398	1.0116	-38.98
	4	15.75	-0.0837	-0.0464	-0.0521	-0.0521	0.4620	-35.74
rimp2-aug-cc-pVTZ	2	0.9320	-0.3822	-0.0040	-0.0006	-0.0116	1.0567	-40.30
	4	5.871	0.3780	-0.0016	-0.0007	-0.0006	0.5108	-35.16
		aug-cc-pVDZ						
rimp2-cc-pVDZ	2	29.35	-0.3405	-0.0835	-0.0825	-0.0830	0.5057	-43.59
	4	30.39	-0.4837	-0.0804	-0.0825	-0.0839	0.1920	-22.78
rimp2-aug-cc-pVTZ	2	21.46	0.5108	-0.00004	-0.0017	-0.0027	0.5677	-18.82
	4	220.16	0.0478	-0.0029	-0.0017	-0.0031	0.2606	-163.75
		cc-pVTZ						
rimp2-cc-pVDZ	2	50.08	-0.4886	-0.1200	-0.1186	-0.1080	0.8054	16.90
	4	-54.40	-0.4137	-0.1140	-0.1188	-0.1186	0.3506	44.95
rimp2-aug-cc-pVTZ	2	46.44	-0.1503	-0.0066	-0.0060	0.0044	0.9000	1.91
	4	-42.84	0.0659	-0.0080	-0.0061	-0.0061	0.4562	0.20

Overall we recommend using the step size of 10^{-3} a.u. and the 2^{nd} order finite difference scheme, since this combination delivers a satisfying compromise between accuracy and computational cost throughout. Perhaps surprisingly, the relatively small rimp2-cc-pVDZ auxiliary basis set when paired with either of the three AO basis sets (cc-pVDZ, aug-cc-pVDZ, cc-pVTZ) appears to be accurate enough for most applications from a numerical

Table 3.3: Numerical performance of the finite difference scheme of 2nd or 4th order (FD order) for the magnetizability of H_4C_2O with varying step size. Values shown as percentage error of RI-MP2with cc-pVDZ, aug-cc-pVDZ, and cc-pVTZ; and respectively with two different auxiliary basis sets. Reference values were calculated analytically at the MP2 level of theory with the respective basis sets.

Auxiliary basis set	FD order	B field step size (log_{10} a.u.)						
		-6	-5	-4	-3	-2	-1	0
		cc-pVDZ						
rimp2-cc-pVDZ	2	22.69	-0.0868	-0.0242	-0.0241	-0.0372	-1.4077	-7.84
	4	6.87	-0.0202	-0.0214	-0.0240	-0.0240	0.1199	-27.83
rimp2-aug-cc-pVTZ	2	-40.04	0.0881	-0.0027	-0.0007	-0.0139	-1.3868	-25.89
	4	12.98	0.2546	-0.0001	-0.0006	-0.0006	0.1421	39.07
		aug-cc-pVDZ						
rimp2-cc-pVDZ	2	27.00	0.0308	-0.0343	-0.0300	-0.0512	-1.7195	-73.74
	4	264.99	0.3917	-0.0284	-0.0299	-0.0306	-0.0700	12.35
rimp2-aug-cc-pVTZ	2	56.31	-0.3953	0.0015	-0.0013	-0.0227	-1.6985	-72.59
	4	304.88	0.4405	-0.0089	-0.0012	-0.0020	-0.0467	76.66
		cc-pVTZ						
rimp2-cc-pVDZ	2	17.16	0.0794	-0.0136	-0.0136	-0.0280	-1.5149	-5.61
	4	8.27	-0.1538	-0.0121	-0.0134	-0.0134	0.0875	-16.71
rimp2-aug-cc-pVTZ	2	-2.55	-0.0372	-0.0013	-0.0018	-0.0162	-1.5077	0.50
	4	8.55	-0.1455	-0.0025	-0.0017	-0.0016	0.0974	-2.83

point of view. In our applications below we will nevertheless always use the auxiliary basis set that corresponds to the chosen AO basis.

3.3 Results and Discussion

3.3.1 Accuracy of κ-OOMP2 Magnetizabilities for the Lutnæs Set

As a first assessment, we utilized the test set of 28 molecules curated by Lutnæs et al.[225] to assess the accuracy of κ-OOMP2 for isotropic magnetizabilities. In Table 3.4 we present various statistics for Hartree-Fock (HF), RI-MP2, OOMP2, and κ-OOMP2 in comparison to CCSD(T) in the aug-cc-pVTZ basis. When calculating the RMSE, MSE and the maximum error for each method, we exclude O_3, which exhibits by far the largest correlation effects because of its multireference character. This procedure is in accordance with previous benchmarking studies.[225, 226]

In terms of magnitudes, mean-field HF theory performs quite well, with nearly zero

Table 3.4: Results and statistics for HF, RI-MP2, OOMP2 and κ-OOMP2 calculations of magnetizability compared to the CCSD(T) reference with the aug-cc-pVTZ basis set, for the Lutnæs data set[225] (10^{-30} JT^{-2}). Note that ozone is excluded from the statistics, because it is a dramatic outlier for HF and MP2.

Molecule	HF	MP2	κ-MP2	OOMP2	κ-OOMP2	CCSD(T)
AlF	-401.02	-406.01	-403.43	-407.81	-404.59	-400.20
C_2H_4	-355.07	-350.16	-348.32	-349.59	-348.29	-345.94
C_3H_4	-478.33	-487.29	-484.23	-485.92	-483.39	-481.68
CH_2O	-139.72	-131.80	-135.15	-128.04	-132.96	-129.14
CH_3F	-318.60	-318.31	-318.19	-316.57	-316.94	-317.36
CH_4	-314.11	-322.03	-319.68	-322.17	-319.66	-318.40
CO	-204.95	-218.34	-215.40	-218.07	-215.12	-213.48
FCCH	-452.94	-448.91	-448.26	-448.53	-448.25	-446.61
FCN	-378.65	-376.50	-376.84	-376.11	-376.78	-374.17
H_2C_2O	-433.22	-440.90	-440.05	-440.17	-439.74	-430.82
H_2O	-231.45	-238.75	-237.05	-239.57	-237.43	-236.21
H_2S	-456.51	-468.40	-463.05	-467.91	-462.61	-461.97
H_4C_2O	-545.26	-542.17	-541.97	-538.21	-539.36	-536.25
HCN	-280.51	-278.44	-277.31	-277.32	-276.86	-275.30
HCP	-512.49	-505.57	-500.33	-504.54	-500.73	-498.39
HF	-172.89	-178.76	-177.97	-179.51	-178.48	-177.43
HFCO	-312.12	-315.12	-315.43	-315.78	-315.85	-310.64
HOF	-244.91	-242.51	-244.11	-238.35	-241.43	-237.34
LiF	-191.32	-198.57	-197.02	-199.71	-197.6	-197.01
LiH	-125.72	-127.04	-122.59	-127.22	-122.71	-129.30
N_2	-203.10	-210.57	-208.46	-209.82	-207.93	-206.15
N_2O	-343.15	-345.39	-345.64	-342.05	-344.05	-340.67
NH_3	-287.56	-294.80	-292.39	-295.23	-292.46	-291.19
O_3	581.49	-637.00	-360.72	-34.59	73.76	112.39
OCS	-598.87	-597.22	-597.26	-592.65	-595.38	-591.09
OF_2	-271.88	-252.39	-258.43	-237.10	-250.43	-249.58
PN	-302.34	-333.65	-324.46	-324.05	-319.92	-314.90
SO_2	-304.00	-336.73	-334.44	-339.45	-334.6	-324.38
RMSE	8.63	6.22	4.93	4.92	3.89	
MSE	-0.93	-4.84	-3.40	-3.18	-2.52	
MaxE	22.30	18.75	10.01	15.07	10.22	

mean signed error (MSE), indicating no systematic over or under-estimation. Comparing HF with CCSD(T), it is evident that correlation effects are relatively small, on the order of a few percent (with the conspicuous exception of ozone). The performance of MP2, as noted previously,[222] is disappointing. The MSE increases by a factor of 5 relative to HF, and the RMS error is reduced by only 28 %. Ten cases show significant overcorrection, and disturbingly, there are four cases where MP2 corrects in the wrong direction.

Orbital optimization with MP2 significantly improves the results for magnetizabilities. Whilst OOMP2 is a method that typically exaggerates electron correlation effects,[185, 233] OOMP2 magnetizabilities nevertheless show improvements in both MSE and RMSE relative to MP2 itself. κ-OOMP2 reduces over-correlation effects in OOMP2 via the use of energy-dependent regularization (Eq. 4.13). As seen in Table 3.4, using the recommended parameter[167] ($\kappa = 1.45$) provides significant further improvement relative to OOMP2. At the κ-OOMP2 level, the maximum and RMS errors are both reduced by more than a factor of 2 relative to HF. Relative to MP2 the main improvement is in the ten cases that showed significant overcorrection; the four cases that MP2 corrects in the wrong direction remain.

Finally, it is useful to assess the role of regularization using the unmodified HF orbitals (i.e. the κ-MP2 column of Table 3.4, again using $\kappa = 1.45$). The improvement of κ-MP2 relative to MP2 is on par with the improvement of κ-OOMP2 relative to OOMP2. At $\kappa = 1.45$, κ-MP2 has similar RMSE and slightly larger MSE than OOMP2, while the max error is significantly reduced, even more so than for κ-OOMP2. Of course κ-MP2 has the benefit of shedding the iterative cost of OOMP2, but it is interesting that the improvements from regularization (κ-MP2) and orbital optimization (OOMP2) are synergistic: κ-OOMP2 is clearly the best-performer of the 4 MP2-based approaches.

It is encouraging that κ-OOMP2 significantly improves upon MP2 for magnetizabilities using the regularization parameter ($\kappa = 1.45$) chosen without reference to this property. To explore the extent to which further improvement is possible, Figure 3.1 displays how the κ-OOMP2 errors on this 27-molecule dataset vary as a function of κ. Note that $\kappa = 0$ (left edge) is HF, and $\kappa \to \infty$ is OOMP2, so strong regularization is to the left of the figure, whilst weak is to the right. It is evident that modest improvements in magnetizabilities beyond the $\kappa = 1.45$ results are obtained by decreasing κ to about 1.2, which corresponds to somewhat stronger damping of electron correlation effects. However, the κ dependence is sufficiently weak that we recommend using the existing parameter. κ-MP2 has qualitatively similar behaviour as κ-OOMP2, but with slightly worse performance for all 3 statistical measures.

3.3.2 Accuracy of κ-OOMP2 Magnetizabilities for Conjugated Cyclic Molecules

As one additional assessment of the performance of this set of quantum chemical methods, we revisit the magnetizability anisotropies of a set of aromatic molecules that were previously examined at the HF level.[203] These species exhibit greater electron delocalization than the small molecules discussed above, and therefore have larger magnetizabilities. For planar

Figure 3.1: Variation of the κ value in κ-MP2 and κ-OOMP2 and its effect on performance on the 27-molecule test set

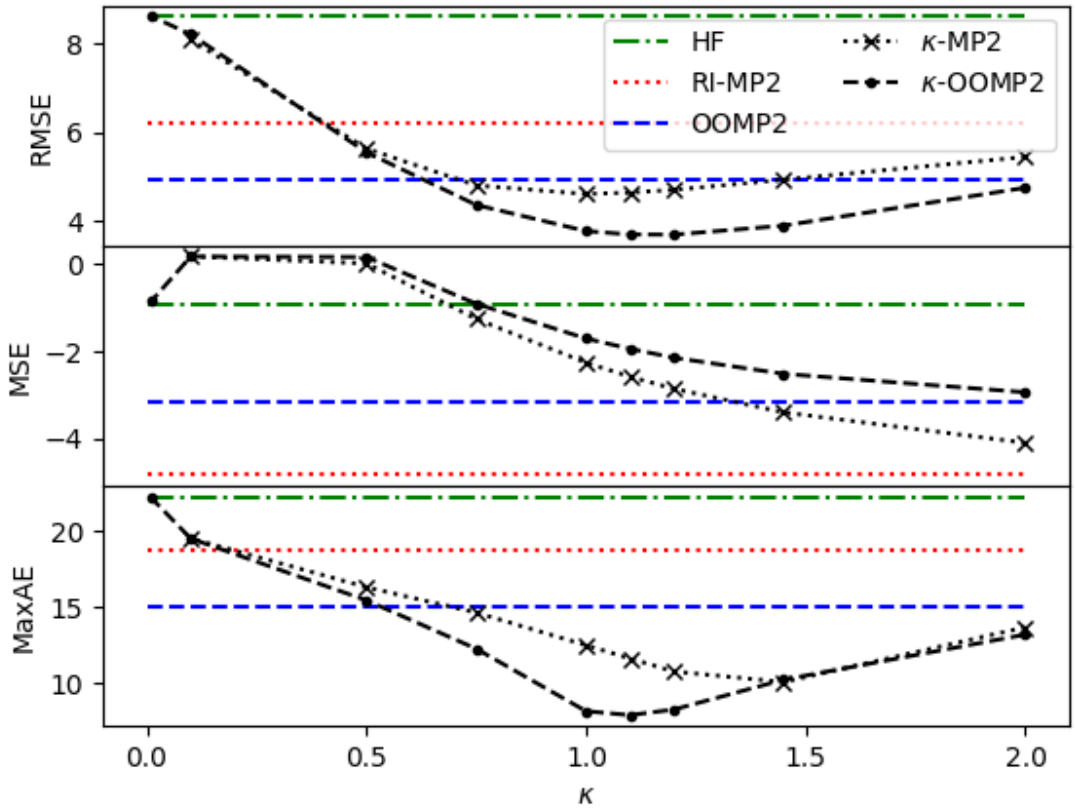

molecules (in the xy plane), the magnetizability anisotropy is defined as

$$\xi_{\text{aniso}} = \xi_{zz} - \frac{1}{2}\left(\xi_{xx} + \xi_{yy}\right) \tag{3.16}$$

As shown in Table 3.5, HF anisotropies with the relatively small aug-cc-pVDZ basis set perform quite well relative to experiment, presumably due to fortuitous cancellation between basis set incompleteness effects and neglect of electron correlation. Nevertheless, at least for aromatic species like these, the aug-cc-pVDZ basis set appears to be quite useful for calculations at the HF level. Basis set incompleteness effects are clearly evident by comparing HF against CCSD(T) relative to experiment: the HF result agrees better in 4 of the 6 cases.

On the other hand, with the larger cc-pVTZ basis set, CCSD(T) compares quite favorably to experiment in most cases (Table 3.6), except for pyridine and to a lesser extent cyclopentadiene. Due to the often unreliable error bars and inaccuracies associated with these

Table 3.5: Calculated magnetizability anisotropies for various conjugated molecules using the aug-cc-pVDZ basis, and and experimental values (10^{-30} JT^{-2}). Deviations are evaluated with respect to the CCSD(T) results.

Molecule	HF	MP2	OOMP2	κ-OOMP2	CCSD	CCSD(T)	exp.
benzene	-1061.26	-939.85	-922.15	-951.55	-905.92	-878.79	-1036±40 [266]
pyridine	-1079.05	-1033.0	-1007.04	-1037.1	-1012.67	-993.19	-953±12 [267]
furan	-644.59	-702.74	-702.31	-691.76	-654.65	-660.30	-643±8 [268]
thiophene	-854.57	-927.42	-930.06	-907.08	-863.56	-871.27	-832±18 [268]
1,3-dioxol-2-one	-242.01	-253.65	-249.35	-250.39	-241.54	-244.136	-240±20 [209]
cyclopentadiene	-558.40	-601.50	-609.76	-593.32	-554.20	-561.91	-570±5 [209]
RMSE	82.88	44.58	40.02	41.87	14.57		
MSE	38.38	41.43	35.18	36.93	3.82		

Table 3.6: Calculated and experimental magnetizability anisotropies for various conjugated molecules. cc-pVTZ unless otherwise noted. Statistics calculated against CCSD(T) (10^{-30} JT^{-2})

Molecule	HF	MP2	OOMP2	κ-OOMP2	CCSD	CCSD(T)	exp.
benzene	-1125.54	-1069.91	-1056.94	-1081.22	-1047.36	-1027.63	-1036±40 [266]
pyridine	-1077.14	-1029.05	-1003.57	-1032.58	-1011.74	-990.68	-953±12 [267]
furan	-633.38	-681.06	-677.95	-669.79	-634.07	-639.10	-643±8 [268]
thiophene	-841.75	-900.07	-899.71	-880.66	-837.80	-844.39	-832±18 [268]
1,3-dioxol-2-one	-239.20	-248.32	-244.00	-244.33	-234.89	-237.40	-234±20 [78]
cyclopentadiene	-553.19	-593.19	-598.75	-584.89	-547.30	-554.69	-570±5 [78]
RMSE	53.40	40.25	35.54	36.16	12.67		
MSE	29.39	37.95	31.17	33.26	3.21		

historical experimental data [203, 210], as well as possible remaining basis set limitations, we shall instead compare the various wavefunction-based methods relative to CCSD(T) for the remainder of this section. The mean and RMS errors for these magnetizability anisotropies relative to CCSD(T) are presented in Table 3.6. Additionally, the corresponding statistics for isotropic magnetizabilities are presented in Table 3.7.

Comparing the magnetizability anisotropies at the HF vs MP2 vs CCSD(T) levels shows that in 4 of the 6 cases, MP2 and OOMP2 overcorrect for correlation effects. These 4 cases (furan, thiophene, 1,3-dioxol-2-one, and cyclopentadiene) are therefore improved by regularization via κ-OOMP2. These 4 cases also shows strikingly small correlation at this level of basis. In the two remaining cases (benzene and pyridine) MP2 and OOMP2 undercorrect relative to CCSD(T), with orbital optimization significantly improving upon the MP2 result. This undercorrection is quite significant. Regularization, which attenuates correlation

Table 3.7: Calculated isotropic magnetizability for various conjugated molecules evaluated in the cc-pVTZ basis (10^{-30} JT^{-2}). Error statistics are given relative to the CCSD(T) results.

Molecule	HF	MP2	κ-MP2	OOMP2	κ-OOMP2	CCSD	CCSD(T)
benzene	-999.36	-964.01	-972.68	-959.99	-971.39	-966.65	-954.09
pyridine	-880.70	-854.52	-862.74	-846.68	-859.40	-858.10	-845.74
furan	-747.79	-759.08	-757.69	-757.09	-756.52	-749.01	-756.54
thiophene	-993.86	-1004.85	-1000.94	-1001.93	-999.46	-987.78	-984.79
1,3-dioxol-2-one	-690.34	-685.18	-687.34	-680.15	-684.81	-682.78	-679.08
cyclopentadiene	-782.81	-794.88	-791.57	-793.97	-791.01	-783.26	-781.37
RMSE	24.36	11.58	13.35	9.03	11.74	8.10	
MSE	15.54	10.15	11.89	6.37	10.16	4.33	

effects associated with the smallest orbital gaps, therefore worsens the benzene and pyridine results. Interestingly, OOMP2 closely approaches CCSD for the benzene and pyridine cases, in contrast to overcorrelating for the other 4 cases.

Isotropic magnetizabilities show slightly different trends. Benzene and pyridine displays smaller correlation effects, around half that of the anisotropic magnetizabilities, whereas the other three molecules (furan, thiophene, 1,3-dioxol-2-one) shows slightly larger correlation effects. Cyclopentadiene shows strikingly small correlation, similar to the anisotropic case. Comparing the isotropic magnetizability at the HF vs MP2 vs CCSD(T) levels, instead of two distinct groups, we observe several distinct behaviours. For benzene and pyridine, MP2 again undercorrects relative to CCSD(T); orbital optimization via OOMP2 significantly improves upon the MP2 result, and even closely approaches CCSD(T). Regularization degrades the MP2 and OOMP2 results. For furan, MP2 overcorrects slightly relative to CCSD(T), while orbital optimization tempers the correlation contribution. For 1,3-dioxol-2-one, MP2 undercorrects relative to CCSD(T), while orbital optimization increases the correlation contribution. In these four molecules, OOMP2 performs surprisingly well relative to CCSD(T). Except for furan, regularization worsens the results for the other three molecules. In contrast, for thiophene, the MP2 correlation contribution has the wrong sign relative to CCSD(T); orbital optimization decreases the correlation contribution but retains the wrong sign.

Given the considerations mentioned above, it is clear that regularization of either the MP2 results for these conjugated species cannot give significant overall improvements since the two largest outliers are cases where correlation effects are underestimated with MP2 and OOMP2. Overall, the statistics suggest that MP2 moderately improves upon HF, reducing the RMSE for the magnetizability anisotropy by roughly 20%; and the isotropic magnetizability by roughly 50%. We also observe that all 4 MP2 methods give higher MSE than HF for anisotropy, similar to the results in Figure 3.1; whereas for the isotropic results, all 4 MP2 methods give lower MSE than HF, particularly OOMP2, which had more than half the MSE of HF's. Relative to MP2, there is a slight overall improvement with OOMP2 and an even

smaller improvement with κ-OOMP2 (Table 3.6).

3.3.3 Evaluation of magnetizability exaltations in cyclic conjugated molecules

Other than energetic stabilization and geometric symmetry breaking, magnetizability exaltations have been suggested as a gauge for aromaticity and anti-aromaticity.[204–206] Qualitatively, with electron delocalization around a ring, the magnetizability perpendicular to the ring, and hence the isotropic magnetizability as well, should be enhanced relative to expected values due to the associated ring current. This exaltation provides a measure of aromaticity that is complementary to the susceptibility anisotropy discussed in the previous subsection. Of course, to define the exaltation of the magnetizability, it is also essential to have a reference. Traditionally, this reference is a theoretical molecule with the same bond structure but without conjugation. For example, benzene's reference would be the theoretical cyclo-hexatriene. Two conventions for calculating the magnetizability for these theoretical molecules have been employed. One is the Pascal system of atomic constants[269], and the other is the Haberditzl semiempirical increment system[270]. The Pascal and Haberditzl systems suffer from accuracy issues related to heteroatoms, small rings, non-cylindrical molecules, and charge[271]; missing constants or bond types also exclude novel systems from consideration, while the bond increment systems focuses on a single Lewis structure of the hypothetical non-aromatic ring system. Partly for these reasons, magnetizability exaltation has fallen out of favor as a criterion for aromaticity over the past 25 years. Indeed a recent review[272] commented that "due to the difficulty in quantifying aromaticity using this method and the need for an empirical reference, together with the development of computational methods that allow a more detailed and direct study of the magnetic properties, in a qualitative and quantitative fashion, this method is rarely used."

Modern alternative computational methods include those based on nucleus-independent chemical shifts[206] and those based on visualizing the current density.[273] While indeed these are valuable approaches, it is worth pointing out that magnetizability exaltations need not rely on empirical references. Here we will define the out-of-plane magnetizability exaltation as the difference between the out-of-plane component of the magnetizability tensor (ξ_{zz}) of the aromatic molecule and that of a suitably chosen open chain analog with the same number of formal double bonds and lone pairs. Experimental comparison remains a possibility when susceptibility data for both ring and chain molecules is available. As a simple example, the open chain reference for benzene is hexatriene, $H_2C{=}CH{-}CH{=}CH{-}CH{=}CH_2$. Of course such references are typically not unique – even hexatriene has multiple conformations, though the all-trans form is a natural choice. Other molecules present more interesting alternative open chain references; for instance, we shall later examine N_2S_2 for which HNSNSH and H_2NSNS are both possible. The out-of-plane exaltation aims to single out the ring current effect by accounting for similar Lewis structures in both the aromatic rings and their open chain counterparts.

Aromatic, non-aromatic, and anti-aromatic molecules are expected to display large negative, around zero, and large positive exaltations respectively. Here we investigate small ring molecules with 2, 4, and 6 π electrons. All structures were optimized with ωB97M-V[274]/def2-TZVPDD.[275] In Table 3.8 we present out-of-plane magnetizability exaltations calculated with HF, MP2, κ-OOMP2, as well as CCSD and CCSD(T). Where different possible open chain references exist, our choice is specified (in some cases we will explore two alternative choices to assess the sensitivity of the exaltations to different reasonable choices of reference). Since our objective here is qualitative, the small cc-pVDZ basis was used for these calculations.

Starting with 6 π electrons, in addition to benzene, thiophene (C_4H_4S), cyclopentadiene anion ($C_5H_5^-$), and pyridine (C_5H_5N) all display the expected large negative magnetizability exaltations, associated with ring currents. In contrast, disulfur dinitride (N_2S_2) behaves as weakly anti-aromatic under the exaltation criteria, relative to the open-chain reference, HNSNSH. Interestingly, the results are virtually unchanged when using the alternative open-chain reference, H_2NSNS. It appears that the two straight chain isomers display similar if not more delocalization than the N_2S_2 ring itself. In addition, calculated at the CCSD(T)/cc-pVTZ level, N_2S_2 has a magnetizability anisotropy of 67.0 10^{-30} JT^{-2}, which is much different from the normally large anisotropy that aromatic molecules possess. N_2S_2 has been previously characterized as weakly aromatic,[276, 277] based on structural, energetic and chemical shift criteria. In simple terms, N_2S_2 is closer to 2-electron aromaticity than 6-electron aromaticity, because the two highest orbitals are essentially in and out of phase linear combinations of π-type lone pair orbitals on the two S atoms, giving bond order 1.25 for the N$-$S bonds. By contrast, other researchers had argued that N_2S_2 has diradicaloid character, for instance based on classical valence bond analysis[278]. On magnetizability grounds, N_2S_2 appears to continue to be an unconventional molecule.

Moving on to 4 π electron systems, cyclobutadiene, being the classic anti-aromatic molecule, displays a large positive exaltation as expected. Likewise, $C_5H_5^+$ also displays a very large positive exaltation. In contrast C_2H_2O, when considering the 70 kcal/mol more stable and electronically more similar $H_2CC(H)OH$ isomer, is predicted to be non-aromatic. For the group of molecules with 2 π electrons, all 4 molecules are predicted to be aromatic, with exaltations comparable to benzene and pyradine if normalized by π electron count.

We also consider cyclopentadiene C_5H_6, which was presented as an illustration against using out-of-plane magnetizability exaltation as an aromaticity criteria [279]. With our method, against both planar s-cis and trans isomers of 1,3-pentadiene, cyclopentadiene displays moderate negative exaltation, around 35 to 50% of benzene's. This suggests that not all of the exaltation results from the ring current effect, as the aforementioned authors stated[279]; nonetheless, given the difference in magnitude, out-of-plane magnetizability exaltation remains to appear to be a useful gauge of aromaticity.

Finally, it is interesting to briefly examine the effect of electron correlation on the magnetizability exaltations. Overall most of the studied molecules with strong magnetizability exaltations display small correlation contributions, of most around 10%, with the striking exception of $C_5H_5^+$. For $C_5H_5^+$, MP2 and κ-OOMP2 provide relatively consistent exaltations,

Table 3.8: Magnetizability exaltations for various molecules with 0, 2, or 6 π electrons calculated in the cc-pVDZ basis (10^{-30} J T^{-2}).

Molecule	Straight chain analog	HF	RI-MP2	κ-OOMP2	CCSD	CCSD(T)
		2 π electrons				
$C_2H_2N^+$	$H_2CC(H)NH$	-54.90	-69.94	-68.42	-65.75	-67.16
	H_2CNCH_2	-234.69	-228.11	-228.74	-221.42	-220.76
$C_3H_3^+$	$H_3CCCH_2^+$	-228.39	-221.02	-221.55	-221.07	-218.99
	$H_2CC(H)CH_2^+$	-47.89	-53.64	-53.10	-51.43	-52.24
CN_2H^+	$HNNCH_2$	-209.93	-205.27	-206.20	-200.96	-200.32
N_3^+		-213.45	-179.99	-189.82	-190.88	-188.09
		4 π electrons				
C_2H_2O	H_2COCH_2	-81.83	-37.54	-24.46	-42.24	-34.71
	$H_2CC(H)OH$	44.27	72.04	86.43	68.48	72.20
C_4H_4	s-trans	743.50	734.72	748.73	640.29	648.11
$C_5H_5^+$	s-cis	1209.29	1961.63	2027.48	1472.01	1598.06
	trans	1323.18	2100.45	2157.77	1596.96	1727.93
C_5H_6	trans 1,3 pentadiene	-175.40	-214.97	-207.72	-181.69	-186.87
	planar s-cis 1,3 pentadiene	-238.96	-296.12	-284.92	-256.29	-265.05
		6 π electrons				
S_2N_2	$SNSNH_2$	152.35	382.44	326.57	261.66	303.17
	HSNSNH	148.76	395.43	340.31	271.87	318.70
$C_5H_5^-$	cis	-718.63	-727.35	-729.51	-708.17	-704.59
	trans	-605.72	-606.83	-606.66	-592.97	-589.94
C_5H_5N	NCCCC	-521.11	-487.88	-491.27	-475.28	-456.70
	CCNCC	-511.46	-463.03	-468.09	-453.73	-432.74
C_6H_6	trans	-601.10	-546.79	-558.10	-534.88	-514.56

and the correlation contribution from both methods is around half of the exaltation from HF. The cause of this difference is in the magnetizability calculation of the ring molecule, where the χ_{zz} computed from CCSD(T) is more than twice that of HF. The exaltation calculated from CCSD(T) for $C_5H_5^+$ is qualitatively consistent with both RI-MP2 and κ-OOMP2.

3.4 Conclusions

In this work we have reported a new finite field implementation of magnetic properties, using gauge-including atomic orbitals, and applied it to the evaluation of magnetizabilities. This required development of software to implement the complex matrix elements, and to enable evaluation of energies using complex orbitals and amplitudes, as a consequence of the matrix elements. In return for overcoming those challenges, analytic derivatives are not required, and thus it is possible to assess the performance of new or uncommon electronic structure methods more readily.

As an illustration, we have reported tests of orbital optimized MP2 (OOMP2), and

a recently proposed regularized OOMP2 method (κ-OOMP2) for magnetizabilities. These results for small molecules in the aug-cc-pVTZ basis show that κ-OOMP2 generally provides a significant improvement over MP2 itself, as well as over OOMP2, for magnetizabilities. However, it does not approach the accuracy of high-quality coupled cluster methods, such as CCSD(T). Results for isotropic magnetizabilities and magnetizability anisotropies for a set of 6 conjugated cyclic species in the smaller cc-pVTZ basis show smaller improvements with regularization for κ-OOMP2 over MP2, and no overall improvement relative to OOMP2.

Additionally we reexamined an old aromaticity criteria: the out-of-plane magnetizability exaltation. Using a single straight chain molecule as reference instead of increment systems or empirical tables allows one to consider the difference in electronic structure and its underlying effects. We then applied this new regime on a set of aromatic and anti-aromatic molecules. These calculations proved interesting in several respects. First, while large negative exaltations are associated with aromaticity, we found one nominally aromatic species, N_2S_2, which displays a positive exaltation. This may rekindle debate about its aromaticity. Second, we found that errors in HF, MP2, and κ-OOMP2 magnetizability exaltations are significantly larger for anti-aromatic species, for the most part, consistent with the presence of stronger correlation effects.

In terms of future work, it will be interesting to see if significant improvements in the magnetizabilities predictions can be obtained by using orbitals from either κ-OOMP2 or density functional theory together with energy evaluation at the MP3 or scaled MP3 levels. Such models have been used with very promising results for relative energies.[236, 280, 281] and the effort to adapt an efficient MP3 code work with the complex orbitals and amplitudes associated with finite applied magnetic fields should be far less than implementing analytical second derivatives. Hopefully the framework built here will be helpful for exploring this and other unconventional possibilities for accurate and reasonably efficient evaluation of molecular magnetizabilities. We also intend to complete the extensions of our implementation necessary to evaluate chemical shifts, and in due course, scalar couplings.

Appendix A: GIAO Matrix Elements of the Diamagnetic Magnetizability

To arrive at a convenient expression for matrix elements of the diamagnetic magnetizability operator, Eq. 3.9, in the complex GIAO basis associated with a finite applied **B**-field, we use the following shorthand notation for the overlap:

$$S_{\mu\nu}(l'+1) = \langle \omega_\mu | \omega_\nu(l'+1) \rangle \tag{3.17}$$

Here, l' is the polynomial power associated with the x-component of the Gaussian orbital that is a part of the GIAO ω_ν. Similarly, m' and n' are used for the y- and z-components, respectively. Hence, $S_{\mu\nu}(l'+1)$ is the overlap between GIAOs ω_μ and ω_ν with increased orbital angular momentum (x-component) of ω_ν. After some straightforward but cumbersome algebra we arrive at the following expression for matrix elements of the diamagnetic magnetizability operator given in Eq. 3.9:

$$\begin{aligned} h_{\mu\nu}^{\mathrm{DM}} =& \frac{1}{8}\big[(B_y^2+B_z^2)\left(S_{\mu\nu}(l'+2)+2R_{\nu,x}S_{\mu\nu}(l'+1)+R_{\nu,x}^2S_{\mu\nu}\right) \\ &+(B_x^2+B_z^2)\left(S_{\mu\nu}(m'+2)+2R_{\nu,y}S_{\mu\nu}(m'+1)+R_{\nu,y}^2S_{\mu\nu}\right) \\ &+(B_x^2+B_y^2)\left(S_{\mu\nu}(n'+2)+2R_{\nu,z}S_{\mu\nu}(n'+1)+R_{\nu,z}^2S_{\mu\nu}\right) \\ &-2B_xB_y\left(S_{\mu\nu}(l'+1,m'+1)+R_{\nu,y}S_{\mu\nu}(l'+1)+R_{\nu,x}S_{\mu\nu}(m'+1)+R_{\nu,x}R_{\nu,y}S_{\mu\nu}\right) \\ &-2B_xB_z\left(S_{\mu\nu}(l'+1,n'+1)+R_{\nu,z}S_{\mu\nu}(l'+1)+R_{\nu,x}S_{\mu\nu}(n'+1)+R_{\nu,x}R_{\nu,z}S_{\mu\nu}\right) \\ &-2B_yB_z\left(S_{\mu\nu}(m'+1,n'+1)+R_{\nu,z}S_{\mu\nu}(m'+1)+R_{\nu,y}S_{\mu\nu}(n'+1)+R_{\nu,y}R_{\nu,z}S_{\mu\nu}\right)\big] \end{aligned} \tag{3.18}$$

$R_{\nu,x}$, $R_{\nu,y}$ and $R_{\nu,z}$ denote the x, y and z-coordinates of the nucleus on which the GIAO ω_ν is centered.

Appendix B: GIAO Matrix Elements of the Paramagnetic Shielding

The matrix elements of the 3 spatial components of the paramagnetic shielding operator, Eq. 3.10 are given separately for clarity (though for instance the y component can be obtained as a cyclic permutation of the coordinates and the quantum numbers from the x component,

and z can be obtained similarly from y).

$$\begin{aligned} h_{\mu\nu}^{\mathrm{PS},x} = -\frac{i}{2}B_x\big[&R_{\nu,z}\left(B_y S_{\mu\nu}(n'-1) + S_{\mu\nu}(m'+1,n'-1)\right) \\ &- 2\beta\left(B_y S_{\mu\nu}(n'+1) + S_{\mu\nu}(m'+1,n'+1)\right) \\ &- \frac{i}{2}\chi_{\nu,z}\left(B_y S_{\mu\nu} + S_{\mu\nu}(m'+1)\right) \\ &- \big[R_{\nu,y}\left(B_z S_{\mu\nu}(m'-1) + S_{\mu\nu}(m'-1,n'+1)\right) \\ &+ 2\beta\left(B_z S_{\mu\nu}(m'+1) + S_{\mu\nu}(m'+1,n'+1)\right) \\ &+ \frac{i}{2}\chi_{\nu,y}\left(B_z S_{\mu\nu} + S_{\mu\nu}(n'+1)\right)\big] \end{aligned} \tag{3.19}$$

$$\begin{aligned} h_{\mu\nu}^{\mathrm{PS},y} = -\frac{i}{2}B_y\big[&R_{\nu,x}\left(B_z S_{\mu\nu}(l'-1) + S_{\mu\nu}(l'-1,n'+1)\right) \\ &- 2\beta\left(B_z S_{\mu\nu}(l'+1) + S_{\mu\nu}(l'+1,n'+1)\right) \\ &- \frac{i}{2}\chi_{\nu,x}\left(B_z S_{\mu\nu} + S_{\mu\nu}(n'+1)\right) \\ &- \big[R_{\nu,z}\left(B_x S_{\mu\nu}(n'-1) + S_{\mu\nu}(l'+1,n'-1)\right) \\ &+ 2\beta\left(B_x S_{\mu\nu}(n'+1) + S_{\mu\nu}(l'+1,n'+1)\right) \\ &+ \frac{i}{2}\chi_{\nu,z}\left(B_x S_{\mu\nu} + S_{\mu\nu}(l'+1)\right)\big] \end{aligned} \tag{3.20}$$

$$\begin{aligned} h_{\mu\nu}^{\mathrm{PS},z} = -\frac{i}{2}B_z\big[&R_{\nu,y}\left(B_x S_{\mu\nu}(m'-1) + S_{\mu\nu}(l'+1,m'-1)\right) \\ &- 2\beta\left(B_x S_{\mu\nu}(m'+1) + S_{\mu\nu}(l'+1,m'+1)\right) \\ &- \frac{i}{2}\chi_{\nu,y}\left(B_x S_{\mu\nu} + S_{\mu\nu}(l'+1)\right) \\ &- \big[R_{\nu,x}\left(B_y S_{\mu\nu}(l'-1) + S_{\mu\nu}(l'-1,m'+1)\right) \\ &+ 2\beta\left(B_y S_{\mu\nu}(l'+1) + S_{\mu\nu}(l'+1,m'+1)\right) \\ &+ \frac{i}{2}\chi_{\nu,x}\left(B_y S_{\mu\nu} + S_{\mu\nu}(m'+1)\right)\big] \end{aligned} \tag{3.21}$$

In the above expressions, β is the gaussian exponent of the primitive GIAO ν and $\boldsymbol{\chi}_\nu$ is the vector

$$\boldsymbol{\chi}_\nu = \mathbf{B} \times \mathbf{R}_\nu \tag{3.22}$$

3.5 Supplementary Information

The S.I. for this data my be readily accessed from the publication source in its citation[99].

Chapter 4

An In-Silico NMR Laboratory for Nuclear Magnetic Shieldings Computed Via Finite Fields

4.1 Introduction

Nuclear magnetic resonance (NMR) spectroscopy is a widely used technique in organic chemistry and biochemistry for determining the identity and structure of molecules[282–285]. It works by applying a strong magnetic field to a sample and measuring the response of the nuclear spins in the sample to the applied field. The resulting spectrum contains information about the chemical shifts and coupling constants of the nuclei in the molecular sample, which can be used to determine the structure (and the identity) of the molecule. For large systems, structure determination from the NMR spectrum is not a straightforward task. As a result, NMR spectra prediction with quantum chemistry methods has become quite widely used in aiding the assignment of experimental spectra[201, 286–288].

To this end, a plethora of methods has been developed over the years. Lower cost methods such as Hartree-Fock (HF) theory [289] and density functional theory (DFT) provide lower accuracy approximations to chemical shifts. The level of accuracy attainable for magnetic properties using pure or hybrid density functionals is generally not considered sufficient for predictive and quantitative applications,[290, 291] in contrast to the steadily continued developments in the accuracy of DFT methods for molecular structures and relative energies[274, 292]. The basic reason for the poor performance of DFT for chemical shifts is that the standard existence theorems upon which modern functional developments are based are formally inapplicable to molecules in magnetic fields[293, 294]. One extension (CDFT) requires that the functionals depend not just upon the electron density, but also the current (or paramagnetic current (C)) density[295, 296], which is typically not done at present, though active progress continues.[297, 298] Another extension (BDFT) requires that the XC functional depends explicitly on both the density and the magnetic field (B)[299], which is

currently not widely used. Routine DFT-based calculations of NMR shieldings and chemical shifts use neither of these extensions, and nonetheless offer significantly improved accuracy over HF theory, although the accuracy of course varies significantly from functional to functional[246, 291, 297, 300–302]. Additionally, linear and sublinear scaling implementations have allowed application of DFT to large systems with more than 1000 heavy atoms[303, 304].

There is ample precedent showing that wave function-based methods based on coupled cluster (CC) theory[305, 306] are the best solution to the problem of inadequate accuracy in DFT for NMR chemical shifts. For example, RMS errors for absolute ^{13}C chemical shieldings of small molecules in the gas phase using coupled cluster with singles and doubles and perturbative triples (CCSD(T))[224] could yield a standard deviation of less than 0.8 ppm versus experiment[290]: these errors are reduced by a further factor of 5-10 or so when relative shieldings in related environments are evaluated.[291, 307–309] However there are very strong size-limitations on the applicability of CCSD(T): CCSD(T) scales as $\mathcal{O}(A^7)$ with the number of atoms, A, which limits production calculations to small molecules and small numbers of calculations. Therefore CCSD(T) has been used to provide most of the benchmark data for assessing and developing computational methods for NMR shielding that have lower compute costs.

Alternatively, second order Møller-Plesset perturbation theory (MP2) is the lowest cost post-HF method that accounts for correlation, which as already implied is essential for accurate chemical shift predictions. [290, 310, 311] MP2 has relatively low computational scaling of $\mathcal{O}(A^5)$ and offers much higher quality prediction than HF. MP2 also improves upon low-level density functionals, particularly for ^{1}H shieldings, and to a lesser degree, for ^{13}C shieldings[300]. As a result, MP2 has seen considerable development for calculating chemical shifts. These include the early z-vector approach[254], local-correlation approximation[257, 312, 313], AO-MP2[314–316], and Cholesky decomposition (CD)[317, 318]. There were efforts to improve accuracy as well, for example, spin component scaled MP2 (SCS-MP2)[319], and spin opposite scaled MP2 (SOS-MP2)[276]. The closely related double-hybrid (DH) DFT has also received attention in this context[301, 320].

Yet MP2 is known to fail dramatically when the energy gap between the highest occupied and lowest unoccupied molecular orbitals (HOMO and LUMO) becomes small, because the correlation amplitudes may diverge. Various novel approaches for relatively low-cost stabilization (or regularization) of MP2 have been developed recently, including the δ[185], σ[233], and κ[233] regularizers. In particular κ-MP2,[321] reviewed in detail below, has been shown to not just avoid divergences, but also significantly improve the accuracy of MP2 for non-bonded interactions where it exhibits large errors.[322] In a related vein, MP3, which scales as $\mathcal{O}(A^6)$, yields such disappointing results for molecular relative energies that one typically does not employ it in practice, resorting instead to the infinite order CCSD method with iterative $\mathcal{O}(A^6)$ compute cost. This problem, associated with poor convergence of the MP series, can be greatly ameliorated for non-bonded interactions by damping the third order contribution by 0.5 in the MP2.5 method, or by some variable fraction X in the MP2.X method. Such scaled MP3 approaches[323–325] have been recently shown to work

even better for relative energies using non-canonical reference orbitals[236, 280, 281].

We are interested in applying novel methods of intermediate compute cost such as those reviewed above to the calculation of NMR properties. However the shielding is a 2nd order property[201, 240], whose analytical implementation (i.e. as second order responses) is enormously challenging in terms of human labor. Selecting a new theory for painstaking implementation is a high-risk project that has historically been addressed one wavefunction method at a time. Instead, building on our recent work on magnetic susceptibilities[99], we have chosen a different approach. Here we report our implementation of an in-silico laboratory for magnetic shielding by applying finite nuclear spins at a nucleus, K, ($\mathbf{m}_K$) and magnetic fields ($\mathbf{B}$) directly to the molecular Hamiltonian:

$$\hat{H}(\mathbf{m}_K, \mathbf{B}) = \hat{H}^{(0)} + \hat{H}^{(1)}(\mathbf{m}_K, \mathbf{B}) + \hat{H}^{(2)}(\mathbf{m}_K, \mathbf{B}) \tag{4.1}$$

Here the superscript (1) indicates linear terms, and the superscript (2) indicates quadratic terms. Solving for the electronic structure energy, $E(\mathbf{m}_K, \mathbf{B})$ for different finite values of $\mathbf{B}$ and $\mathbf{m}_K$ in principle permits the evaluation of the magnetic shielding as second order finite differences, approximating the true derivative. Thus the usual laborious implementation of the analytical derivative is completely avoided. This approach has been successfully used before by other groups[214, 242, 326] for diverse purposes, including properties of molecules in strong fields, and magnetic properties. There has also been development of the first order finite difference approach to shieldings, using finite differences of gradients.[327]

The organization of the remainder of the paper is as follows. In Section 4.2, we discuss the theoretical background of the calculation of NMR shielding tensors with κ-MP2 and MP2.X, describe details of our implementation, introduce the test set from Lutnæs and coworkers,[225, 291] and evaluate the accuracy of the numerical procedure. In Section 4.3, we assess the performance of κ-MP2 and MP2.X compared to CCSD(T) reference data, using the Lutnæs test set. Finally, conclusions are given in Section 4.4.

4.2 Theoretical Background

For in-depth treatment of the quantum chemical calculation of magnetic properties, we refer interested readers to these reviews on the subject.[201, 239, 240] We will present our approach by first introducing the general design idea of our code (Section 4.2.1), then discuss the matrix elements that are required for the calculation of nuclear shieldings (Section 4.2.2). We then briefly introduce the theoretical basis of κ-MP2 and MP3 for calculating the nuclear shielding tensor (Section 4.2.3, 4.2.4). Lastly, we will discuss the implementation and verification of our code (Section 4.2.5), the data set we will employ to generate the results (Section 4.2.6), as well as the numerical performance of finite difference shieldings compared to analytical results (Section 4.2.7).

4.2.1 General Approach

The nuclear shielding $\boldsymbol{\sigma}^K$ for nucleus K is a 3x3 tensor and can be calculated as the derivative of the energy E with respect to the magnetic field $\mathbf{B}$ and the induced magnetic moment $\mathbf{m}_K$,[201] with elements

$$\sigma_{ij}^K = \left.\frac{\partial^2 E\left(\{\mathbf{R}_N\}, \mathbf{B}, \mathbf{m}_K\right)}{\partial \mathrm{m}_{K,i} \partial \mathrm{B}_j}\right|_{\mathbf{B}=\mathbf{0}, \mathbf{m}_K=\mathbf{0}} . \tag{4.2}$$

Here, $\{\mathbf{R}_N\}$ is the nuclear configuration. The isotropic shielding is $\sigma_{\mathrm{iso}} = \frac{1}{3}\mathrm{tr}(\boldsymbol{\sigma})$. The nuclear shielding tensor is related to the experimentally observed chemical shift

$$\delta = \frac{\sigma_{\mathrm{iso,ref}} - \sigma_{\mathrm{iso}}}{1 - \sigma_{\mathrm{iso,ref}}} \tag{4.3}$$

where σ_{ref} is some reference system.

We use Gauge-Including Atomic Orbitals (GIAOs),[238] also known as London orbitals, in the calculation of NMR properties to address the gauge-origin problem.[201] A GIAO ω_μ, centered on nucleus N, is given as

$$\omega_\mu(\mathbf{r}; \mathbf{A}_N) = \exp\left(-i\mathbf{A}_N \cdot \mathbf{r}\right) \cdot \chi(\mathbf{r}), \tag{4.4}$$

where $\mathbf{r}$ is the electron coordinate and $\chi(\mathbf{r})$ is a regular Gaussian-type orbital and the vector potential $\mathbf{A}_N$ is

$$\mathbf{A}_N = \frac{1}{2}\mathbf{B} \times \left(\mathbf{R}_N - \mathbf{R}_O\right). \tag{4.5}$$

$\mathbf{R}_O$ is the vector of an arbitrarily chosen gauge-origin O, which we choose to be the zero vector for convenience.

We calculate the second derivative of the energy with respect to the magnetic field and induced magnetic moment to second order *via*[241]

$$\sigma_{ij}^K = \frac{E(\Delta B_i, \Delta m_{K,j}) - E(\Delta B_i, -\Delta m_{K,j}) - E(-\Delta B_i, \Delta m_{K,j}) + E(-\Delta B_i, -\Delta m_{K,j})}{4\Delta B_i \Delta m_{K,j}} \tag{4.6}$$

ΔB_i and $\Delta m_{K,i}$ are steps in the Cartesian component i of the magnetic field and nuclear magnetic moment respectively. The magnitude of the two steps determines the accuracy of the numerical results via roundoff error and/or contamination from higher derivatives. An assessment of ΔB_i, $\Delta m_{K,i}$ and their relation to the numerical error is given in Section 4.2.7. The calculation of the nuclear shieldings *via* eq. 4.6 necessitates the calculation of several energies at different values of the magnetic field and nuclear magnetic moment. Due to the use of GIAOs, we use a fully complex-valued code throughout our calculations.

4.2.2 Required Matrix Elements

The Hamiltonian in an external magnetic field is discussed in detail in ref. 245 and an excellent overview on the calculation of matrix elements involving GIAOs can be found in ref. 246. For the sake of brevity, we will discuss only the terms in the field Hamiltonian that enter the nuclear magnetic shielding expression. The Hamiltonian with explicit dependence on the external magnetic field and nuclear magnetic moment is given by

$$\begin{aligned}\hat{H} = &-\frac{1}{2}\sum_{i}^{n}\nabla_i^2 - \sum_{i}^{n}\sum_{K}^{N}\frac{Z_K}{|\mathbf{r}_{iK}|} + \frac{1}{2}\sum_{i}^{n}\boldsymbol{B}\cdot\boldsymbol{L}_i + \alpha^2\sum_{i}^{n}\sum_{K}^{N}\frac{\boldsymbol{m}_K\cdot\boldsymbol{L}_{iK}}{r_{iK}^3} \\ &+ \frac{\alpha^2}{2}\sum_{i}^{n}\sum_{K}^{N}\frac{(\boldsymbol{B}\cdot\boldsymbol{m}_K)(\boldsymbol{r}_{iN}\cdot\boldsymbol{r}_{iK}) - (\boldsymbol{B}\cdot\boldsymbol{r}_{iK})(\boldsymbol{r}_{iN}\cdot\boldsymbol{m}_K)}{r_{iK}^3} + \sum_{i\neq j}\frac{1}{|\mathbf{r}_i - \mathbf{r}_j|}\end{aligned} \tag{4.7}$$

Indexes i, j refer to electrons, K refers to nuclei, the angular momentum operator of electron j around nucleus K is $\boldsymbol{L}_{jK} = -i\mathbf{r}_K \times \nabla_j$, and α is the fine structure constant.

The terms in the Hamiltonian are, in order, kinetic, nuclear attraction, paramagnetic shielding, paramagnetic spin-orbit, diamagnetic shielding, and electron-electron repulsion. For details on the implementation of matrix elements of GIAO matrix elements of kinetic, nuclear attraction, paramagnetic shielding, and electron-electron repulsion, we refer readers to our previous work[99].

The diamagnetic shielding (DS) operator is[245]

$$\hat{h}_i^{\mathrm{DS}} = \frac{\alpha^2}{2}\sum_{K}^{N}\left[\frac{(\boldsymbol{B}\cdot\boldsymbol{m}_K)(\boldsymbol{r}_{iN}\cdot\boldsymbol{r}_{iK}) - (\boldsymbol{B}\cdot\boldsymbol{r}_{iK})(\boldsymbol{r}_{iN}\cdot\boldsymbol{m}_K)}{r_{iK}^3}\right]. \tag{4.8}$$

The paramagnetic spin-orbit coupling (PSO) operator is [245]

$$\hat{h}_i^{\mathrm{PSO}} = \alpha^2\sum_{K}^{N}\left(\frac{\boldsymbol{m}_K\cdot\boldsymbol{L}_{iK}}{r_{iK}^3}\right). \tag{4.9}$$

After some straightforward yet cumbersome algebra, the DS and PSO operators lead to energy expressions that involve only field integrals with increased or decreased angular momentum on GIAO ω_ν. The field integrals can also be further decomposed into nuclear attraction integrals with increased or decreased angular momentum on GIAO ω_ν. (see Appendix) The first field integral based approach is much less cumbersome than using modified nuclear attraction integrals, and is used for all the results in this paper.

4.2.3 Nuclear Shieldings with κ-MP2

The following is a brief description of regularization theory and the κ regularized MP2 approach (κ-MP2), recently proposed by our group.[186, 233, 234, 321] We begin from the

textbook canonical MP2 correlation energy expression, which is given by

$$E_{\text{MP2}} = -\frac{1}{4}\sum_{ijab}\frac{|\langle ab||ij\rangle|^2}{\Delta_{ij}^{ab}} \tag{4.10}$$

Here $\Delta_{ij}^{ab} = \epsilon_a + \epsilon_b - \epsilon_i - \epsilon_j$, which is composed of sums and differences of orbital energies, ϵ, of virtual levels, a, b and occupied levels, i, j.

The above expression, Eq. 4.10, for E_{MP2}, diverges when Δ_{ij}^{ab} is small. This will be the case for metals, and is almost the case for small gap systems such as semiconductor clusters, or, in particular, some unstable reactive species, such as molecules with stretched bonds or high energy transition structures. Addressing this issue defines the regularization problem.

The simplest possible approach is to use a level shift, defining δ regularization. We thus shift the denominator Δ_{ij}^{ab} by a constant factor δ: $\Delta_{ij}^{ab} \longleftarrow \Delta_{ij}^{ab} + \delta$. This achieves the dual purpose of preventing divergence and damping MP2's over correlation. However, it was found that for the purpose of Coulson-Fischer point restoration for double and triple bond dissociations, δ had to be really large.[231] Such a large level shift deteriorates the performance of δ-MP2 for thermochemistry and other properties because it damps all correlation contributions, regardless of how close Δ_{ij}^{ab} is to zero. This is clearly not a satisfactory approach.

An alternative approach is the σ-regularizer, with the idea of adjusting the damping strength of the correlation contribution as a function of Δ_{ij}^{ab}. The σ regularized MP2 (σ-MP2) expression is given by

$$E_{\sigma\text{-MP2}} = -\frac{1}{4}\sum_{ijab}\frac{|\langle ab||ij\rangle|^2}{\Delta_{ij}^{ab}}\left(1-\exp\left(-\sigma\Delta_{ij}^{ab}\right)\right), \tag{4.11}$$

A closely related scheme is κ regularization. In κ regularized MP2 (κ-MP2), the two-electron integrals are damped via $\langle ab||ij\rangle \longleftarrow \langle ab||ij\rangle\left(1-\exp\left(-\kappa\Delta_{ij}^{ab}\right)\right)$ such that the MP2 amplitudes t are modified as

$$t_{ij}^{ab} = \frac{\langle ab||ij\rangle}{\Delta_{ij}^{ab}}\left(1-\exp\left(-\kappa\Delta_{ij}^{ab}\right)\right), \tag{4.12}$$

These regularized amplitudes lead to the κ-MP2 energy expression

$$E_{\kappa\text{-MP2}} = -\frac{1}{4}\sum_{ijab}\frac{|\langle ab||ij\rangle|^2}{\Delta_{ij}^{ab}}\left(1-\exp\left(-\kappa\Delta_{ij}^{ab}\right)\right)^2, \tag{4.13}$$

In the limit of $\Delta_{ij}^{ab} \to 0$, $t_{ij}^{ab} \to \kappa\langle ab||ij\rangle$ instead of ∞, and the corresponding correlation energy contribution is accordingly also zero. At the same time, when Δ_{ij}^{ab} is large, t_{ij}^{ab} is undamped, and the correlation contribution approaches the MP2 value. This energy-dependent regularization (small gap amplitudes strongly damped, large gap amplitudes unaffected) has been demonstrated to significantly improve chemical results for intermolecular interactions, ligand binding energies, and chemical bond and atomization energies.[321]

4.2.4 Nuclear Shieldings with MP3

Adding the next order correction in the MP series defines the MP3 method. The MP3 correlation energy is given by

$$E_{\mathrm{MP3}} = \frac{1}{8}\sum_{ijabcd}(t_{ij}^{ab})^{*}\,\langle ab||cd\rangle\,t_{ij}^{cd} + \frac{1}{8}\sum_{ijklab}(t_{ij}^{ab})^{*}\,\langle kl||ij\rangle\,t_{kl}^{ab} - \sum_{ijkabc}(t_{ij}^{ab})^{*}\,\langle kb||ic\rangle\,t_{kj}^{ac} \tag{4.14}$$

MP3 formally scales as $\mathcal{O}(A^6)$ with respect to molecule size. At the expense of some loss of accuracy, applying tensor hypercontraction (THC) techniques[328] allows a lower scaling of $\mathcal{O}(A^4)$.

From an accuracy standpoint, it is well known that MP3 often produces results that are deteriorated relative to the simpler and less computationally costly MP2 method.[179, 329] This is due to the often oscillating behaviour of the MP series, in which even orders of perturbation increases the number of electrons correlated simultaneously, while odd orders of perturbation theory recouple the existing correlation amplitudes. In effect, the odd orders temper the over-correlation which is present at even orders. However, MP3 correlation often overcorrects, resulting in an overall under-correlation. This observation has inspired several attempts to damp the third order overcorrection. Grimme proposed the SCS-MP3 method [319], where MP3 correlation contribution was scaled by 0.25 in addition to the SCS-MP2 scaling parameters. Improvements in atomization, reaction, and ionization energies were reported, in some cases approaching the quality of the more costly QCISD method. Alternatively, Hobza and coworkers proposed MP2.5 and MP2.X methods [323–325], where the MP3 correlation contribution is scaled with a single empirical parameter, c, usually less than 1. The MP2.X energy is given by

$$E_{\mathrm{MP2.X}}(c) = E_{\mathrm{HF}} + E_{\mathrm{MP2}} + cE_{\mathrm{MP3}} \tag{4.15}$$

For MP2.5 (i.e. $c = 0.5$), Hobza et al. reported significant improvements in the description of non-covalent interactions. Like κ-MP2, MP2.X has the attractive quality of having only one semi-empirical parameter.

4.2.5 Implementation and Code Verification

We have implemented all one- and two-electron integrals given in Section 4.2.2 and κ-MP2 and MP3 using GIAOs in the integral library `libqints` in a developer's version of Q-Chem 6.[173] Our code is able to run complex-restricted[186, 234] and complex-general[235, 259] SCF procedures as implemented in `libgscf` and `libgmbpt`, the latter of which is important for the calculation of indirect spin-spin coupling constants (to be presented in a future publication).

In a first step, the new matrix elements were tested in order to verify our code. Since the nuclear attraction integrals were already tested,[99] we tested the field integral based implementation against the nuclear attraction integral based implementation.

In the second verification step, nuclear shieldings at the Hartree-Fock level and at the RI-MP2 level with very large auxiliary basis sets were tested against analytical shieldings evaluated using the CFOUR[265] code. We also employed the CFOUR package to generate CCSD and CCSD(T) results against which the various MP methods can be assessed.

4.2.6 Lutnæs data set

In the following sections, we will use the data set curated by Lutnæs and coworkers [225, 291] with the purpose of benchmarking magnetic properties. The data set contains the following 28 small molecules: AlF, C_2H_4, C_3H_4, CH_2O, CH_3F, CH_4, CO, FCCH, FCN, H_2C_2O, H_2O, H_2S, H_4C_2O, HCN, HCP, HF, HFCO, HOF, LiF, LiH, N_2, N_2O, NH_3, O_3, OCS, OF_2, PN, SO_2. Geometries were optimized at the CCSD(T)/cc-pVTZ level of theory. Of the 28 molecules, 4 are considered "difficult" cases for NMR shieldings. They are O_3, OF_2, PN, and SO_2. O_3 exhibits significant multireference character, while SO_2 exhibits moderate multireference character. PN does not display distinct multireference character, but has a large paramagnetic contribution to the nuclear shielding tensor. For OF_2, inclusion of triple excitations is important for accurate nuclear shieldings. The rest of the 24 molecules are considered "easy" in the sense that electron correlation effects are not strong. Even so, electron correlation effects are essential to obtain results of useful accuracy. Given the large absolute value of the ^{17}O shieldings of O_3, we will exclude it from all statistical assessment in order to avoid skew. This procedure is in line with previous benchmark studies.[225, 226, 330] The data set then consists of unique nuclear shieldings for 18 ^{1}H nuclei, 17 ^{13}C nuclei, 7 ^{15}N nuclei, 11 ^{17}O nuclei, and 9 ^{17}F nuclei.

4.2.7 Numerical Accuracy of Finite Differences Nuclear Shieldings

To evaluate the numerical accuracy of the finite difference scheme, we compared the finite difference HF isotropic nuclear shieldings of the Lutnæs data set against analytical HF isotropic nuclear shieldings obtained via CFOUR. The cc-pVDZ basis was used for this purpose. The SCF convergence criteria was 10^{-11} a.u., and the cutoff threshold for two electron integrals was 10^{-17} a.u.

In Table 4.1 we present the mean error (ME) and root mean square error (RMSE) for HF nuclear shieldings for the Lutnæs data set. With both the second order and fourth order finite difference scheme, the optimal step size of $10^{-2.3}$ a.u. in both external magnetic field B and nuclear magnetic moment m_K leads to mean errors on the order of 10^{-2} ppm and 10^{-6} ppm respectively. Second order differences with the optimal step size of $10^{-2.3}$ a.u. for both perturbations are then used to evaluate all results reported here.

Table 4.1: Numerical performance of the 2nd and 4th order finite difference schemes for the HF/cc-pVDZ nuclear shieldings of 28 molecules with varying step sizes. Values presented are the ME and RMSE (where the latter is given in parentheses), in units of ppm. Reference values were calculated analytically at the same level of theory.

2nd order	B step size (log_{10} a.u.)	
m_k step size (log_{10} a.u.)	-2.3	-2
-2.3	0.027 (0.096)	0.113 (0.384)
-2	0.029 (0.096)	0.112 (0.382)
4th order	B step size (log_{10} a.u.)	
m_k step size (log_{10} a.u.)	-2.3	-2
-2.3	-1.5×10^{-6} (0.008)	0.002 (0.007)
-2	7×10^{-4} (0.005)	0.002 (0.006)

4.3 Results and Discussion

We assess the performance of various MP2 and MP3 alternatives with the Lutnæs data set. To contextualize the errors in the following sections, we introduce a 3 level target error scale. The high accuracy target is 0.1 ppm for ^{1}H nuclei, 1 ppm for ^{13}C nuclei, 3 ppm for ^{15}N nuclei, and 4 ppm for ^{17}O nuclei. The medium accuracy target is 0.2 ppm for ^{1}H nuclei, 2 ppm for ^{13}C nuclei, 6 ppm for ^{15}N nuclei, and 8 ppm for ^{17}O nuclei. Finally the low accuracy target is 0.4 ppm for ^{1}H nuclei, 4 ppm for ^{13}C nuclei, 12 ppm for ^{15}N nuclei, and 16 ppm for ^{17}O nuclei. This can be loosely applied to statistical error measures of either RMSE or MAE. Various benchmark studies[297, 300, 302] have investigated the nuclear shielding performance of HF, MP2, and many DFT functionals with various basis sets. Notably, for ^{1}H, HF and DFT at various rungs with a large basis set achieve the medium accuracy target of 0.2 ppm, while MP2 comes close to the high accuracy target of 0.1 ppm. With a small basis, most DFT functionals are in the range of the low accuracy target. ^{13}C proved to be slightly more difficult, with MP2 at large basis achieving the medium accuracy target of 2 ppm, and rung 5 DFT functionals achieving the low accuracy target of 4 ppm. ^{15}N and ^{17}O shieldings were shown to be difficult problems. MP2 performed poorly, beyond the range of the low accuracy target. Only a few rung 5 DFT functionals were in the low accuracy target range. It is therefore a worthwhile endeavor to explore alternatives in the MPn family of methods, seeking further improvements over MP2's already impressive performance for ^{1}H and ^{13}C, and seeking suitable methods for the more difficult ^{15}N and ^{17}O shieldings.

4.3.1 Accuracy of κ-MP2 nuclear shieldings for the Lutnæs set

First, we consider the κ-MP2 method. We present κ-MP2 shielding results in Table 4.2, using the medium-sized aug-cc-pVTZ basis set. Since κ-MP2 energies depend non-linearly on

κ, each chosen value requires its own calculations. Therefore we compare MP2 (or $\kappa \to \infty$) against HF (or $\kappa = 0$) and three judiciously chosen finite non-zero κ values. The strongest regularization used is $\kappa = 1.1$, which is a value that was demonstrated to work well for ligand binding energies to transition metal complexes as well as strong intermolecular dispersion interactions.[321] The intermediate value is $\kappa = 1.45$, which was originally recommended for the orbital optimized version, based on thermochemistry.[167] To provide weak regularization, we also assess $\kappa = 2$.

Turning to the results in Table 4.2, we first observe that compared to MP2, overall error (i.e. across *all* nuclei) is reduced at all three regularization strengths. The largest gain is for the intermediate regularization parameter of $\kappa = 1.45$, with a one quarter reduction in RMSE relative to MP2, and more than two thirds error reduction relative to HF. However, it is still double the error of CCSD. Furthermore we notice that the overall RMSE is very similar for all three κ values. At first glance this does not appear too encouraging. However, we recall the conclusion from other recent work[168, 321] assessing relative energies using κ-MP2 and κ-OOMP2 stating that no single κ value is optimal for all classes of relative energies. It may well be that the optimal κ value varies from nucleus to nucleus. Therefore we will next inspect the results for each individual nucleus type.

Table 4.2: κ-MP2 aug-cc-pVTZ Isotropic NMR shielding statistics in ppm

			κ-MP2			
All	HF	κ=1.1	1.45	2	MP2	CCSD
ME	-19.01	2.35	4.85	7.24	8.90	-1.44
RMSE	49.03	15.93	14.18	15.82	19.92	7.83
^{1}H						
ME	0.01	-0.0004	-0.015	-0.035	-0.08	0.06
RMSE	0.39	0.22	0.17	0.14	0.13	0.09
^{13}C						
ME	-11.31	-2.97	-1.24	0.40	1.65	-1.56
RMSE	15.07	4.34	2.59	1.95	3.20	2.43
^{15}N						
ME	-58.12	1.18	10.77	19.02	26.07	-7.41
RMSE	76.67	3.21	15.41	26.71	37.98	9.52
^{17}O						
ME	-38.17	16.91	19.39	21.40	19.00	-0.06
RMSE	50.54	24.50	27.29	29.26	27.36	8.93
^{19}F						
ME	19.76	16.69	12.16	8.18	3.97	5.87
RMSE	34.73	20.80	14.68	9.67	5.59	7.50

For ^{1}H, no improvement over MP2 was observed: with the strongest regularization ($\kappa = 1.1$), RMSE almost doubles to 0.22 ppm from the unregularized MP2 value of 0.13. The weakest regularization ($\kappa = 2$) has similar RMSE as MP2. In fact that RMS changes monotonically across all 4 regularization values: $\kappa = 0, 1.1, 1.45, 2$. This is not unexpected, given the relatively high accuracy of unregularized MP2. We also note the trade-off between RMSE and ME. To say it another way, unregularized MP2 evidently does not systematically overestimate correlation effects in ^{1}H magnetic shieldings across the set of molecules studied here.

For ^{13}C, the situation is qualitatively different. While MP2 performs reasonably well, a subset of regularization strengths lead to quite noticeable improvements over MP2 in the RMSE over our dataset. In particular, intermediate regularization ($\kappa = 1.45$) modestly decreases the RMSE from 3.2 ppm for MP2 to 2.6 ppm, while the ME changes sign from 1.7 ppm for MP2 to -1.2 ppm. The RMSE increases further (along with the ME) as we move to strong regularization. We observe optimal results with weak regularization ($\kappa = 2$), where RMSE is reduced by a third to 2.0 ppm, and the ME is only 0.4 ppm. In fact, the RMSE and ME for weak regularization was lower than for CCSD, and reaches the medium level of accuracy (≤ 2 ppm). From the fact that the ME changes sign between HF and MP2, whilst it does not change sign for CCSD, we infer that unregularized MP2 slightly overcorrelates ^{13}C shieldings, whilst CCSD slightly undercorrelates them. Therefore κ-MP2 with weak regularization ($\kappa = 2$) can be a useful improvement over MP2 for ^{13}C shieldings.

For ^{15}N, the statistics summarized in Table 4.2 reveal a far more dramatic role for regularization than was the case for either ^{1}H or ^{13}C. Comparing HF and MP2, we see only a 2-fold reduction in RMSE for MP2, which is accompanied by only a 2-fold reduction in ME, together with a change of sign. This indicates significant overestimation of the correlation effects on ^{15}N shielding by MP2. As a consequence, we observe error reduction at all κ's, with strong regularization ($\kappa = 1.1$) being optimal. With strong regularization, RMSE is reduced dramatically from 38 ppm for MP2 to only 3.2 ppm, which is an extraordinary 12-fold reduction in error. This results in a nearly three times smaller error than CCSD, and approaches the high accuracy target we identified for ^{15}N. Evidently a large part of the systematic overestimation of correlation effects by MP2 is removed by the strong regularization. This is confirmed by the very large 22-fold reduction in ME from 26 ppm to 1.2 ppm. Furthermore, it is not just the systematic error that is improved. Comparing ME and RMSE, it is clear that the spread of errors significantly narrows with strong regularization.

Why is strong regularization preferred for ^{15}N whilst weak regularization is optimal for ^{13}C? We cannot be entirely sure, although we note that the subset of molecules containing nitrogen nuclei includes many nitriles where N is triple bonded to its neighbor. It is reasonable to speculate that triply bonded molecules exhibit stronger correlation effects than singly bonded species, and this could be a plausible explanation for why stronger regularization leads to error reduction for ^{15}N. However, each nitrile also has a ^{13}C nucleus, and inspection of individual results (see Supporting Information) shows that the ^{13}C shieldings in nitriles are generally better predicted via κ-MP2 with weak regularization than strong regularization. Furthermore chemical shieldings at sp^3 ^{15}N are also better predicted with

strong regularization. We provisionally conclude that the character of correlation effects on shielding at ^{15}N are systematically different to ^{13}C, and each is systematically different to ^{1}H. Accordingly optimal regularization is different for each case.

For ^{17}O, MP2 also performs rather poorly with slightly less than a 2-fold reduction in RMSE relative to HF (from 50.5 ppm to 27.4 ppm). The ME for MP2 changes sign relative to HF and is reduced by only a little more than a factor of two, to a value of 19 ppm. At first glance this appears similar to the case of ^{15}N, and suggests the possibility of significant improvements due to regularization. However, no significant changes over MP2 are observed! Strong regularization ($\kappa = 1.1$) leads to slight improvements, from the RMSE of 27.4 ppm for MP2 to 24.5 ppm. The weaker regularizers lead to results that are essentially unchanged from MP2. Even strong regularization leads to only modest reductions in ME vs MP2, and the sign of the ME is the same as MP2, indicating that correlation effects on ^{17}O shieldings are *still* overestimated.

It is clearly interesting to assess still stronger regularization for ^{17}O shieldings, as values of $\kappa \leq 1$ should apparently yield systematic improvements. From a regularized MP2 perspective, ^{17}O shieldings appear to require extremely strong regularization, perhaps comparable to the values for transition metal energetics (e.g. $\kappa = 0.8$ was optimal for the MOR39 data set[321]). The results of performing these additional numerical experiments are presented in Figure 4.1. In fact, the optimal κ for ^{17}O shieldings is 0.6, giving an RMSE of 16.6 ppm and ME of 2.4 ppm. This reflects an almost 2-fold reduction in MP2's RMSE.

Finally we consider the case of ^{19}F magnetic shieldings. In this case, unregularized MP2 outperforms CCSD, and also exhibits a lower ME than CCSD. The improvement over HF is dramatic at the MP2 level: a five-fold reduction in ME, and a most impressive six-fold reduction in RMSE. There is also no change of sign in the ME from HF to MP2, suggesting that on average, correlation effects on ^{19}F nuclei are not overestimated by MP2. This situation is unpromising for κ-MP2 because all regularization strengths provide some damping of correlation effects. Not surprisingly we indeed observe that all 3 finite regularization strengths in κ-MP2 lead to higher error, with $\kappa = 2$ having the lowest RMSE of 9.7 ppm, versus 5.6 ppm for MP2 and 7.5 ppm for CCSD.

4.3.2 Accuracy of MP3 and MP2.X nuclear shieldings for the Lutnæs Set

Following the detailed discussion of κ-MP2 discussed above, where regularization was used to damp the MP2 contribution to magnetic shieldings, we now turn to the inclusion of third order correlation as an alternative strategy to improve upon MP2. We will assess 3 models. First, as a reference calculation, standard MP3. Second, in light of its very good performance for non-covalent interactions, MP2.5, which damps the third order contribution by a factor of two. And finally, because MP2.X depends linearly on the third order contribution, we can optimize the fraction, either nucleus by nucleus, or for the overall dataset. Bearing in mind the significant increase in computational cost relative to MP2 or κ-MP2, we must also

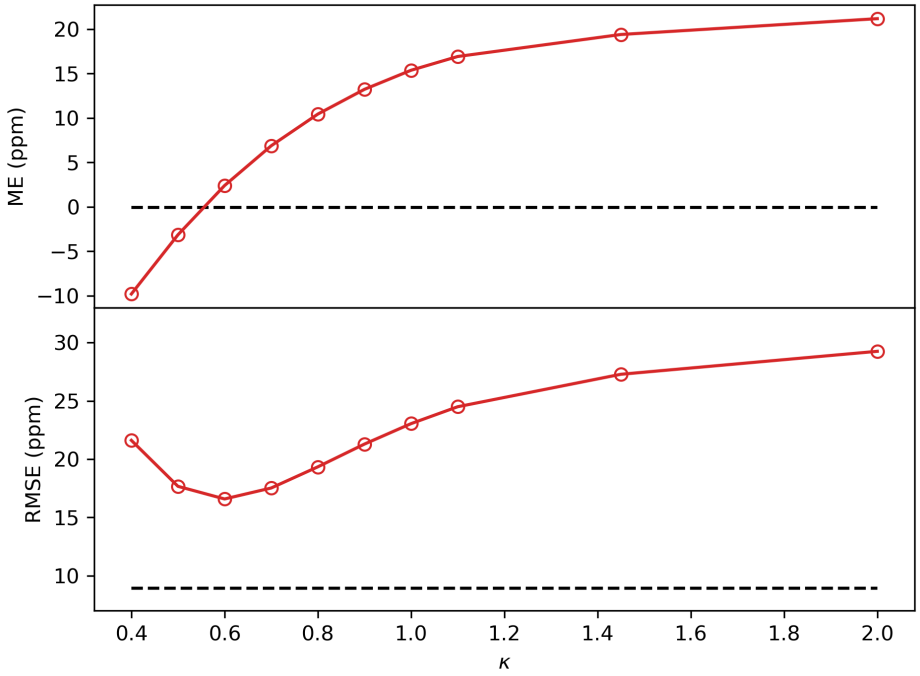

Figure 4.1: κ-MP2 ME and RMSE (in units of ppm) for magnetic shielding at ^{17}O nuclei, plotted as a function of κ. The ME and RMSE corresponding to CCSD are shown as the horizontal dashed lines.

achieve significant improvements in accuracy in order to justify the additional computing expense.

Table 4.3 contains the shielding results obtained with the MP3, MP2.5 and MP2.X models. Considering all atoms, adding the third order correction (ie. MP3) slightly improves upon MP2, by reducing the MP2 RMSE of 20.0 ppm to the MP3 RMSE of 15.1 ppm. We also note that the ME changes sign from the MP2 value of +8.9 ppm to the MP3 value of -5.46 ppm, showing that the third order correction statistically overcorrects MP2 to yield an ME with the same sign as HF. Scaling with the optimal parameter of X = 0.6 leads to remarkable improvements, with RMSE reduced to 3.3 ppm, and ME reduced to 0.72 ppm. This represents half the RMSE of CCSD. The traditional scaling of 0.5 was slightly less effective, giving an RMSE of 4.7 ppm and ME of 2.3 ppm. We can contrast these scaled MP3 results with the κ-MP2 data discussed above. In the κ-MP2 case, there was only modest improvement over MP2 by using either weak, medium or strong regularization, indicating that regularization strength was element-specific rather transferable. By contrast, these large improvements in scaled MP3 over MP3 across the entire data set imply rather good transferability from one element to another. This is very encouraging.

Nevertheless, it may be possible to do even better by optimizing the scaling factor for each nucleus individually. The element-specific results are contained in Table 4.3, and are

Table 4.3: MP3 , MP2.5, and MP2.X Isotropic NMR shielding errors calculated with the aug-cc-pVTZ basis set. All values in units of ppm.

All	MP3	MP2.5	MP2.X	Optimal scaling (c)
ME	-5.46	2.27	0.72	0.6
RMSE	15.1	4.67	3.29	
^{1}H				
ME	0.074	0.002	-0.027	0.3
RMSE	0.177	0.113	0.106	
^{13}C				
ME	-3.13	-0.41	-0.41	0.5
RMSE	4.35	1.15	1.15	
^{15}N				
ME	-17.58	4.90	0.41	0.6
RMSE	25.31	7.28	1.45	
^{17}O				
ME	-11.0	4.51	2.18	0.575
RMSE	21.29	6.22	4.98	
^{19}F				
ME	2.78	3.63	3.29	0.7
RMSE	4.39	4.16	4.01	

also graphically summarized in Figure 4.2. Let us begin with ^{1}H shieldings, where MP2 performed quite remarkably, and where regularization did not lead to any improvements. Standard MP3 performs slightly worse than MP2, with RMSE of 0.19 ppm and ME of 0.09 ppm, compared to the RMSE of 0.13 ppm for MP2. This is consistent with the poor reputation of MP3. By contrast, with the optimal scaling factor of 0.3, the MP2.3 RMSE is reduced to 0.11 ppm, which is a slight improvement over MP2. In fact, MP2.3 approaches the high accuracy target of 0.1 ppm. Nonetheless, it is perhaps debatable as to whether the 0.02 ppm reduction in RMSE is justifiable for the higher cost of the third order correction.

For ^{13}C shieldings, MP2's already very good performance was improved by weak regularization, reducing RMSE from 3.2 ppm to 2.0 ppm. By contrast, MP3 exhibits an RMSE of 4.4 ppm and ME of -3.13 ppm, which is slightly worse than MP2. This situation is significantly improved with the optimal scaling factor of 0.5, whereupon we observe RMSE reduction to 1.2 ppm and ME to -0.4 ppm. This is a quite impressive result, which is not only better than both MP2 and CCSD, but also approaches the high accuracy target of 1 ppm at far less compute cost than CCSD(T). Accordingly, we suggest that MP2.5 may be a potentially valuable first principles approach to ^{13}C magnetic shieldings.

For ^{15}N shieldings, MP3 has quite large errors, with an RMSE of 25.3 ppm and a ME of -17.6 ppm. This however is still a useful improvement over MP2 (RMSE 38.0 ppm).

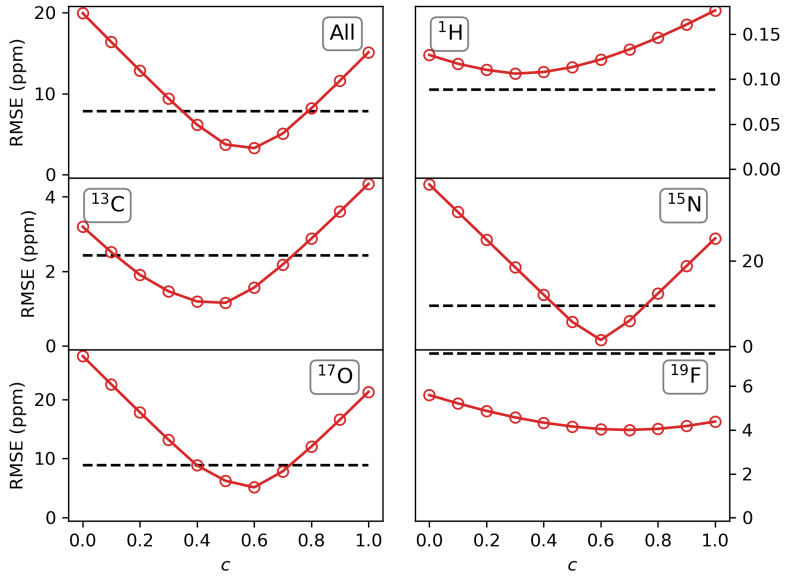

Figure 4.2: MP2.X RMSE (in units of ppm) plotted as a function of scaling factor c. The MP2 RMSE is the left-most data point ($c = 0$), whilst the MP3 RMSE is the right-most data point. For all nuclei, scaled MP2.X with the optimal c outperforms both MP2 and MP3. The RMSE corresponding to CCSD is shown as the horizontal dashed line, and it is evident that for all elements except ^{1}H, scaled MP2.X with the optimal c outperforms CCSD.

With the optimal scaling factor of 0.6, RMSE is dramatically reduced to only 1.5 ppm (ME reduced to 0.4 ppm). This is more than a factor of two better than the κ-MP2 with strong regularization (RMSE of 3.2 ppm), and well within the range of the high accuracy target of 3 ppm for ^{15}N. It is an extraordinary six-fold improvement over CCSD itself, indicating that the optimal scaling is effectively accounting for a very significant fraction of the triples correlation effect by a simple and apparently very effective renormalization of the doubles. It appears that MP2.6 may be a very promising method for ^{15}N magnetic shieldings.

Similarly for ^{17}O shieldings, MP3 again has quite large errors, with RMSE of 21.3 ppm and ME of -11 ppm, which can be compared against the MP2 value of 27.4 ppm. With the optimal scaling factor of 0.575, RMSE reduced by a striking factor of four to 5.0 ppm, while the ME is reduced to 2.2. This represents close to a factor of two improvement over CCSD's 8.9 ppm RMSE, as well as approaching the 4 ppm high accuracy target. While not quite as strikingly high quality as the ^{15}N shieldings, this improvement suggests that approximately half of the triples contribution to ^{17}O shieldings is captured by optimally scaled MP3.

Lastly for ^{19}F, where MP2 with RMSE 5.7 ppm outperformed CCSD's 7 ppm RMSE, and where regularization led to no improvements, unscaled MP3 has RMSE of 4.4 ppm and ME of 2.8 ppm. This is a particularly interesting case, because it is a rare outcome where standard MP3 already statistically performs better than CCSD. With optimal scaling factor

of 0.7, we observe a slightly improved RMSE of 4.0 ppm, while the ME is slightly increased to 3.3 ppm. Relative to the CCSD RMSE of 7.5 ppm, we infer that almost half of the triples contribution to correlation (i.e. the CCSD error) is captured by the renormalization associated with scaled MP2.7. This is a quite similar outcome to the ^{17}O and ^{13}C shielding results.

Overall, considering ^{1}H, MP2.4 gives a slight but meaningful improvement over MP2, albeit at a higher computational cost. Considering only heavy atoms, 0.6 seems to be a suitable scaling factor overall, giving greatly improved shieldings for ^{13}C, ^{15}N, and ^{17}O, in all cases producing smaller RMSE than CCSD. The value of 0.6 is quite close to the *ad hoc* scaling factor of 0.5, and in all cases gives similar statistical performance. In addition, with optimal scaling factors, we observe very promising performance, where RMSE's have either neared or reached the respective high accuracy targets.

4.4 Conclusions

We have implemented and tested a method-independent finite difference based software using gauge including atomic orbitals to calculate NMR shieldings. This finite field approach uses second order finite differences of the energy, as a function of an applied magnetic field and an applied nuclear spin to evaluate the magnetic shielding tensor. This required development of the appropriate complex matrix elements for magnetically perturbed Hamiltonian, as well as generalization of the corresponding self-consistent field and correlation energies to work with complex orbitals and amplitudes. Once this infrastructure is in place, assessment of magnetic properties of non-standard methods may then be accomplished with much less effort than if it were necessary to implement analytic second derivatives. The finite difference approach is also trivially parallelizable, and is well suited for use with locally dense basis sets that augment the 1-particle basis set on just the atom of interest and its immediate neighbors.[98, 331] For evaluation of shieldings at all nuclei in a molecule using a given basis set, the energy-based finite difference approach will be significantly less efficient, as well as less numerically precise, than analytical approaches, when available.

The MP2 method is known to have excellent performance for ^{1}H shieldings and good performance for ^{13}C, but poor performance for ^{15}N and ^{17}O on normal closed-shell molecules. This motivated us to assess the possibility of using regularized MP2 (κ-MP2)[321] to improve upon MP2. We tested on a set of 28 small molecules[225] that was used previously to benchmark approximate electronic structure methods for magnetic properties. The results showed that κ-MP2 could perform very well, provided element-specific regularization was used. For ^{1}H zero regularization is optimal; for ^{13}C, weak regularization reduces MP2 errors by 30%; for ^{15}N, strong regularization reduces MP2 errors by a remarkable 90%, and for ^{19}F zero regularization is optimal. For ^{13}C and ^{15}N, κ-MP2 with element-specific regularization yields errors that are smaller than CCSD.

On the other hand, we found that the scaled third order perturbative method MP2.X is the best performing among the methods we have inspected. Our results showed that with use

of element-specific scaling factors c, MP2.X performs very well. For ^{1}H $c = 0.3$ is optimal, reducing MP2 errors by almost 20%; for ^{13}C, $c = 0.5$ reduces MP2 errors by more than 60%; for ^{15}N, $c = 0.6$ reduces MP2 errors by an impressive 95%; for ^{17}O, $c = 0.575$ reduces MP2 errors by a remarkable 80%, and for ^{19}F, $c = 0.7$ reduces MP2 errors by close to 30%. For all those elements but ^{1}H, MP2.X with element-specific scaling factor yields errors that are smaller than CCSD, making these approaches promising for chemical applications with accuracy significantly higher than is attainable with DFT.[302, 309]

The success of the κ-MP2 and MP2.X methods can be viewed in two different ways. First, one may consider that these approaches heuristically cure failures of the parent MP2 and MP3 methods. Thus regularization of MP2 (i.e. κ-MP2) damps the overestimation of correlation effects that is commonly characteristic of MP2, while scaling MP3 to partially include perturbative third order correlation reduces the overdamping of MP2 that is commonly seen with MP3. A second point of view, that is equally valid, is that the exact correlation energy can be given just in terms of doubles correlation amplitudes when used with Brueckner orbitals. Therefore either regularizing the MP2 amplitudes or partially including third order correlation is renormalizing the doubles amplitudes of MP2 and MP3 theory respectively. If such a heuristic renormalization succeeds in achieving accuracy beyond the CCSD level, as we have demonstrated here, then it seems to be partially accounting for the neglected triple and higher correlation effects. Finally, the fact that the optimal renormalization parameters are highly element-specific in the case of κ-MP2 suggests that element-specific correlation effects are important when correlation is treated at such a simple level of theory as MP2. The fact that there is much better transferability of the optimal scaling parameter from element to element in MP2.X seems to imply that the additional complexity of this approach indeed reflects substantially improved treatment of electron correlation.

To solidify the utility of these methods for NMR shielding calculations, further investigations should be conducted with a larger data set.[300, 309] There are also other potentially interesting extensions of the approach described here. For instance, one could assess whether orbital optimized MP2[166, 228] and its regularized generalizations[167, 168] are capable of providing further improvements, and whether the choice of different orbitals in MP3 and MP2.X[236, 280] could provide any advantage. Additionally, it will be potentially very useful to extend our framework to evaluate scalar couplings.

Appendix A: GIAO matrix element of the paramagnetic spin-orbit coupling

To arrive at a convenient expression for matrix elements of the paramagnetic spin-orbit coupling operator, Eq. 4.9, in the complex GIAO basis associated with a finite applied **B**-field and induced magnetic moment $\mathbf{m}_K$, we use the following shorthand notation for the charge-less three center field integral and the charge-less three center nuclear attraction integral for center **K**:

$$F^x(l'+1) = \left\langle \omega_\mu | \frac{x_K}{|\mathbf{r}-\mathbf{R}_K|^3} | \omega_\nu(l'+1) \right\rangle \tag{4.16}$$

$$I(l'+1) = \left\langle \omega_\mu | |\mathbf{r}-\mathbf{R}_K|^{-1} | \omega_\nu(l'+1) \right\rangle \tag{4.17}$$

Here, l' is the polynomial power associated with the x-component of the Gaussian orbital that is a part of the GIAO ω_ν. Similarly, m' and n' are used for the y- and z-components, respectively. l, m, n, refers to the GIAO ω_μ. Hence, $F^x(l'+1)$ is the field integral in the x-direction between GIAOs ω_μ and ω_ν and center K with increased orbital angular momentum (x-component) of ω_ν; similarly $I(l'+1)$ is the nuclear attraction integral between GIAOs ω_μ and ω_ν and center K with increased orbital angular momentum (x-component) of ω_ν.

Field Integral approach

Expanding as sum of charge-less three center field integrals, we arrive at the following expressions for matrix elements of the paramagnetic spin-orbit operator given in Eq. 4.9:

$$\begin{aligned} h_{\mu\nu}^{\mathrm{PSO},x} = & -i\alpha^2 \sum_K m_{K,x} \times \\ & \Big[n' F^y(n'-1) - \frac{i}{2}\chi_{\nu,z} F^y - 2\beta' F^y(n'+1) \\ & -m' F^z(m'-1) + \frac{i}{2}\chi_{\nu,y} F^z + 2\beta' F^z(m'+1) \Big] \end{aligned} \tag{4.18}$$

$$\begin{aligned} h_{\mu\nu}^{\mathrm{PSO},y} = & -i\alpha^2 \sum_K m_{K,y} \times \\ & \Big[l' F^z(l'-1) - \frac{i}{2}\chi_{\nu,x} F^z - 2\beta' F^z(l'+1) \\ & -n' F^x(n'-1) + \frac{i}{2}\chi_{\nu,z} F^x + 2\beta' F^x(n'+1) \Big] \end{aligned} \tag{4.19}$$

$$
\begin{aligned}
h_{\mu\nu}^{\mathrm{PSO},z} = & -i\alpha^2 \sum_K m_{K,z} \times \\
& \Big[m' F^x (m'-1) - \frac{i}{2} \chi_{\nu,y} F^x - 2\beta' F^x (m'+1) \\
& - l' F^y (l'-1) + \frac{i}{2} \chi_{\nu,x} F^y + 2\beta' F^y (l'+1) \Big]
\end{aligned} \tag{4.20}
$$

Nuclear Attraction Integral approach

Alternatively, we can expand the paramagnetic spin-orbit coupling matrix element into sum of nuclear attraction integrals by explicitly treating the $|r^{-3}|$ operator. We employ the following equation:

$$
\int dx \frac{x_K}{|r_K|^3} \omega_\mu \omega_\nu = \int dx \frac{1}{|r_K|} \frac{\partial \omega_\mu}{\partial x} \omega_\nu + \int dx \frac{1}{|r_K|} \omega_\nu \frac{\partial \omega_\nu}{\partial x} \tag{4.21}
$$

After some straightforward but cumbersome algebra we arrive at the following expressions for matrix elements of the paramagnetic spin-orbit coupling operator given in Eq. 4.9:

$$
\begin{aligned}
h_{\mu\nu}^{\mathrm{PSO,x}} = & -i\alpha^2 \sum_K m_{K,x} \big[4\beta\beta' I(m+1,n'+1) - 2\beta' m I(m-1,n'+1) - i\beta' \chi_{\mu,y} I(n'+1) \\
& - 2\beta n' I(m+1,n'-1) + m n' I(m-1,n'-1) + \frac{i}{2} n' \chi_{\mu,y} I(n'-1) \\
& + i\beta \chi_{\nu,z} I(m+1) - \frac{i}{2} m \chi_{\nu,z} I(m-1) + \frac{1}{4} \left(\chi_{\mu,y} \chi_{\nu,z} - \chi_{\mu,z} \chi_{\nu,y} \right) I \\
& - 4\beta\beta' I(n+1,m'+1) + 2\beta' n I(n-1,m'+1) + i\beta' \chi_{\mu,z} I(m'+1) \\
& + 2\beta m' I(n+1,m'-1) - n m' I(n-1,m'-1) - \frac{i}{2} m' \chi_{\mu,z} I(m'-1) \\
& - i\beta \chi_{\nu,z} I(l+1) + \frac{i}{2} l \chi_{\nu,z} I(l-1) \big]
\end{aligned} \tag{4.22}
$$

$$
\begin{aligned}
h_{\mu\nu}^{\mathrm{PSO,y}} = & -i\alpha^2 \sum_K m_{K,y} \big[4\beta\beta' I(n+1,l'+1) - 2\beta' n I(n-1,l'+1) - i\beta' \chi_{\mu,z} I(l'+1) \\
& - 2\beta l' I(n+1,l'-1) + n l' I(n-1,l'-1) + \frac{i}{2} l' \chi_{\mu,z} I(l'-1) \\
& + i\beta \chi_{\nu,x} I(l+1) - \frac{i}{2} n \chi_{\nu,x} I(n-1) + \frac{1}{4} \left(\chi_{\mu,x} \chi_{\nu,z} - \chi_{\mu,z} \chi_{\nu,x} \right) I \\
& - 4\beta\beta' I(l+1,n'+1) + 2\beta' n' I(l-1,n'+1) + i\beta' \chi_{\mu,z} I(m'+1) \\
& + 2\beta m' I(n+1,m'-1) - n m' I(n-1,m'-1) - \frac{i}{2} m' \chi_{\mu,z} I(m'-1) \\
& - i\beta \chi_{\nu,y} I(n+1) + \frac{i}{2} n \chi_{\nu,y} I(n-1) \big]
\end{aligned} \tag{4.23}
$$

$$
\begin{aligned}
h_{\mu\nu}^{\mathrm{PSO},z} = &- i\alpha^2 \sum_K m_{K,z} \big[4\beta\beta' I(m+1,n'+1) - 2\beta' m I(m-1,n'+1) - i\beta' \chi_{\mu,y} I(n'+1) \\
&- 2\beta n' I(m+1,n'-1) + m n' I(m-1,n'-1) + \frac{i}{2} n' \chi_{\mu,y} I(n'-1) \\
&+ i\beta \chi_{\nu,z} I(m+1) - \frac{i}{2} m \chi_{\nu,z} I(m-1) + \frac{1}{4} \left(\chi_{\mu,y}\chi_{\nu,z} - \chi_{\mu,z}\chi_{\nu,y} \right) I \\
&- 4\beta\beta' I(n+1,m'+1) + 2\beta' n I(n-1,m'+1) + i\beta' \chi_{\mu,z} I(m'+1) \\
&+ 2\beta m' I(n+1,m'-1) - n m' I(n-1,m'-1) - \frac{i}{2} m' \chi_{\mu,z} I(m'-1) \\
&- i\beta \chi_{\nu,y} I(n+1) + \frac{i}{2} n \chi_{\nu,y} I(n-1) \big]
\end{aligned} \tag{4.24}
$$

Appendix B: GIAO matrix elements of the diamagnetic shielding

Field Integral approach

The following are the expressions for matrix elements of the diamagnetic shielding operator, given in Eq. 4.8, expanded as sum of charge-less three center field integrals:

$$
\begin{aligned}
h_{\mu\nu}^{\mathrm{DS},x} = &\frac{\alpha^2}{2} \sum_K \{ (B_y m_{K,y} + B_z m_{K,z}) F^x(l'+1) - B_x m_{K,y} F^x(m'+1) - B_x m_{K,z} F^x(n'+1) \\
&+ [(B_y m_{K,y} + B_z m_{K,z}) R_{\nu,x} - B_x m_{K,y} R_{\nu,y} - B_x m_{K,z} R_{\nu,z}] F^x) \}
\end{aligned} \tag{4.25}
$$

$$
\begin{aligned}
h_{\mu\nu}^{\mathrm{DS},y} = &\frac{\alpha^2}{2} \sum_K \{ (B_x m_{K,x} + B_z m_{K,z}) F^y(m'+1) - B_y m_{K,x} F^y(l'+1) - B_y m_{K,z} F^y(n'+1) \\
&+ [(B_x m_{K,x} + B_z m_{K,z}) R_{\nu,y} - B_y m_{K,x} R_{\nu,x} - B_y m_{K,z} R_{\nu,z}] F^y) \}
\end{aligned} \tag{4.26}
$$

$$
\begin{aligned}
h_{\mu\nu}^{\mathrm{DS},z} = &\frac{\alpha^2}{2} \sum_K \{ (B_x m_{K,x} + B_y m_{K,y}) F^z(n'+1) - B_x m_{K,z} F^z(l'+1) - B_z m_{K,y} F^z(m'+1) \\
&+ [(B_x m_{K,x} + B_y m_{K,y}) R_{\nu,z} - B_z m_{K,x} R_{\nu,x} - B_z m_{K,y} R_{\nu,y}] F^z) \}
\end{aligned} \tag{4.27}
$$

Nuclear Attraction Integral approach

Similarly, the diamagnetic shielding matrix element can also be expanded as sums of nuclear attraction integrals employing Eq. 4.21. After some manipulation we can obtain alternative expressions for the matrix elements of the paramagnetic spin-orbit coupling operator given in Eq. 4.8:

$$
\begin{aligned}
h_{\mu\nu}^{\mathrm{DS},x} =& \frac{\alpha^2}{2}\sum_K \{(B_y m_{K,y} + B_z m_{K,z})\{lI(l-1,l'+1) - 2\beta I(l+1,l'+1) \\
& -(2R_{\nu,x}\beta' + i\cdot\frac{\chi_{\mu,x}+\chi_{\nu,x}}{2})I(l'+1) + [(l'+1) - i\cdot\frac{R_{\nu,x}(\chi_{\mu,x}+\chi_{\nu,x})}{2}]I \\
& -2\beta' I(l'+2) - 2R_{\nu,x}\beta I(l+1) + R_{\nu,x}lI(l-1) + R_{\nu,x}l'I(l'-1)\} \\
& -B_x m_{K,y}[lI(l-1,m'+1) - 2\beta I(l+1,m'+1) - i\cdot\frac{\chi_{\mu,x}+\chi_{\nu,x}}{2}I(m'+1) \\
& +l'I(l'-1,m'+1) - 2\beta' I(l'+1,m'+1) - 2R_{\nu,y}\beta' I(l'+1) - 2R_{\nu,y}\beta I(l+1) \\
& +R_{\nu,y}l'I(l'-1) + R_{\nu,y}lI(l-1) - i\cdot\frac{R_{\nu,y}(\chi_{\mu,x}+\chi_{\nu,x})}{2}I] \\
& -B_x m_{K,z}[lI(l-1,n'+1) - 2\beta I(l+1,n'+1) - i\cdot\frac{\chi_{\mu,x}+\chi_{\nu,x}}{2}I(n'+1) \\
& +l'I(l'-1,n'+1) - 2\beta' I(l'+1,n'+1) - 2R_{\nu,z}\beta' I(n'+1) - 2R_{\nu,z}\beta I(l+1) \\
& +R_{\nu,z}l'I(l'-1) + R_{\nu,z}lI(l-1) - i\cdot\frac{R_{\nu,z}(\chi_{\mu,x}+\chi_{\nu,x})}{2}I]\Big\}
\end{aligned}
\tag{4.28}
$$

$$
\begin{aligned}
h_{\mu\nu}^{\mathrm{DS},y} =& \frac{\alpha^2}{2}\sum_K \{(B_x m_{K,x} + B_z m_{K,z})\{mI(m-1,m'+1) - 2\beta I(m+1,m'+1) \\
& -(2R_{\nu,y}\beta' + i\cdot\frac{\chi_{\mu,y}+\chi_{\nu,y}}{2})I(m'+1) + [(m'+1) - i\cdot\frac{R_{\nu,y}(\chi_{\mu,y}+\chi_{\nu,y})}{2}]I \\
& -2\beta' I(m'+2) - 2R_{\nu,x}\beta I(m+1) + R_{\nu,y}mI(m-1) + R_{\nu,y}m'I(m'-1)\} \\
& -B_y m_{K,x}[mI(m-1,l'+1) - 2\beta I(m+1,l'+1) - i\cdot\frac{\chi_{\mu,y}+\chi_{\nu,y}}{2}I(l'+1) \\
& +m'I(l'+1,m'-1) - 2\beta' I(l'+1,m'+1) - 2R_{\nu,x}\beta' I(m'+1) - 2R_{\nu,x}\beta I(m+1) \\
& +R_{\nu,x}m'I(m'-1) + R_{\nu,x}mI(m-1) - i\cdot\frac{R_{\nu,x}(\chi_{\mu,y}+\chi_{\nu,y})}{2}I] \\
& -B_y m_{K,z}[mI(m-1,n'+1) - 2\beta I(m+1,n'+1) - i\cdot\frac{\chi_{\mu,z}+\chi_{\nu,z}}{2}I(n'+1) \\
& +m'I(m'-1,n'+1) - 2\beta' I(m'+1,n'+1) - 2R_{\nu,z}\beta' I(m'+1) - 2R_{\nu,z}\beta I(m+1) \\
& +R_{\nu,z}m'I(m'-1) + R_{\nu,z}mI(m-1) - i\cdot\frac{R_{\nu,z}(\chi_{\mu,y}+\chi_{\nu,y})}{2}I]\Big\}
\end{aligned}
\tag{4.29}
$$

$$
\begin{aligned}
h_{\mu\nu}^{\mathrm{DS},z} =& \frac{\alpha^2}{2}\sum_K \{(B_x m_{K,x} + B_y m_{K,y})\{nI(n-1,n'+1) - 2\beta I(n+1,n'+1) \\
& -(2R_{\nu,z}\beta' + i\cdot\frac{\chi_{\mu,z}+\chi_{\nu,z}}{2})I(n'+1) + [(n'+1) - i\cdot\frac{R_{\nu,z}(\chi_{\mu,z}+\chi_{\nu,z})}{2}]I \\
& -2\beta' I(n'+2) - 2R_{\nu,z}\beta I(n+1) + R_{\nu,z}nI(n-1) + R_{\nu,z}n'I(n'-1)\} \\
& -B_z m_{K,x}[nI(n-1,l'+1) - 2\beta I(n+1,l'+1) - i\cdot\frac{\chi_{\mu,z}+\chi_{\nu,z}}{2}I(l'+1) \\
& +n'I(l'+1,n'-1) - 2\beta' I(l'+1,n'+1) - 2R_{\nu,x}\beta' I(n'+1) - 2R_{\nu,x}\beta I(n+1) \\
& +R_{\nu,x}n'I(n'-1) + R_{\nu,x}nI(n-1) - i\cdot\frac{R_{\nu,x}(\chi_{\mu,z}+\chi_{\nu,z})}{2}I] \\
& -B_z m_{K,y}[nI(n-1,m'+1) - 2\beta I(n+1,m'+1) - i\cdot\frac{\chi_{\mu,z}+\chi_{\nu,z}}{2}I(m'+1) \\
& +m'I(m'+1,n'-1) - 2\beta' I(m'+1,n'+1) - 2R_{\nu,y}\beta' I(n'+1) - 2R_{\nu,y}\beta I(n+1) \\
& +R_{\nu,y}n'I(n'-1) + R_{\nu,y}nI(n-1) - i\cdot\frac{R_{\nu,y}(\chi_{\mu,z}+\chi_{\nu,z})}{2}I]\Big\}
\end{aligned}
\tag{4.30}
$$

In the above expressions, β, β' are the Gaussian exponents of the primitive GIAO's μ, ν. $R_{\nu,x}$, $R_{\nu,y}$, $R_{\nu,z}$ are the x, y, z Cartesian components of the primitive GIAO ν. And $\boldsymbol{\chi}_\nu$ is the vector

$$\boldsymbol{\chi}_\nu = \mathbf{B}\times\mathbf{R}_\nu \tag{4.31}$$

4.5 Supplementary Information

The S.I. for this data my be readily accessed from the publication source in its citation[100].

Bibliography

(1) Heisenberg, W.; Pauli, W. Zur Quantendynamik der Wellenfelder. *Zeitschrift fur Physik* **1929**, *56*, 1–61.

(2) Born, M.; Oppenheimer, R. Zur Quantentheorie der Molekeln. *Ann. Phys.* **1927**, *389*, 457–484.

(3) Löwdin, P.-O. Quantum Theory of Many-Particle Systems. I. Physical Interpretations by Means of Density Matrices, Natural Spin-Orbitals, and Convergence Problems in the Method of Configurational Interaction. *Phys. Rev.* **1955**, *97*, 1474–1489.

(4) Haag, R.; Kastler, D. An Algebraic Approach to Quantum Field Theory. *Journal of Mathematical Physics* **2004**, *5*, 848–861.

(5) Haag, R. Discussion of the 'axioms' and the asymptotic properties of a local field theory with composite particles. *EPJ H* **2010**, *35*, 243–253.

(6) Feynman, R. P. Space-Time Approach to Quantum Electrodynamics. *Phys. Rev.* **1949**, *76*, 769–789.

(7) Brunetti, R.; Fredenhagen, K. Microlocal Analysis and Interacting Quantum Field Theories: Renormalization on Physical Backgrounds. *Communications in Mathematical Physics* **2000**, *208*, 623–661.

(8) Dyson, F. J. Divergence of Perturbation Theory in Quantum Electrodynamics. *Phys. Rev.* **1952**, *85*, 631–632.

(9) 't Hooft, G.; Veltman, M., *Diagrammar*; Springer: 1974.

(10) Witten, E. 2 + 1 dimensional gravity as an exactly soluble system. *Nuclear Physics B* **1988**, *311*, 46–78.

(11) Deser, S.; Jackiw, R.; 't Hooft, G. Three-dimensional Einstein gravity: Dynamics of flat space. *Annals of Physics* **1984**, *152*, 220–235.

(12) Lorentz, H. A.; Einstein, A.; Minkowski, H.; Weyl, H., *Das Relativitätsprinzip*; Springer: 1922.

(13) Gödel, K., *On formally undecidable propositions of Principia Mathematica and related systems*; Courier Corporation: 1992.

(14) Hilbert, D. Die Grundlegung der elementaren Zahlenlehre. *Mathematische Annalen* **1931**, *104*, 485–494.

(15) Gentzen, G. Die Widerspruchsfreiheit der reinen Zahlentheorie. *Mathematische Annalen* **1936**, *112*, 493–565.

(16) Dütsch, M.; Fredenhagen, K. Algebraic Quantum Field Theory, Perturbation Theory, and the Loop Expansion. *Commun. Math. Phys.* **2001**, *219*, 5–30.

(17) Morel, L.; Yao, Z.; Cladé, P.; Guellati-Khélifa, S. Determination of the fine-structure constant with an accuracy of 81 parts per trillion. *Nature* **2020**, *588*, 61–65.

(18) Aoyama, T.; Hayakawa, M.; Kinoshita, T.; Nio, M. Quantum electrodynamics calculation of lepton anomalous magnetic moments: Numerical approach to the perturbation theory of QED. *Progress of Theoretical and Experimental Physics* **2012**, *2012*, 01A107.

(19) Yarkony, D. R. Diabolical conical intersections. *Reviews of Modern Physics* **1996**, *68*, 985.

(20) Köuppel, H.; Domcke, W.; Cederbaum, L. S. Multimode molecular dynamics beyond the Born-Oppenheimer approximation. *Advances in chemical physics* **1984**, 59–246.

(21) Bunker, P. R.; Moss, R. E. The effect of the breakdown of the Born-Oppenheimer approximation on the rotation-vibration Hamiltonian of a triatomic molecule. *Journal of Molecular Spectroscopy* **1980**, *80*, 217–228.

(22) Dirac, P. a. M. Note on Exchange Phenomena in the Thomas Atom. *Mathematical Proceedings of the Cambridge Philosophical Society* **1930**, *26*, 376–385.

(23) Bohr, N. I. On the constitution of atoms and molecules. *The London, Edinburgh, and Dublin Philosophical Magazine and Journal of Science* **1913**, *26*, 1–25.

(24) Lennard-Jones, J. E. Cohesion. *Proc. Phys. Soc.* **1931**, *43*, 461.

(25) Slater, J. C. The Theory of Complex Spectra. *Phys. Rev.* **1929**, *34*, 1293–1322.

(26) Langhoff, S. R.; Davidson, E. R. Configuration interaction calculations on the nitrogen molecule. *International Journal of Quantum Chemistry* **1974**, *8*, 61–72.

(27) Löwdin, P.-O. Quantum Theory of Many-Particle Systems. III. Extension of the Hartree-Fock Scheme to Include Degenerate Systems and Correlation Effects. *Phys. Rev.* **1955**, *97*, 1509–1520.

(28) Mazziotti, D. A. Quantum chemistry without wave functions: two-electron reduced density matrices. *Acc Chem Res* **2006**, *39*, 207–215.

(29) Mazziotti, D. A. Structure of Fermionic Density Matrices: Complete N -Representability Conditions. *Phys. Rev. Lett.* **2012**, *108*, 263002.

(30) Slater, J. C. Note on Hartree's Method. *Phys. Rev.* **1930**, *35*, 210–211.

(31) Fock, V. „Selfconsistent field“ mit Austausch für Natrium. *Z. Physik* **1930**, *62*, 795–805.

(32) Dunning Jr, T. H. Gaussian basis sets for use in correlated molecular calculations. I. The atoms boron through neon and hydrogen. *The Journal of chemical physics* **1989**, *90*, 1007–1023.

(33) Kaldor, U. Many-Body Perturbation-Theory Calculations with Finite, Bound Basis Sets. *Phys. Rev. A* **1973**, *7*, 427–434.

(34) Baerends, E. J.; Ros, P. Evaluation of the LCAO Hartree—Fock—Slater method: Applications to transition-metal complexes. *International Journal of Quantum Chemistry* **1978**, *14*, 169–190.

(35) Szabo, A.; Ostlund, N. S., *Modern Quantum Chemistry: Introduction to Advanced Electronic Structure Theory*, First; Dover Publications, Inc.: Mineola, 1996.

(36) Löwdin, P.-O. A Note on the Quantum-Mechanical Perturbation Theory. *The Journal of Chemical Physics* **1951**, *19*, 1396–1401.

(37) Hammes-Schiffer, S.; Andersen, H. C. The advantages of the general Hartree–Fock method for future computer simulation of materials. *The Journal of Chemical Physics* **1993**, *99*, 1901–1913.

(38) Ostlund, N. S. Complex and Unrestricted Hartree-Fock Wavefunctions. *The Journal of Chemical Physics* **2003**, *57*, 2994–2997.

(39) Pople, J. A. Nobel Lecture: Quantum chemical models. *Rev. Mod. Phys.* **1999**, *71*, 1267–1274.

(40) Horn, D.; Weinstein, M. The t-expansion: A nonperturbative analytic tool for Hamiltonian systems. *Phys. Rev. D* **1984**, *30*, 1256–1270.

(41) Roothaan, C. C. J. New Developments in Molecular Orbital Theory. *Rev. Mod. Phys.* **1951**, *23*, 69–89.

(42) Pople, J. A.; McIver Jr., J. W.; Ostlund, N. S. Self-Consistent Perturbation Theory. I. Finite Perturbation Methods. *The Journal of Chemical Physics* **2003**, *49*, 2960–2964.

(43) Shavitt, I.; Bartlett, R. J., *Many-Body Methods in Chemistry and Physics: MBPT and Coupled-Cluster Theory*; Cambridge Molecular Science; Cambridge University Press: Cambridge, 2009.

(44) Löwdin, P.-O. Studies in perturbation theory XIII. Treatment of constants of motion in resolvent method, partitioning technique, and perturbation theory. *International Journal of Quantum Chemistry* **1968**, *2*, 867–931.

(45) Löwdin, P.-O. Studies in Perturbation Theory. IV. Solution of Eigenvalue Problem by Projection Operator Formalism. *Journal of Mathematical Physics* **2004**, *3*, 969–982.

(46) Coester, F. Bound states of a many-particle system. *Nuclear Physics* **1958**, *7*, 421–424.

(47) Hugenholtz, N. M. Perturbation theory of large quantum systems. *Physica* **1957**, *23*, 481–532.

(48) Mathews, J.; Walker, R. L., *Mathematical Methods of Physics*; W. A. Benjamin: 1970.

(49) Linderberg, J.; Öhrn, Y., *Propagators in quantum chemistry*; John Wiley & Sons: 2004.

(50) Lindgren, I. The Rayleigh-Schrodinger perturbation and the linked-diagram theorem for a multi-configurational model space. *J. Phys. B: At. Mol. Phys.* **1974**, *7*, 2441–2470.

(51) Goldstone, J.; Mott, N. F. Derivation of the Brueckner many-body theory. *Proceedings of the Royal Society of London. Series A. Mathematical and Physical Sciences* **1997**, *239*, 267–279.

(52) Hubbard, J.; Peierls, R. E. The description of collective motions in terms of many-body perturbation theory. *Proceedings of the Royal Society of London. Series A. Mathematical and Physical Sciences* **1997**, *240*, 539–560.

(53) Lennard-Jones, J. E. Perturbation Problems in Quantum Mechanics. *Proceedings of the Royal Society of London. Series A, Containing Papers of a Mathematical and Physical Character* **1930**, *129*, 598–615.

(54) Møller, C.; Plesset, M. S. Note on an Approximation Treatment for Many-Electron Systems. *Phys. Rev.* **1934**, *46*, 618–622.

(55) Epstein, H.; Glaser, V. The role of locality in perturbation theory. *Annales de l'institut Henri Poincaré. Section A, Physique Théorique* **1973**, *19*, 211–295.

(56) Rayleigh, J. W. S. B., *The Theory of Sound*; Macmillan: 1896.

(57) Brillouin, L. Les problèmes de perturbations et les champs self-consistents. *J. Phys. Radium* **1932**, *3*, 373–389.

(58) Brillouin, L. Le champ self-consistent de Fock pour les électrons des métaux. *J. Phys. Radium* **1934**, *5*, 413–418.

(59) Brandow, B. In *Advances in quantum chemistry*; Elsevier: 1977; Vol. 10, pp 187–249.

(60) Bartlett, R. J. Coupled-cluster approach to molecular structure and spectra: a step toward predictive quantum chemistry. *J. Phys. Chem.* **1989**, *93*, 1697–1708.

(61) Čížek, J. On the Correlation Problem in Atomic and Molecular Systems. Calculation of Wavefunction Components in Ursell-Type Expansion Using Quantum-Field Theoretical Methods. *Journal of Chemical Physics* **1966**, *45*, 4256–4266.

(62) Kümmel, H.; Lührmann, K. H.; Zabolitzky, J. G. Many-fermion theory in expS- (or coupled cluster) form. *Physics Reports* **1978**, *36*, 1–63.

(63) Noga, J.; Bartlett, R. J.; Urban, M. Towards a full CCSDT model for electron correlation. CCSDT-n models. *Chemical Physics Letters* **1987**, *134*, 126–132.

(64) Hirata, S.; Fan, P.-D.; Auer, A. A.; Nooijen, M.; Piecuch, P. Combined coupled-cluster and many-body perturbation theories. *The Journal of Chemical Physics* **2004**, *121*, 12197–12207.

(65) Rishi, V.; Perera, A.; Bartlett, R. J. Behind the success of modified coupled-cluster methods: addition by subtraction. *Molecular Physics* **2019**, *117*, 2201–2216.

(66) Scuseria, G. E.; Henderson, T. M.; Sorensen, D. C. The Ground State Correlation Energy of the Random Phase Approximation from a Ring Coupled Cluster Doubles Approach. *The Journal of Chemical Physics* **2008**, *129*, 231101.

(67) Raghavachari, K.; Trucks, G. W.; Pople, J. A.; Head-Gordon, M. A fifth-order perturbation comparison of electron correlation theories. *Chemical Physics Letters* **1989**, *157*, 479–483.

(68) Löwdin, P.-O. To reach for the unreachable - psi and gamma. *Journal of Molecular Structure: THEOCHEM* **1988**, *165*, 177–188.

(69) Surján, P. R.; Szabados, Á. Constant denominator perturbative schemes and the partitioning technique. *International Journal of Quantum Chemistry* **2002**, *90*, 20–26.

(70) Stubbins, C. Methods of extrapolating the t-expansion series. *Phys Rev D Part Fields* **1988**, *38*, 1942–1949.

(71) Knowles, P. J. On the validity and applicability of the connected moments expansion. *Chemical Physics Letters* **1987**, *134*, 512–518.

(72) Cioslowski, J. Connected moments expansion: A new tool for quantum many-body theory. *Phys. Rev. Lett.* **1987**, *58*, 83–85.

(73) Cioslowski, J. Connected moments expansion for the ground-state energy of systems described by nonlinear Hamiltonians. *Phys. Rev. A* **1987**, *36*, 374–376.

(74) Cioslowski, J.; Kertesz, M.; Surjan, P. R.; Poirier, R. A. Connected moments expansion calculations of the correlation energy in small molecules. *Chemical Physics Letters* **1987**, *138*, 516–519.

(75) Lorentz, H. A. In *Collected Papers: Volume V*, Lorentz, H. A., Ed.; Springer Netherlands: Dordrecht, 1937, pp 172–197.

(76) Larmor, J. IX. A dynamical theory of the electric and luminiferous medium.—Part III. Relations with material media. *Philosophical Transactions of the Royal Society of London. Series A, Containing Papers of a Mathematical or Physical Character* **1897**, 205–300.

(77) Hameka, H. F. Theory of Magnetic Properties of Molecules with Particular Emphasis on the Hydrogen Molecule. *Rev. Mod. Phys.* **1962**, *34*, 87–101.

(78) Flygare, W.; Benson, R. The molecular Zeeman effect in diamagnetic molecules and the determination of molecular magnetic moments (g values), magnetic susceptibilities, and molecular quadrupole moments. *Molecular Physics* **1971**, *20*, 225–250.

(79) Buckingham, A. D. Permanent and induced molecular moments and long-range intermolecular forces. *Advances in Chemical Physics: Intermolecular Forces* **1967**, 107–142.

(80) Sauer, S. P. A., *Molecular Electromagnetism: A Computational Chemistry Approach*; Oxford Graduate Texts; Oxford University Press: Oxford, New York, 2011.

(81) Rabi, I. I.; Ramsey, N. F.; Schwinger, J. Use of Rotating Coordinates in Magnetic Resonance Problems. *Rev. Mod. Phys.* **1954**, *26*, 167–171.

(82) Fukui, H. Theory and calculation of nuclear shielding constants. *Progress in Nuclear Magnetic Resonance Spectroscopy* **1997**, *31*, 317–342.

(83) Helgaker, T.; Jaszuński, M.; Ruud, K. Ab Initio Methods for the Calculation of NMR Shielding and Indirect SpinSpin Coupling Constants. *Chem. Rev.* **1999**, *99*, 293–352.

(84) Gauss, J. Accurate Calculation of NMR Chemical Shifts. *Berichte der Bunsengesellschaft für physikalische Chemie* **1995**, *99*, 1001–1008.

(85) McWeeny, R. On the Origin of Spin-Hamiltonian Parameters. *The Journal of Chemical Physics* **1965**, *42*, 1717–1725.

(86) Ruud, K.; Helgaker, T.; Bak, K. L.; Jo/rgensen, P.; Jensen, H. J. A. Hartree–Fock limit magnetizabilities from London orbitals. *The Journal of chemical physics* **1993**, *99*, 3847–3859.

(87) Cohen, H. D.; Roothaan, C. Electric dipole polarizability of atoms by the Hartree—Fock method. I. Theory for closed-shell systems. *The Journal of chemical physics* **1965**, *43*, S34–S39.

(88) Ditchfield, R. Self-consistent perturbation theory of diamagnetism. *Molecular Physics* **1974**, *27*, 789–807.

(89) Malkin, V. G.; Malkina, O. L.; Casida, M. E.; Salahub, D. R. Nuclear magnetic resonance shielding tensors calculated with a sum-over-states density functional perturbation theory. *Journal of the American Chemical Society* **1994**, *116*, 5898–5908.

(90) Stanton, R. E. Hellmann-Feynman Theorem and Correlation Energies. *The Journal of Chemical Physics* **2004**, *36*, 1298–1300.

(91) Slater, J. C. Hellmann-Feynman and Virial Theorems in the X Method. *The Journal of Chemical Physics* **2003**, *57*, 2389–2396.

(92) Handy, N. C.; Schaefer III, H. F. On the evaluation of analytic energy derivatives for correlated wave functions. *The Journal of Chemical Physics* **1984**, *81*, 5031–5033.

(93) Kállay, M.; Gauss, J. Analytic second derivatives for general coupled-cluster and configuration-interaction models. *The Journal of chemical physics* **2004**, *120*, 6841–6848.

(94) Amos, R. D.; Rice, J. E. Implementation of analytic derivative methods in quantum chemistry. *Computer Physics Reports* **1989**, *10*, 147–187.

(95) Pople, J. A.; Krishnan, R.; Schlegel, H. B.; Binkley, J. S. Derivative studies in hartree-fock and møller-plesset theories. *Int. J. Quantum Chem.* **2009**, *16*, 225–241.

(96) Tellgren, E. I.; Helgaker, T.; Soncini, A. Non-perturbative magnetic phenomena in closed-shell paramagnetic molecules. *Phys Chem Chem Phys* **2009**, *11*, 5489–5498.

(97) Liu, S. et al. Multiresolution 3D-DenseNet for chemical shift prediction in NMR crystallography. *The journal of physical chemistry letters* **2019**, *10*, 4558–4565.

(98) Liang, J. et al. Efficient calculation of NMR shielding constants using composite method approximations and locally dense basis sets. *Journal of Chemical Theory and Computation* **2023**, *19*, 514–523.

(99) Stauch, T. et al. Molecular magnetisabilities computed via finite fields: assessing alternatives to MP2 and revisiting magnetic exaltations in aromatic and antiaromatic species. *Molecular Physics* **2021**, *119*.

(100) Wong, J. et al. An in-silico NMR laboratory for nuclear magnetic shieldings computed via finite fields: Exploring nucleus-specific renormalizations of MP2 and MP3. *The Journal of chemical physics* **2023**, *158*.

(101) Löwdin, P.-O. Studies in Perturbation Theory. IV. Solution of Eigenvalue Problem by Projection Operator Formalism. *J. Math. Phys.* **1962**, *3*, 969–982.

(102) Brillouin, L. Les problèmes de perturbations et les champs self-consistents. *J. Phys. Radium* **1932**, *3*, 373–389.

(103) Schrödinger, E. Quantisierung als Eigenwertproblem. *Ann. Phys.* **1926**, *385*, 437–490.

(104) Møller, C.; Plesset, M. S. Note on an Approximation Treatment for Many-Electron Systems. *Phys. Rev.* **1934**, *46*, 618.

(105) Coester, F. Bound states of a many-particle system. *Nucl. Phys.* **1958**, *7*, 421–424.

(106) Coester, F.; Kümmel, H. Short-range correlations in nuclear wave functions. *Nucl. Phys.* **1960**, *17*, 477–485.

(107) Čıžek, J. On the Correlation Problem in Atomic and Molecular Systems. Calculation of Wavefunction Components in Ursell-Type Expansion Using Quantum-Field Theoretical Methods. *J. Chem. Phys.* **1966**, *45*, 4256–4266.

(108) Čižek, J. On the use of the cluster expansion and the technique of diagrams in calculations of correlation effects in atoms and molecules. *Adv. Chem. Phys.* **1969**, 35–89.

(109) Andersson, K.; Malmqvist, P.-Å.; Roos, B. Second-Order Perturbation Theory with a Complete Active Space Self-Consistent Field Reference Function. *J. Chem. Phys.* **1992**, *96*, 1218–1226.

(110) Chan, G. K.-L.; Sharma, S. The Density Matrix Renormalization Group in Quantum Chemistry. *Annu. Rev. Phys. Chem.* **2011**, *62*, 465–481.

(111) Small, D.; Head-Gordon, M. Correction to constrained coupled cluster doubles models based on the second coupled cluster central moment. *J. Chem. Phys.* **2007**, *127*, 064102.

(112) Horn, D.; Weinstein, M. The t expansion: A nonperturbative analytic tool for Hamiltonian systems. *Phys. Rev. D* **1984**, *30*, 1256–1270.

(113) Metropolis, N.; Ulam, S. The monte carlo method. *Journal of the American statistical association* **1949**, *44*, 335–341.

(114) Kalos, M. H. Monte Carlo calculations of the ground state of three-and four-body nuclei. *Physical Review* **1962**, *128*, 1791.

(115) Kalos, M. H. Monte Carlo Calculations of the Ground State of Three- and Four-Body Nuclei. *Phys. Rev.* **1962**, *128*, 1791–1795.

(116) Reynolds, P. J.; Ceperley, D. M.; Alder, B. J.; Lester Jr, W. A. Fixed-node quantum Monte Carlo for molecules. *The Journal of Chemical Physics* **1982**, *77*, 5593–5603.

(117) Sugiyama, G.; Koonin, S. Auxiliary field Monte-Carlo for quantum many-body ground states. *Annals of Physics* **1986**, *168*, 1–26.

(118) Horn, D.; Karliner, M.; Weinstein, M. The t expansion and SU(2) lattice gauge theory. *Phys. Rev. D* **1985**, *31*, 2589–2599.

(119) Stubbins, C. Methods of extrapolating the t-expansion series. *Phys. Rev. D* **1988**, *38*, 1942–1949.

(120) Cioslowski, J. Connected moments expansion: A new tool for quantum many-body theory. *Phys. Rev. Lett.* **1987**, *58*, 83–85.

(121) Knowles, P. On the validity and applicability of the connected moments expansion. *Chem. Phys. Lett.* **1987**, *134*, 512–518.

(122) Mancini, J. D.; Zhou, Y.; Meier, P. F. Analytic properties of connected moments expansions. *Int. J. Quantum Chem.* **1994**, *50*, 101–107.

(123) Mancini, J. D.; Murawski, R. K.; Fessatidis, V.; Bowen, S. P. Generalized moments expansion applied to the two-dimensional $S = \frac{1}{2}$ Heisenberg model. *Phys. Rev. B* **2005**, *72*, 214405.

(124) Surján, P. R.; Szabados, Á. Constant denominator perturbative schemes and the partitioning technique. *Int. J. Quantum Chem.* **2002**, *90*, 20–26.

(125) Mancini, J. D.; Prie, J. D.; Massano, W. J. Approximations to the ground-state energy of the single-impurity Kondo model using variational and connected-moments expansions. *Phys. Rev. A* **1991**, *43*, 1777.

(126) Lo, C.; Wong, Y. J. Connected-moments expansion for the S = 1/2 antiferromagnetic spin chain. *Phys. Lett. A* **1994**, *187*, 269–272.

(127) Fernández, F. M. Rayleigh–Ritz variation method and connected-moments polynomial approach. *Int. J. Quantum Chem.* **2009**, *109*, 717–719.

(128) Fernández, F. M. On perturbation theory for the Fokker–Planck equation. *Phys. Scr.* **2009**, *80*, 065010.

(129) Fessatidis, V.; Mancini, J. D.; Bowen, S. P.; Campuzano, M. Zero point energy of the Pullen–Edmonds Hamiltonian. *J. Math. Chem.* **2008**, *44*, 20–27.

(130) Mancini, J. D.; Zhou, Y.; Meier, P. F.; Massano, W. J.; Prie, J. D. Numerical analysis of moments expansions. *Phys. Lett. A* **1994**, *185*, 435–439.

(131) Fessatidis, V.; Corvino, F. A.; Mancini, J. D.; Murawski, R. K.; Mikalopas, J. Analytic properties of moments matrices. *Phys. Lett. A* **2010**, *374*, 2890–2893.

(132) Cioslowski, J. Connected moments expansion for the ground-state energy of systems described by nonlinear Hamiltonians. *Phys. Rev. A* **1987**, *36*, 374.

(133) Cioslowski, J. A study of the connected moments expansions for the correlation energy via an exactly soluble problem. *Int. J. Quantum Chem.* **1987**, *32*, 563–567.

(134) Cioslowski, J. Estimation of the overlap between the approximate and exact wave function of the ground state from the connected-moments expansion. *Phys. Rev. A* **1987**, *36*, 3441.

(135) Cioslowski, J. The connected moments expansion for the zero-point energy of coupled anharmonic oscillators. *Chem. Phys. Lett.* **1987**, *136*, 515–518.

(136) Amore, P.; Fernandez, F.; Rodriguez, M. High-order connected moments expansion for the Rabi Hamiltonian. *Open Phys.* **2012**, *10*, 102–108.

(137) Fessatidis, V.; Mancini, J. D.; Bowen, S. P. Moments expansion study of the Rabi Hamiltonian. *Phys. Lett. A* **2002**, *297*, 100–104.

(138) Massano, W. J.; Bowen, S. P.; Mancini, J. D. Application of the connected-moment expansion to single-impurity Anderson Hamiltonians. *Phys. Rev. A* **1989**, *39*, 4301.

(139) Mancini, J. D.; Massano, W. J. Ground-state energy of the Wolff model. *Phys. Lett. A* **1991**, *160*, 457–460.

(140) Zhuravlev, A. Cumulant t-expansion for strongly correlated fermions. *Phys. Lett. A* **2016**, *380*, 1995–1999.

(141) Amore, P.; Fernández, F. M.; Rodriguez, M. Further analysis of the connected moments expansion. *J. Phys. A* **2011**, *44*, 505302.

(142) Lee, K.; Lo, C. Application of the connected-moments expansion to the half-filled Hubbard model. *Il Nuovo Cimento D* **1993**, *15*, 1483–1487.

(143) Mancini, J. D.; Zhou, Y.; Meier, P. F. Analytic properties of connected moments expansions. *Int. J. Quantum Chem.* **1994**, *50*, 101–107.

(144) Ullah, N. Removal of the singularity in the moment-expansion formalism. *Phys. Rev. A* **1995**, *51*, 1808.

(145) Amore, P.; Fernández, F. Solution to the equations of the moment expansions. *Open Phys.* **2013**, *11*, 195–205.

(146) Mancini, J. D.; Murawski, R. K.; Fessatidis, V.; Bowen, S. P. Generalized moments expansion applied to the two-dimensional S = 1/2 Heisenberg model. *Phys. Rev. B* **2005**, *72*, 214405.

(147) Yoshida, T.; Iguchi, K. Connected moments expansion with variational Monte Carlo technique. *Chem. Phys. Lett.* **1988**, *143*, 329–331.

(148) Noga, J.; Szabados, A.; Surján, P. On the Use of Connected Moments Expansion with Coupled Cluster Reference. *Int. J. Mol. Sci.* **2002**, *3*, 508–521.

(149) Kowalski, K.; Piecuch, P. The method of moments of coupled-cluster equations and the renormalized CCSD [T], CCSD (T), CCSD (TQ), and CCSDT (Q) approaches. *The Journal of Chemical Physics* **2000**, *113*, 18–35.

(150) Piecuch, P.; Kowalski, K.; Pimienta, I. S.; Mcguire, M. J. Recent advances in electronic structure theory: Method of moments of coupled-cluster equations and renormalized coupled-cluster approaches. *International Reviews in Physical Chemistry* **2002**, *21*, 527–655.

(151) Pimienta, I. S.; Kowalski, K.; Piecuch, P. Method of moments of coupled-cluster equations: The quasivariational and quadratic approximations. *The Journal of chemical physics* **2003**, *119*, 2951–2962.

(152) Cioslowski, J.; Kertesz, M.; Surjan, P.; Poirier, R. Connected moments expansion calculations of the correlation energy in small molecules. *Chemical physics letters* **1987**, *138*, 516–519.

(153) Kowalski, K.; Peng, B. Quantum simulations employing connected moments expansions. *J. Chem. Phys.* **2020**, *153*, 201102.

(154) Claudino, D.; Peng, B.; Bauman, N. P.; Kowalski, K.; Humble, T. S. Improving the accuracy and efficiency of quantum connected moments expansions. *Quantum Sci. Technol.* **2021**, *6*, 034012.

(155) Ren, X.; Rinke, P.; Joas, C.; Scheffler, M. Random-phase approximation and its applications in computational chemistry and materials science. *J. Mat. Sci.* **2012**, *47*, 7447–7471.

(156) Bartlett, R. J.; Shavitt, I. Comparison of high-order many-body perturbation theory and configuration interaction for H2O. *Chem. Phys. Lett.* **1977**, *50*, 190–198.

(157) Čižek, J.; Paldus, J. Correlation problems in atomic and molecular systems III. Rederivation of the coupled-pair many-electron theory using the traditional quantum chemical methods. *Int. J. Quantum Chem.* **1971**, *5*, 359–379.

(158) Čižek, J. On the correlation problem in atomic and molecular systems. Calculation of wavefunction components in Ursell-type expansion using quantum-field theoretical methods. *J. Chem. Phys.* **1966**, *45*, 4256–4266.

(159) Raghavachari, K.; Pople, J. A.; Replogle, E. S.; Head-Gordon, M. Fifth order Moeller-Plesset perturbation theory: comparison of existing correlation methods and implementation of new methods correct to fifth order. *J. Phys. Chem.* **1990**, *94*, 5579–5586.

(160) Purvis III, G.; Bartlett, R. A full coupled-cluster singles and doubles model: The inclusion of disconnected triples. *J. Chem. Phys.* **1982**, *76*, 1910–1918.

(161) Noga, J.; Bartlett, R. J. The full CCSDT model for molecular electronic structure. *J. Chem. Phys.* **1987**, *86*, 7041–7050.

(162) Raghavachari, K.; Trucks, G.; Pople, J.; Head-Gordon, M. A fifth-order perturbation comparison of electron correlation theories. *Chem. Phys. Lett.* **1989**, *157*, 479–483.

(163) Bartlett, R. J.; Watts, J.; Kucharski, S.; Noga, J. Non-iterative fifth-order triple and quadruple excitation energy corrections in correlated methods. *Chemical physics letters* **1990**, *165*, 513–522.

(164) Stanton, J. F. Why CCSD(T) works: a different perspective. *Chem. Phys. Lett.* **1997**, *281*, 130–134.

(165) Rishi, V.; Perera, A.; Bartlett, R. J. Behind the success of modified coupled-cluster methods: addition by subtraction. *Mol. Phys.* **2019**, *117*, 2201–2216.

(166) Lochan, R. C.; Head-Gordon, M. Orbital-optimized opposite-spin scaled second-order correlation: An economical method to improve the description of open-shell molecules. *J. Chem. Phys.* **2007**, *126*, 164101.

(167) Lee, J.; Head-Gordon, M. Regularized orbital-optimized second-order Møller–Plesset perturbation theory: A reliable fifth-order-scaling electron correlation model with orbital energy dependent regularizers. *J. Chem. Theory Comput.* **2018**, *14*, 5203–5219.

(168) Rettig, A.; Shee, J.; Lee, J.; Head-Gordon, M. Revisiting the orbital energy-dependent regularization of orbital-optimized second-order Møller–Plesset theory. *J. Chem. Theory Comput.* **2022**, *18*, 5382–5392.

(169) Handy, N. C.; Pople, J. A.; Head-Gordon, M.; Raghavachari, K.; Trucks, G. W. Size-consistent Brueckner theory limited to double substitutions. *Chem. Phys. Lett.* **1989**, *164*, 185–192.

(170) Raghavachari, K.; Pople, J. A.; Replogle, E. S.; Head-Gordon, M.; Handy, N. C. Size-consistent Brueckner theory limited to double and triple substitutions. *Chem. Phys. Lett.* **1990**, *167*, 115–121.

(171) Cremer, D. Møller–Plesset perturbation theory: from small molecule methods to methods for thousands of atoms. *Wiley Interdiscip. Rev.: Comput. Mol. Sci.* **2011**, *1*, 509–530.

(172) Shao, Y. et al. Advances in molecular quantum chemistry contained in the Q-Chem 4 program package. *Mol. Phys.* **2015**, *113*, 184–215.

(173) Epifanovsky, E. et al. Software for the frontiers of quantum chemistry: An overview of developments in the Q-Chem 5 package. *J. Chem. Phys.* **2021**, *155*, 084801.

(174) Tubman, N. M.; Freeman, C. D.; Levine, D. S.; Hait, D.; Head-Gordon, M.; Whaley, K. B. Modern approaches to exact diagonalization and selected configuration interaction with the adaptive sampling CI method. *J. Chem. Theory Comput.* **2020**, *16*, 2139–2159.

(175) Pople, J. A.; Head-Gordon, M.; Fox, D. J.; Raghavachari, K.; Curtiss, L. A. Gaussian-1 theory: A general procedure for prediction of molecular energies. *J. Chem. Phys.* **1989**, *90*, 5622–5629.

(176) Grossman, J. C. Benchmark quantum Monte Carlo calculations. *J. Chem. Phys.* **2002**, *117*, 1434–1440.

(177) Ma, A.; Towler, M. D.; Drummond, N. D.; Needs, R. J. Scheme for adding electron-nucleus cusps to Gaussian orbitals. *J. Chem. Phys.* **2005**, *122*, 224322.

(178) Marko š, P.; Olejnık, S. Š. t-expansion and connected-moment expansion: A generalization to excited states. *Phys. Rev. D* **1990**, *42*, 2943–2946.

(179) Handy, N.; Knowles, P.; Somasundram, K. On the convergence of the Møller-Plesset perturbation series. *Theor. Chem. Acc.* **1985**, *68*, 87–100.

(180) Christiansen, O.; Olsen, J.; Jørgensen, P.; Koch, H.; Malmqvist, P.-Å. On the inherent divergence in the Møller-Plesset series. The neon atom—A test case. *Chem. Phys. Lett.* **1996**, *261*, 369–378.

(181) Krogh, J. W.; Olsen, J. A general coupled cluster study of the N2 molecule. *Chem. Phys. Lett.* **2001**, *344*, 578–586.

(182) Chan, G. K.-L.; Kállay, M.; Gauss, J. State-of-the-art density matrix renormalization group and coupled cluster theory studies of the nitrogen binding curve. *J. Chem. Phys.* **2004**, *121*, 6110–6116.

(183) Engels-Putzka, A.; Hanrath, M. Dissociating N2: a multi-reference coupled cluster study on the potential energy surfaces of ground and excited states. *Mol. Phys.* **2009**, *107*, 143–155.

(184) Kurlancheek, W.; Head-Gordon, M. Violations of N-representability from spin-unrestricted orbitals in Møller–Plesset perturbation theory and related double-hybrid density functional theory. *Mol. Phys.* **2009**, *107*, 1223–1232.

(185) Stück, D.; Head-Gordon, M. Regularized orbital-optimized second-order perturbation theory. *J. Chem. Phys.* **2013**, *139*, 244109.

(186) Lee, J.; Lin, L.; Head-Gordon, M. Systematically improvable tensor hypercontraction: Interpolative separable density-fitting for molecules applied to exact exchange, second-and third-order Møller–Plesset perturbation theory. *J. Chem. Theory Comput.* **2019**, *16*, 243–263.

(187) Hurley, A. C.; Lennard-Jones, J. E.; Pople, J. A. The molecular orbital theory of chemical valency XVI. A theory of paired-electrons in polyatomic molecules. *Proc. Roy. Soc. Ser. A* **1953**, *220*, 446–455.

(188) Small, D. W.; Head-Gordon, M. Tractable spin-pure methods for bond breaking: Local many-electron spin-vector sets and an approximate valence bond model. *J. Chem. Phys.* **2009**, *130*, 084103.

(189) Small, D. W.; Head-Gordon, M. Post-modern valence bond theory for strongly correlated electron spins. *Phys. Chem. Chem. Phys.* **2011**, *13*, 19285–19297.

(190) Davies, D. *The Theory of the Electric and Magnetic Properties of Molecules* **1967**.

(191) Hinchliffe, A.; Munn, R. Molecular Electromagnetism. *Molecular Electromagnetism* **1985**.

(192) Sauer, S. Molecular Electromagnetism. A Computational Chemistry Approach. *Molecular Electromagnetism: A Computational Chemistry Approach* **2011**.

(193) Ramsey, N. The internal diamagnetic field correction in measurements of the proton magnetic moment. *Physical Review* **1950**, *77*, 567.

(194) Ramsey, N. Dependence of magnetic shielding of nuclei upon molecular orientation. *Physical Review* **1951**, *83*, 540–541.

(195) Ramsey, N. Chemical effects in nuclear magnetic resonance and in diamagnetic susceptibility. *Physical Review* **1952**, *86*, 243–246.

(196) Ramsey, N. Electron coupled interactions between nuclear spins in molecules. *Physical Review* **1953**, *91*, 303–307.

(197) Ramsey, N. Magnetic shielding of nuclei in molecules. *Physical Review* **1950**, *78*, 699–703.

(198) Ramsey, N.; Purcell, E. Interactions between nuclear spins in molecules. *Physical Review* **1952**, *85*, 143–144.

(199) Ramsey, N. Spin interactions of accelerated nuclei in molecules. *Physical Review* **1953**, *90*, 232–233.

(200) Ramsey, N. Pseudo-quadrupole effect for nuclei in molecules. *Physical Review* **1953**, *89*, 527.

(201) Helgaker, T.; Jaszuński, M.; Ruud, K. Ab initio methods for the calculation of NMR shielding and indirect spin-spin coupling constants. *Chemical Reviews* **1999**, *99*, 293–352.

(202) Van Eldik, R.; Reedijk, J. Advances in Inorganic Chemistry. *Advances in Inorganic Chemistry* **2006**.

(203) Ruud, K.; Skaane, H.; Helgaker, T.; Bak, K.; Jorgensen, P. Magnetizability of Hydrocarbons. *Journal of the American Chemical Society* **1994**, *116*, 10135–10140.

(204) Pauling, L. The diamagnetic anisotropy of aromatic molecules. *The Journal of Chemical Physics* **1936**, *4*, 673–677.

(205) Schleyer, P.; Jiao, H. What is aromaticity? *Pure and Applied Chemistry* **1996**, *68*, 209–218.

(206) Jiao, H.; Von Ragué Schleyer, P.; Mo, Y.; McAllister, M.; Tidwell, T. Magnetic evidence for the aromaticity and antiaromaticity of charged fluorenyl, indenyl, and cyclopentadienyl systems. *Journal of the American Chemical Society* **1997**, *119*, 7075–7083.

(207) Ruud, K.; Helgaker, T.; Bak, K.; Jørgensen, P.; Olsen, J. Accurate magnetizabilities of the isoelectronic series BeH-, BH, and CH+. The MCSCF-GIAO approach. *Chemical Physics* **1995**, *195*, 157–169.

(208) Shoemaker, R.; Flygare, W. Molecular quadrupole moment, molecular magnetic susceptibilities, and molecular g values in benzene. *The Journal of Chemical Physics* **1969**, *51*, 2988–2991.

(209) Flygare, W.; Benson, R. The molecular zeeman effect in diamagnetic molecules and the determination of molecular magnetic moments (G values), magnetic susceptibilities, and molecular quadrupole moments. *Molecular Physics* **1971**, *20*, 225–250.

(210) Ruud, K.; Helgaker, T.; Jørgensen, P. The effect of correlation on molecular magnetizabilities and rotational g tensors. *Journal of Chemical Physics* **1997**, *107*, 10599–10606.

(211) Hyams, P.; Gerratt, J.; Cooper, D.; Raimondi, M. The calculation of molecular response properties using perturbed spin-coupled wave functions. II. Polarizability and magnetic susceptibility of H2 and LiH as functions of internuclear distance. *The Journal of Chemical Physics* **1994**, *100*, 4417–4431.

(212) Loibl, S.; Manby, F.; Schutz, M. Density fitted, local Hartree-Fock treatment of NMR chemical shifts using London atomic orbitals. *Molecular Physics* **2010**, *108*, 477–485.

(213) Wilson, P.; Amos, R.; Handy, N. Density functional predictions for magnetizabilities and nuclear shielding constants. *Molecular Physics* **1999**, *97*, 757–768.

(214) Tellgren, E. I.; Teale, A. M.; Furness, J. W.; Lange, K.; Ekström, U.; Helgaker, T. Non-perturbative calculation of molecular magnetic properties within current-density functional theory. *The Journal of chemical physics* **2014**, *140*.

(215) Reimann, S.; Borgoo, A.; Tellgren, E.; Teale, A.; Helgaker, T. Magnetic-Field Density-Functional Theory (BDFT): Lessons from the Adiabatic Connection. *Journal of Chemical Theory and Computation* **2017**, *13*, 4089–4100.

(216) Sauer, S.; Enevoldsen, T.; Oddershede, J. Paramagnetism of closed shell diatomic hydrides with six valence electrons. *The Journal of Chemical Physics* **1993**, *98*, 9748–9757.

(217) Cybulski, S.; Bishop, D. Calculation of magnetic properties. VI. Electron correlated nuclear shielding constants and magnetizabilities for thirteen small molecules. *Journal of Chemical Physics* **1997**, *106*, 4082–4090.

(218) Cybulski, S.; Bishop, D. Calculation of magnetic properties VII. Electron-correlated magnetizability polarizabilities and nuclear shielding polarizabilities for nine small molecules. *Molecular Physics* **1998**, *93*, 739–750.

(219) Gauss, J.; Ruud, K.; Kállay, M. Gauge-origin independent calculation of magnetizabilities and rotational g tensors at the coupled-cluster level. *Journal of Chemical Physics* **2007**, *127*.

(220) Cybulski, S.; Bishop, D. Electron-correlated calculations of magnetic properties: I. Magnetizability of H2 and HF. *Molecular Physics* **1992**, *76*, 1289–1301.

(221) Cybulski, S.; Bishop, D. Calculations of magnetic properties. IV. Electron-correlated magnetizabilities and rotational g factors for nine small molecules. *The Journal of Chemical Physics* **1994**, *100*, 2019–2026.

(222) Loibl, S.; Schütz, M. Magnetizability and rotational g tensors for density fitted local second-order Møller-Plesset perturbation theory using gauge-including atomic orbitals. *Journal of Chemical Physics* **2014**, *141*.

(223) Yoshizawa, T.; Hada, M. Relativistic and electron-correlation effects on magnetizabilities investigated by the douglas-kroll-hess method and the second-order møller-plesset perturbation theory. *Journal of Computational Chemistry* **2009**, *30*, 2550–2566.

(224) Raghavachari, K.; Trucks, G.; Pople, J.; Head-Gordon, M. A fifth-order perturbation comparison of electron correlation theories. *Chemical Physics Letters* **1989**, *157*, 479–483.

(225) Lutns, O.; Teale, A.; Helgaker, T.; Tozer, D.; Ruud, K.; Gauss, J. Benchmarking density-functional-theory calculations of rotational g tensors and magnetizabilities using accurate coupled-cluster calculations. *Journal of Chemical Physics* **2009**, *131*.

(226) Lehtola, S.; Dimitrova, M.; Fliegl, H.; Sundholm, D. Benchmarking Magnetizabilities with Recent Density Functionals. *Journal of Chemical Theory and Computation* **2021**, *17*, 1457–1468.

(227) Lochan, R.; Head-Gordon, M. Orbital-optimized opposite-spin scaled second-order correlation: An economical method to improve the description of open-shell molecules. *Journal of Chemical Physics* **2007**, *126*.

(228) Neese, F.; Schwabe, T.; Kossmann, S.; Schirmer, B.; Grimme, S. Assessment of orbital-optimized, spin-component scaled second-order many-body perturbation theory for thermochemistry and kinetics. *Journal of Chemical Theory and Computation* **2009**, *5*, 3060–3073.

(229) Bozkaya, U.; Turney, J.; Yamaguchi, Y.; Schaefer III, H.; Sherrill, C. Quadratically convergent algorithm for orbital optimization in the orbital-optimized coupled-cluster doubles method and in orbital-optimized second-order Mller-Plesset perturbation theory. *Journal of Chemical Physics* **2011**, *135*.

(230) Bozkaya, U. Orbital-optimized second-order perturbation theory with density-fitting and cholesky decomposition approximations: An efficient implementation. *Journal of Chemical Theory and Computation* **2014**, *10*, 2371–2378.

(231) Razban, R.; Stück, D.; Head-Gordon, M. Addressing first derivative discontinuities in orbital-optimised opposite-spin scaled second-order perturbation theory with regularisation. *Molecular Physics* **2017**, *115*, 2102–2109.

(232) Lan, T.; Yanai, T. Correlated one-body potential from second-order Møller-Plesset perturbation theory: Alternative to orbital-optimized MP2 method. *Journal of Chemical Physics* **2013**, *138*.

(233) Lee, J.; Head-Gordon, M. Regularized Orbital-Optimized Second-Order Møller-Plesset Perturbation Theory: A Reliable Fifth-Order-Scaling Electron Correlation Model with Orbital Energy Dependent Regularizers. *Journal of Chemical Theory and Computation* **2018**, *14*, 5203–5219.

(234) Lee, J.; Head-Gordon, M. Two single-reference approaches to singlet biradicaloid problems: Complex, restricted orbitals and approximate spin-projection combined with regularized orbital-optimized Møller-Plesset perturbation theory. *Journal of Chemical Physics* **2019**, *150*.

(235) Lee, J.; Head-Gordon, M. Distinguishing artificial and essential symmetry breaking in a single determinant: Approach and application to the C60, C36, and C20 fullerenes. *Physical Chemistry Chemical Physics* **2019**, *21*, 4763–4778.

(236) Bertels, L.; Lee, J.; Head-Gordon, M. Third-Order Møller-Plesset Perturbation Theory Made Useful? Choice of Orbitals and Scaling Greatly Improves Accuracy for Thermochemistry, Kinetics, and Intermolecular Interactions. *Journal of Physical Chemistry Letters* **2019**, *10*, 4170–4176.

(237) Sen, S.; Tellgren, E. I. Non-perturbative calculation of orbital and spin effects in molecules subject to non-uniform magnetic fields. *The Journal of Chemical Physics* **2018**, *148*.

(238) London, F. The general theory of molecular forces. *Transactions of the Faraday Society* **1937**, *33*, 8b–26.

(239) Vaara, J. Theory and computation of nuclear magnetic resonance parameters. *Physical Chemistry Chemical Physics* **2007**, *9*, 5399–5418.

(240) Helgaker, T.; Coriani, S.; Jørgensen, P.; Kristensen, K.; Olsen, J.; Ruud, K. Recent advances in wave function-based methods of molecular-property calculations. *Chemical Reviews* **2012**, *112*, 543–631.

(241) Fornberg, B. Generation of finite difference formulas on arbitrarily spaced grids. *Mathematics of Computation* **1988**, *51*, 699–706.

(242) Stopkowicz, S.; Gauss, J.; Lange, K.; Tellgren, E.; Helgaker, T. Coupled-cluster theory for atoms and molecules in strong magnetic fields. *Journal of Chemical Physics* **2015**, *143*.

(243) Lehtola, S.; Dimitrova, M.; Sundholm, D. *Mol. Phys.* **2019**, 1.

(244) Beer, M.; Kussmann, J.; Ochsenfeld, C. Nuclei-selected NMR shielding calculations: A sublinear-scaling quantum-chemical method. *Journal of Chemical Physics* **2011**, *134*.

(245) Helgaker, T.; Joørgensen, P. An electronic Hamiltonian for origin independent calculations of magnetic properties. *The Journal of Chemical Physics* **1991**, *95*, 2595–2801.

(246) Irons, T.; Zemen, J.; Teale, A. Efficient Calculation of Molecular Integrals over London Atomic Orbitals. *Journal of Chemical Theory and Computation* **2017**, *13*, 3636–3649.

(247) Taketa, H.; Huzinaga, S.; O-ohata, K. Gaussian-expansion methods for molecular integrals. *Journal of the Physical Society of Japan* **1966**, *21*, 2313–2324.

(248) McMurchie, L.; Davidson, E. One- and two-electron integrals over cartesian gaussian functions. *Journal of Computational Physics* **1978**, *26*, 218–231.

(249) Dupuis, M.; Rys, J.; King, H. Evaluation of molecular integrals over Gaussian basis functions. *The Journal of Chemical Physics* **1976**, *65*, 111–116.

(250) King, H.; Dupuis, M. Numerical integration using rys polynomials. *Journal of Computational Physics* **1976**, *21*, 144–165.

(251) Gill, P.; Johnson, B.; Pople, J. Two-electron repulsion integrals over Gaussian s functions. *International Journal of Quantum Chemistry* **1991**, *40*, 745–752.

(252) Head-Gordon, M.; Pople, J. A method for two-electron Gaussian integral and integral derivative evaluation using recurrence relations. *The Journal of Chemical Physics* **1988**, *89*, 5777–5786.

(253) Pausch, A.; Klopper, W. Efficient evaluation of three-centre two-electron integrals over London orbitals. *Molecular Physics* **2020**, *118*.

(254) Handy, N.; Pople, J.; Head-Gordon, M.; Raghavachari, K.; Trucks, G. Size-consistent Brueckner theory limited to double substitutions. *Chemical Physics Letters* **1989**, *164*, 185–192.

(255) Sherrill, C.; Krylov, A.; Byrd, E.; Head-Gordon, M. Energies and analytic gradients for a coupled-cluster doubles model using variational Brueckner orbitals: Application to symmetry breaking in O4+. *Journal of Chemical Physics* **1998**, *109*, 4171–4181.

(256) Ortiz, J. Brueckner orbitals, Dyson orbitals, and correlation potentials. *International Journal of Quantum Chemistry* **2004**, *100*, 1131–1135.

(257) Loibl, S.; Schütz, M. NMR shielding tensors for density fitted local second-order Moller-Plesset perturbation theory using gauge including atomic orbitals. *Journal of Chemical Physics* **2012**, *137*.

(258) Shao, Y. et al. Advances in molecular quantum chemistry contained in the Q-Chem 4 program package. *Molecular Physics* **2015**, *113*, 184–215.

(259) Valatin, J. Generalized Hartree-Fock method. *Physical Review* **1961**, *122*, 1012–1020.

(260) Paul, C. A. In *Revival: The Handbook of Software for Engineers and Scientists (1995)*; CRC Press: 2018, pp 926–962.

(261) Hô, M.; Hernández-Pérez, J. M. Evaluation of Gaussian Molecular Integrals I. *The Mathematica Journal* **2012**, *14*.

(262) Hô, M.; Hernández-Pérez, J. Evaluation of Gaussian molecular integrals II. Kinetic-energy integrals. *Math J* **2013**, *15*, 1–1510.

(263) Hô, M.; Hernández-Pérez, J. Evaluation of Gaussian molecular integrals III. Nuclear-electron attraction integrals. *Math J* **2014**, *16*, 1–13.

(264) Aidas, K. et al. The Dalton quantum chemistry program system. *Wiley Interdisciplinary Reviews: Computational Molecular Science* **2014**, *4*, 269–284.

(265) Matthews, D. A. et al. Coupled-cluster techniques for computational chemistry: The CFOUR program package. *The Journal of Chemical Physics* **2020**, *152*.

(266) Lukins, P.; Laver, D.; Buckingham, A.; Ritchie, G. Cotton-Mouton effect, magnetic anisotropy and charge distribution of cyclopropane. *The Journal of Physical Chemistry* **1985**, *89*, 1309–1312.

(267) Wang, Y.-L.; Cooper, B. R. Collective excitations and magnetic ordering in materials with singlet crystal-field ground state. *Physical Review* **1968**, *172*, 539.

(268) Sutter, D.; Flygare, W. H. Molecular g values, magnetic susceptibility anisotropies, second moment of the charge distribution, and molecular quadrupole moments in ethylenimine and pyrrole. *Journal of the American Chemical Society* **1969**, *91*, 6895–6902.

(269) Pascal, B., *Thoughts*; PF Collier & son: 1910; Vol. 48.

(270) Haberditzl, W. Advances in molecular diamagnetism. *Angewandte Chemie International Edition in English* **1966**, *5*, 288–298.

(271) Dauben Jr, H. J.; Wilson, J. D.; Laity, J. L. Diamagnetic susceptibility exaltation as a criterion of aromaticity. *Journal of the American Chemical Society* **1968**, *90*, 811–813.

(272) Gershoni-Poranne, R.; Stanger, A. Magnetic criteria of aromaticity. *Chemical Society Reviews* **2015**, *44*, 6597–6615.

(273) Guo, Y.; Wang, B.; Zhang, X.; Yuan, S.; Ma, L.; Wang, J. Magnetic two-dimensional layered crystals meet with ferromagnetic semiconductors. *InfoMat* **2020**, *2*, 639–655.

(274) Mardirossian, N.; Head-Gordon, M. Thirty years of density functional theory in computational chemistry: An overview and extensive assessment of 200 density functionals. *Molecular Physics* **2017**, *115*, 2315–2372.

(275) Weigend, A.; Rumelhart, D.; Huberman, B. Generalization by weight-elimination with application to forecasting. *Advances in neural information processing systems* **1990**, *3*.

(276) Jung, Y.; Heine, T.; Schleyer, P.; Head-Gordon, M. Aromaticity of Four-Membered-Ring 6-Electron Systems: N 2S2 and Li2C4H4. *Journal of the American Chemical Society* **2004**, *126*, 3132–3138.

(277) Karadakov, P. B.; Hearnshaw, P.; Horner, K. E. Magnetic shielding, aromaticity, antiaromaticity, and bonding in the low-lying electronic states of benzene and cyclobutadiene. *The Journal of Organic Chemistry* **2016**, *81*, 11346–11352.

(278) Ramozzi, R.; Chéron, N.; Braıda, B.; Hiberty, P. C.; Fleurat-Lessard, P. A valence bond view of isocyanides' electronic structure. *New Journal of Chemistry* **2012**, *36*, 1137–1140.

(279) Herges, R.; Jiao, H.; von Ragué Schleyer, P. Magnetic properties of aromatic transition states: The Diels–Alder reactions. *Angewandte Chemie International Edition in English* **1994**, *33*, 1376–1378.

(280) Rettig, A.; Hait, D.; Bertels, L.; Head-Gordon, M. Third-Order Møller-Plesset Theory Made More Useful? The Role of Density Functional Theory Orbitals. *Journal of Chemical Theory and Computation* **2020**, *16*, 7473–7489.

(281) Loipersberger, M.; Bertels, L.; Lee, J.; Head-Gordon, M. Exploring the Limits of Second- And Third-Order Møller-Plesset Perturbation Theories for Noncovalent Interactions: Revisiting MP2.5 and Assessing the Importance of Regularization and Reference Orbitals. *Journal of Chemical Theory and Computation* **2021**, *17*, 5582–5599.

(282) Gil, R. Constitutional, configurational, and conformational analysis of small organic molecules on the basis of NMR residual dipolar couplings. *Angewandte Chemie - International Edition* **2011**, *50*, 7222–7224.

(283) Becette, O.; Zong, G.; Chen, B.; Taiwo, K.; Case, D.; Dayie, T. Solution NMR readily reveals distinct structural folds and interactions in doubly 13C- And 19F-labeled RNAs. *Science Advances* **2020**, *6*.

(284) Krivdin, L. Computational protocols for calculating 13C NMR chemical shifts. *Progress in Nuclear Magnetic Resonance Spectroscopy* **2019**, *112-113*, 103–156.

(285) Krivdin, L. Computational 1H NMR: Part 1. Theoretical background. *Magnetic Resonance in Chemistry* **2019**, *57*, 897–914.

(286) Gauss, J. Effects of electron correlation in the calculation of nuclear magnetic resonance chemical shifts. *The Journal of Chemical Physics* **1993**, *99*, 3629–3643.

(287) Casabianca, L.; De Dios, A. Ab initio calculations of NMR chemical shifts. *Journal of Chemical Physics* **2008**, *128*.

(288) Grimblat, N.; Sarotti, A. Computational Chemistry to the Rescue: Modern Toolboxes for the Assignment of Complex Molecules by GIAO NMR Calculations. *Chemistry - A European Journal* **2016**, *22*, 12246–12261.

(289) Wolinski, K.; Hinton, J.; Pulay, P. Efficient Implementation of the Gauge-Independent Atomic Orbital Method for NMR Chemical Shift Calculations. *Journal of the American Chemical Society* **1990**, *112*, 8251–8260.

(290) Auer, A.; Gauss, J.; Stanton, J. Quantitative prediction of gas-phase 13C nuclear magnetic shielding constants. *Journal of Chemical Physics* **2003**, *118*, 10407–10417.

(291) Teale, A.; Lutnæs, O.; Helgaker, T.; Tozer, D.; Gauss, J. Benchmarking density-functional theory calculations of NMR shielding constants and spin-rotation constants using accurate coupled-cluster calculations. *Journal of Chemical Physics* **2013**, *138*.

(292) Goerigk, L.; Hansen, A.; Bauer, C.; Ehrlich, S.; Najibi, A.; Grimme, S. A look at the density functional theory zoo with the advanced GMTKN55 database for general main group thermochemistry, kinetics and noncovalent interactions. *Physical Chemistry Chemical Physics* **2017**, *19*, 32184–32215.

(293) Grayce, C.; Harris, R. Magnetic-field density-functional theory. *Physical Review A* **1994**, *50*, 3089–3095.

(294) Tellgren, E.; Kvaal, S.; Sagvolden, E.; Ekström, U.; Teale, A.; Helgaker, T. Choice of basic variables in current-density-functional theory. *Physical Review A - Atomic, Molecular, and Optical Physics* **2012**, *86*.

(295) Furness, J. et al. Current Density Functional Theory Using Meta-Generalized Gradient Exchange-Correlation Functionals. *Journal of Chemical Theory and Computation* **2015**, *11*, 4169–4181.

(296) Tao, J.; Mo, Y. Accurate Semilocal Density Functional for Condensed-Matter Physics and Quantum Chemistry. *Physical Review Letters* **2016**, *117*.

(297) Schattenberg, C.; Kaupp, M. Effect of the Current Dependence of Tau-Dependent Exchange-Correlation Functionals on Nuclear Shielding Calculations. *Journal of Chemical Theory and Computation* **2021**, *17*, 1469–1479.

(298) Franzke, Y.; Holzer, C. Impact of the current density on paramagnetic NMR properties. *Journal of Chemical Physics* **2022**, *157*.

(299) Reimann, S. et al. Kohn–Sham energy decomposition for molecules in a magnetic field. *Molecular Physics* **2019**, *117*, 97–109.

(300) Flaig, D. et al. Benchmarking Hydrogen and Carbon NMR Chemical Shifts at HF, DFT, and MP2 Levels. *Journal of Chemical Theory and Computation* **2014**, *10*, 572–578.

(301) Stoychev, G.; Auer, A.; Izsák, R.; Neese, F. Self-Consistent Field Calculation of Nuclear Magnetic Resonance Chemical Shielding Constants Using Gauge-Including Atomic Orbitals and Approximate Two-Electron Integrals. *Journal of Chemical Theory and Computation* **2018**, *14*, 619–637.

(302) Liang, J. et al. Efficient Calculation of NMR Shielding Constants Using Composite Method Approximations and Locally Dense Basis Sets. *Journal of Chemical Theory and Computation* **2023**, *19*, 514–523.

(303) Ochsenfeld, C.; Kussmann, J.; Koziol, F. Ab initio NMR spectra for molecular systems with a thousand and more atoms: A linear-scaling method. *Angewandte Chemie - International Edition* **2004**, *43*, 4485–4489.

(304) Kussmann, J.; Ochsenfeld, C. Linear-scaling method for calculating nuclear magnetic resonance chemical shifts using gauge-including atomic orbitals within Hartree-Fock and density-functional theory. *Journal of Chemical Physics* **2007**, *127*.

(305) Bartlett, R.; Musiał, M. Coupled-cluster theory in quantum chemistry. *Reviews of Modern Physics* **2007**, *79*, 291–352.

(306) Bartlett, R. Coupled-cluster theory and its equation-of-motion extensions. *Wiley Interdisciplinary Reviews: Computational Molecular Science* **2012**, *2*, 126–138.

(307) Gauss, J.; Stanton, J. Electron-correlated approaches for the calculation of nmr chemical shifts. *Advances in Chemical Physics* **2002**, *123*, 355–422.

(308) Reid, D.; Collins, M. Approximating CCSD(T) nuclear magnetic shielding calculations using composite methods. *Journal of Chemical Theory and Computation* **2015**, *11*, 5177–5181.

(309) Schattenberg, C.; Kaupp, M. Extended Benchmark Set of Main-Group Nuclear Shielding Constants and NMR Chemical Shifts and Its Use to Evaluate Modern DFT Methods. *Journal of Chemical Theory and Computation* **2021**, *17*, 7602–7621.

(310) Prochnow, E.; Auer, A. Quantitative prediction of gas-phase 15N and 31P nuclear magnetic shielding constants. *Journal of Chemical Physics* **2010**, *132*.

(311) Harding, M.; Lenhart, M.; Auer, A.; Gauss, J. Quantitative prediction of gas-phase 19F nuclear magnetic shielding constants. *Journal of Chemical Physics* **2008**, *128*.

(312) Gauss, J.; Werner, H.-J. NMR chemical shift calculations within local correlation methods: The GIAO-LMP2 approach. *Physical Chemistry Chemical Physics* **2000**, *2*, 2083–2090.

(313) Stoychev, G.; Auer, A.; Gauss, J.; Neese, F. DLPNO-MP2 second derivatives for the computation of polarizabilities and NMR shieldings. *Journal of Chemical Physics* **2021**, *154*.

(314) Almlöf, J.; Taylor, P. R. In *Advances in Quantum Chemistry*; Elsevier: 1991; Vol. 22, pp 301–373.

(315) Ayala, P. Y.; Scuseria, G. E. Linear scaling second-order Moller–Plesset theory in the atomic orbital basis for large molecular systems. *The Journal of chemical physics* **1999**, *110*, 3660–3671.

(316) Maurer, M.; Ochsenfeld, C. Spin component-scaled second-order Møller-Plesset perturbation theory for calculating NMR shieldings. *Journal of Chemical Theory and Computation* **2015**, *11*, 37–44.

(317) Glasbrenner, M.; Vogler, S.; Ochsenfeld, C. Efficient low-scaling computation of NMR shieldings at the second-order Møller-Plesset perturbation theory level with Cholesky-decomposed densities and an attenuated Coulomb metric. *Journal of Chemical Physics* **2021**, *155*.

(318) Blaschke, S.; Stopkowicz, S. Cholesky decomposition of complex two-electron integrals over GIAOs: Efficient MP2 computations for large molecules in strong magnetic fields. *Journal of Chemical Physics* **2022**, *156*.

(319) Grimme, S. Improved second-order Møller-Plesset perturbation theory by separate scaling of parallel- and antiparallel-spin pair correlation energies. *Journal of Chemical Physics* **2003**, *118*, 9095–9102.

(320) Yan, W.; Xu, X. Accurate Prediction of Nuclear Magnetic Resonance Parameters via the XYG3 Type of Doubly Hybrid Density Functionals. *Journal of Chemical Theory and Computation* **2022**.

(321) Shee, J.; Loipersberger, M.; Rettig, A.; Lee, J.; Head-Gordon, M. Regularized Second-Order Møller–Plesset Theory: A More Accurate Alternative to Conventional MP2 for Noncovalent Interactions and Transition Metal Thermochemistry for the Same Computational Cost. *Journal of Physical Chemistry Letters* **2021**, *12*, 12084–12097.

(322) Nguyen, B.; Chen, G.; Agee, M.; Burow, A.; Tang, M.; Furche, F. Divergence of Many-Body Perturbation Theory for Noncovalent Interactions of Large Molecules. *Journal of Chemical Theory and Computation* **2020**, *16*, 2258–2273.

(323) Pitoňák, M.; Neogrády, P.; Černỳ, J.; Grimme, S.; Hobza, P. Scaled MP3 noncovalent interaction energies agree closely with accurate CCSD (T) benchmark data. *ChemPhysChem* **2009**, *10*, 282–289.

(324) Riley, K.; Řezáč, J.; Hobza, P. The performance of MP2.5 and MP2.X methods for nonequilibrium geometries of molecular complexes. *Physical Chemistry Chemical Physics* **2012**, *14*, 13187–13193.

(325) Sedlak, R.; Riley, K.; Řezáč, J.; Pitoňák, M.; Hobza, P. MP2.5 and MP2.X: Approaching CCSD(T) quality description of noncovalent interaction at the cost of a single CCSD iteration. *ChemPhysChem* **2013**, *14*, 698–707.

(326) Sen, S.; Tellgren, E. Benchmarking Density Functional Approximations for Diamagnetic and Paramagnetic Molecules in Nonuniform Magnetic Fields. *Journal of Chemical Theory and Computation* **2021**, *17*, 1480–1496.

(327) Nakatsuji, H.; Kanda, K.; Yonezawa, T.; Endo, K. Theoretical Study of the Metal Chemical Shift in Nuclear Magnetic Resonance. Ag, Cd, Cu, and Zn Complexes. *Journal of the American Chemical Society* **1984**, *106*, 4653–4660.

(328) Hohenstein, E. G.; Parrish, R. M.; Martınez, T. J. Tensor hypercontraction density fitting. I. Quartic scaling second-and third-order Møller-Plesset perturbation theory. *The Journal of chemical physics* **2012**, *137*.

(329) Alberts, I. L.; Rowlands, T. W.; Handy, N. C. Stationary points on the potential energy surfaces of (C2H2) 2,(C2H2) 3, and (C2H4) 2. *The Journal of chemical physics* **1988**, *88*, 3811–3816.

(330) Auer, A. A. High-level ab-initio calculation of gas-phase NMR chemical shifts and secondary isotope effects of methanol. *Chemical Physics Letters* **2009**, *467*, 230–232.

(331) Chestnut, D.; Wright, D. W.; Krizek, B. A. NMR chemical shifts and intramolecular Van der Waals interactions: carbonyl and ether systems. *Journal of Molecular Structure* **1988**, *190*, 99–111.